REPORT NO. DOT-TSC-FAA-72-6

MONOPULSE AZIMUTH MEASUREMENT IN THE ATC RADAR BEACON SYSTEM

transpo 72

U.S. International Transportation Exposition
Dulles International Airport
Washington, D.C.
May 27-June 4, 1972

BERNHARD KULKE
BRUCE RUBINGER
GEORGE G. HAROULES
TRANSPORTATION SYSTEMS CENTER
55 BROADWAY
CAMBRIDGE, MA. 02142

DECEMBER 1971
TECHNICAL REPORT

PREPARED FOR:

DEPARTMENT OE OF TRANSPORTATION
FEDERAL AVIATION ADMINISTRATION
WASHINGTON, D.C. 20590

TECHNICAL REPORT STANDARD TITLE PAGE

1. Report No.	2. Government Accession No.	3. Recipient's Catalog No.
DOT-TSC-FAA-72-6		

4. Title and Subtitle	5. Report Date
MONOPULSE AZIMUTH MEASUREMENT IN THE ATC RADAR BEACON SYSTEM	December 1971
	6. Performing Organization Code

7. Author(s)	8. Performing Organization Report No.
Bernhard Kulke, Bruce Rubinger, George G. Haroules	

9. Performing Organization Name and Address	10. Work Unit No.
Department of Transportation Transportation Systems Center 55 Broadway Cambridge, MA 02142	R-2135
	11. Contract or Grant No. FA 219
	13. Type of Report and Period Covered Technical Report
12. Sponsoring Agency Name and Address Department of Transportation Federal Aviation Administration Washington, D.C. 20590	14. Sponsoring Agency Code

15. Supplementary Notes

16. Abstract

A review is made of the application of sum-difference beam techniques to the ATC Radar Beacon System. A detailed error analysis is presented for the case of a monopulse azimuth measurement based on the existing beacon antenna with a modified feed network. A comparison of the total expected monopulse error with the azimuth error of the existing ATCRBS indicates that there is little to be gained by a monopulse modification. Without beam sharpening, the single-reply monopulse accuracy is less than that of the existing system. With beam sharpening and/or by using multiple reply information, the azimuth error is estimated to be as little as 1 or 2 Azimuth Change Pulses (ACP's), compared to 3 ACP's measured error for the Common Digitizer. However, the monopulse modification implies a considerable increase in system cost and complexity, and the estimated accuracy has not so far been demonstrated in the field. A monopulse modification for azimuth measurement in ATCRBS therefore is not recommended. In terms of fruit reduction, an advantage is obtainable by utilizing sum-difference techniques for artificial beam sharpening, but other solutions may be preferable.

17. Key Words	18. Distribution Statement
ATC Radar Beacon System, Monopulse Azimuth Measurement, Error Analysis, Sum-Difference Techniques	Availability is unlimited. Document may be released to the National Technical Information Service, Springfield, VA 22151, for sale to the public.

19. Security Classif. (of this report)	20. Security Classif. (of this page)	21. No. of Pages	22. Price
Unclassified	Unclassified	121 133	$3.00

Form DOT F 1700.7 (8-69)

TABLE OF CONTENTS

Page

ACKNOWLEDGMENTS xi

SUMMARY xiii

INTRODUCTION 1

AZIMUTH ACCURACY AND RESOLUTION IN THE PRESENT ATCRBS 4

SUM-DIFFERENCE TECHNIQUES IN THE BEACON RADAR SYSTEM 8
- Interrogator Sidelobe Suppression (ISLS) 8
- Receiver Sidelobe Suppression (RSLS) 12
- Monopulse Azimuth Measurement 14
  - Antenna Parameters 15
  - Sources of Error for a Monopulse Angle Measurement in the Beacon System 19
    - Thermal Noise 20
    - Monopulse Network Error 23
    - Mechanical Errors 30
    - Error Due to Pattern Asymmetry 36
    - Off-Boresight Error 37
    - Error Due to Interfering Targets 40
      - Adjacent Target Interference 42
      - Sidelobe Target Interference 47
    - Multipath Error 49
    - Summary of Error Contributions 51
  - Application to the NAS En Route System with the Common Digitizer 53
  - Application to the En Route Manual System 55

CONCLUSIONS AND RECOMMENDATIONS 57

APPENDIX A (THE MANUAL BEACON SYSTEM) A-1

APPENDIX B (THE NAS EN ROUTE SYSTEM) B-1
- System Detection Capability B-6
- System Position Accuracy B-8
- System Resolution B-9
- Summary B-11

APPENDIX C (SLIDING-WINDOW TARGET DETECTION) C-1

TABLE OF CONTENTS (CONT.)

Page

APPENDIX D (DESIGN AND ANALYSIS OF MONOPULSE PRIMARY RADAR SYSTEMS) D-1
Introduction D-2
A Brief Literature Survey of Monopulse Tracking Radars D-2
Optimum Design of Monopulse Antennas D-5

APPENDIX E (BORESIGHT SHIFT DUE TO RF AND IF PHASE ERRORS) E-1

APPENDIX F (SOURCES OF MULTIPATH ERROR) F-1
Multipath Errors Arising From Surface Reflections F-2
Reflections From The Sea F-8
Reflections From The Ground F-14

APPENDIX G (MULTIPATH ERROR INTRODUCED BY BUILDING REFLECTIONS) G-1
The Reflecting Structure Viewed As An Antenna G-2
Worst-Case Pointing Error Introduced By Building Reflections G-6

REFERENCES

LIST OF ILLUSTRATIONS

Page

1. Measured Azimuth Accuracy With TPX-42 Interrogator System..... 7

2. Interrogator Sidelobe Suppression By Transmitting P_2 Via the Difference Pattern..... 9

3. Modifications on the Beacon Antenna That Provide a Rudimentary Capability for Sum-Difference Operation..... 11

4. Receiver Connections for RSLS..... 13

5. Monopulse Angle Measurement..... 15

6. Sum and Difference Pattern, FA 7202 Antenna with Modified Feed Network..... 17

7. Power Ratio of Difference Pattern Gain to Sum Pattern Gain, FA 7202 Antenna with Modified Feed Network..... 18

8. Difference Pattern Voltage Vs Angle Off Boresight, FA 7202 Antenna with Modified Feed Network..... 18

9. Monopulse Error Curve, FA 7202 Antenna with Modified Feed Network..... 20

10. Calculated Signal-to-Noise Ratio Vs Distance for the ATC Beacon System, With Parameters as in Table 1..... 22

11. Transponder Reply Code Format..... 23

12. Azimuth Pointing Error Caused by Thermal Noise, Based on Signal Extraction From One Pair of Bracket Pulses..... 24

13. Illustrating Monopulse Network Error In An Amplitude Monopulse System..... 25

14. Calculated Beam Pointing Error For a 22.5° Phase Error in Two Symmetrically Placed Elements, Plotted Vs Element Position..... 26

LIST OF ILLUSTRATIONS (CONT.)

Page

15. Pointing Error Induced by a Phase Error Associated with the Feed for a Centrally Located Element..... 28

16. Measured H-Plane Pattern for AN/GPA-123 and AN/GPA-128 Antennas..... 36

17. Normalized Increase of σ with Angle Off-Boresight, Due to Decreasing S/N Ratio..... 38

18. Illustrating the Bias Error that Arises from an Off-Boresight Monopulse Measurement..... 39

19. Bias Error Associated with an Off-Boresight Measurement, Using the Sum-Difference Patterns of Fig. 6..... 39

20. Assumed Typical Interference (Fruit) Background Monopulse Measurement When the Sidelobe Level is High..... 41

21. Target Geometry for Single-Target Interference Close to Boresight..... 43

22. Composite Sum and Difference Signals Generated by Two Targets..... 43

23. Complex Indicated Angle in One Coordinate..... 45

24A. Bias and Random Errors Due to a Single Adjacent Interfering Target at Angle B..... 46

24B. Extension of Figure 24A for Large Off-Boresight Angles..... 46

25. Single-Reply Angle Error Caused by Single Interfering Target, Not Adjacent, Plotted vs the Power Ratio of the Sum Pattern Peak to the Difference Pattern Sidelobe Level at the Interfering Target Azimuth..... 49

26. False Target Indications Caused by Multipath Returns..... 50

LIST OF ILLUSTRATIONS (CONT.)

Page

27. Monopulse Vernier Azimuth Capability Added to the Common Digitizer..... 54

28. A Method of Generating a Centermark in the Manual Beacon System..... 56

A1. "Current ATCRBS" Data Acquisition and Transfer System..... A-3

B1. Received Signal Flow in the Common Digitizer..... B-3

B2. Target Orientation Considerations In Resolution.... B-10

B3. Separation Measurement Errors for NAS Operational Program Data vs FPS-16 Radar Data..... B-12

B4. Separation Measurement Errors for Controllers vs FPS-16..... B-13

C1. Interrelationship of Parameters for Sliding-Window Detection in the Beacon System..... C-3

E1. Hybrid Bridge Circuit for Tracking Feed..... E-2

E2. Trigonometric Relationships for the Condition $\alpha+\beta-\eta=\pi/2$..... E-6

E3. Azimuth Pointing Error Due to RF and IF Phase Errors..... E-6

F1. Geometry of Surface-Reflected Multipath Interference..... F-2

F2. Magnitude and Phase of the Surface Reflection Coefficient Plotted Vs Angle of Incidence for Different Types of Terrain..... F-5

F3a. Reflection Coefficient of a Perfectly Plane Earth vs Angle of Incidence, with $\varepsilon/\varepsilon_0=10$, $\sigma=10^{-3}$ mho m..... F-6

F3b. Reflection Coefficient of a Very Smooth Sea vs Angle of Incidence, $\varepsilon/\varepsilon_0=80$, $\sigma=4$ mho m..... F-6

LIST OF ILLUSTRATIONS (CONT.)

		Page
F4	Scattering Factor vs Surface Roughness	F-7
F5.	Glistening Surface Associated with Various Degrees of Surface Roughness	F-7
F6.	Normalized Antenna Gain Ratio $G_r/G(0)$ vs Azimuth Angle, FA 7202 Antenna Sum Pattern	F-11
F7.	Variation of Antenna Gain with Elevation, FA 7202 Antenna	F-12
F8.	Azimuth Multipath Error Introduced by Diffuse Reflections from the Sea vs Elevation Angle for the FA 7202 Antenna	F-13
F9.	Azimuth Multipath Error Introduced by Ground Reflections	F-17
G1.	Target Reflector Geometry	G-4
G2.	Target Reflector Geometry Projected Upon the Ground Plane	G-4
G3.	Relative Reflection Strength From Two Buildings of Widths W and W/2	G-5
G4.	Azimuth Error Caused by Reflections from Buildings	G-8

LIST OF TABLES

Page

1. Parameters For The FA 7202 Antenna With Modified Feed Network..... 19

2. Assumptions Made In Calculating S/N Ratio For The ATC Beacon System..... 21

3. Characteristics Of A Military, Monopulse Tracking Radar, AN/FPS 16..... 30

4. Sources Of Angle Error In A Precision Tracking Radar..... 31

B1. Performance Summary For FPS-16 Precision Tracking Radar..... B-7

F1. Electromagnetic Parameters For Various Surface Types..... F-3

F2. Wave Height Encountered For Various Sea States..... F-8

F3. Azimuth Multipath Error Introduced By Scattering From The Sea..... F-13

F4. Characteristics Of Clutter Spectra..... F-16

F5. Azimuth Multipath Error Introduced By Ground Reflections..... F-17

ACKNOWLEDGEMENTS

It is a pleasure to acknowledge the support of and the constructive criticism offered by Mr. Martin Natchipolsky. The many helpful comments and suggestions made by Mr. Joseph E. Herrmann also are sincerely appreciated.

SUMMARY

This report investigates the application of sum-difference beam techniques to the ATC Radar Beacon System. A detailed error analysis is presented for the case of a monopulse azimuth measurement based on a modified beacon antenna. The modification would consist of providing the existing antenna with a sum-difference capability by means of a new feed network and then deriving synthetic beam narrowing and/or monopulse azimuth measurements from this pattern.

As the monopulse measurement is inherently analog in nature, its information is contained in terms of the received pulse amplitude, and thus it is highly sensitive to interference from the superimposed signals of undesired targets. The problem of multi-target interference is made worse by the fact that the antenna difference patterns which are the basic sensors for the monopulse error signal tend to have a high sidelobe level.

This study is addressed only toward a modification of the present en route surveillance system, represented by the old manual system and by NAS En Route Stage A with the Common Digitizer. The ARTS III terminal surveillance system has not been addressed explicitly, but it is not believed that its inclusion in the tradeoff would change the overall conclusions. These are as follows.

The addition of a sum-difference antenna capability is evidently feasible. The use of artificial beam narrowing that employs the SLS feature of airborne transponders in principle can be effective in reducing the fruit rate. However, other methods such as improved interrogator management may be adequate as well as more cost-effective. The use of a single-reply monopulse azimuth measurement in conjunction with the present ATCRBS is not expected to improve on the accuracy of the existing system, unless beam sharpening is used simultaneously, and even then the improvement is marginal, with σ going from 3 ACP's to 2 ACP's. If monopulse information from more than one beacon reply is utilized, the error in principle can be reduced to σ - 1 ACP. For the NAS en route system, the corresponding estimated improvement in site accuracy may justify the increased system complexity and cost, depending on the site requirements. For the broadband (manual) system, the monopulse information could be used to generate an accurate centermark. Again, this would require a series of complex and costly system modifications,

with relatively high technical risk. On the other hand, the Common Digitizer delivers known accuracy at a known price, and therefore appears preferable where an improvement on the broadband system is considered.

As has been pointed out, the quoted errors for a monopulse azimuth measurement are only calculated estimates. It is recommended, therefore, that a series of measurements be made that will provide a solid data base to confirm these error estimates. These would include measurements of monopulse azimuth accuracy, both with and without beam sharpening; direct measurement of the signal-to-interference power ratio; isolation and measurement of multipath error; and measurement of the monopulse network error. Data on the effect of short run lengths on sliding-window detector performance would also be of interest. Finally, a combined analytical/experimental effort should be launched to improve the difference pattern of the 28-foot beacon antenna.

INTRODUCTION

The Air Traffic Control Advisory Committee (ATCAC) has suggested the use of monopulse techniques, or more accurately, sum-difference techniques, as a method of improving the performance of the Air Traffic Control Radar Beacon System (ATCRBS, Ref. 1).

While such techniques are well-known to improve angular accuracy in primary-radar tracking applications, their use in a beacon scanning system so far has been demonstrated only to a limited extent. An experimental system for generating a centermark has been described (Ref. 2), and limited field test data with beam-sharpening techniques have been reported (Ref. 3). Sum-difference, beam sharpening techniques appear to have found wide acceptance in military beacon systems, for example (Refs. 4, 5), for the suppression of unwanted replies (fruit) by threshold comparison of the sum and difference signals. However, no work has been published to date on the application of a true monopulse measurement, i.e., using continuous comparison of the sum and difference signals for the determination of target azimuth in the beacon radar system. This report is intended to fill this gap and, implicitly, to determine whether the introduction of such a technique into the present ATCRBS is feasible and worthwhile.

This report therefore is mainly an error analysis of monopulse azimuth measurement within the framework of the ATC beacon system. To lend concreteness, the error components have been calculated with a set of assumptions that appeared reasonable. One of these is that a sum-difference pattern derived from the existing 28-foot beacon antenna be used, as such patterns were readily available to support the calculations.

While these patterns probably do not represent the optimum sum-difference characteristic that can be realized with the 28-foot antenna, given an arbitrarily complex feed network, they are quite representative of current antenna design as far as the difference pattern sidelobe level is concerned. To date, it has not been shown how the latter can be diminished significantly by improved antenna design. The broad shoulders and the high sidelobe level of the difference pattern cause great difficulty for a monopulse measurement in a multi-target environment, and some method of simultaneous, artificial beam sharpening is essential to exclude off-boresight targets.

In systems where surveillance is based on very short dwell times, such as in the electronically scanned discrete-address beacon system (DABS) planned for the 1980's, the statistical detection scheme of the existing beacon reply processor can no longer be used, and the use of some reliable method of target identification based on just one or two beacon replies becomes essential.

A monopulse measurement in principle is capable of doing this, and, as there would be much less interference from undesired targets in a discrete-address system, the shape of the difference pattern becomes less important. The present report therefore is not intended to question the efficacy of monopulse measurement in the discrete-address system.

A further, less stringent assumption is implied by the emphasis on the en route surveillance system, as distinct from the terminal system. This emphasis resulted primarily from the fact that at this time the documentation is far more complete and accessible for NAS En Route Stage A than for the ARTS III system. Another reason for this choice was that one of the beam narrowing techniques that is likely to be used in conjunction with a monopulse azimuth measurement (ISLS) will reduce the number of beacon replies received per scan from any one target. For the en route case, the number of replies under present conditions is of the order of 40 per sweep, and a reduction can well be tolerated without deleterious effects on the detection capability of the system. However, for the terminal area the number of replies per target sweep is of the order of 16, and with normal practices of mode interleaving the number of Mode A (identity) replies is already such that a reduction in this number could cause a serious degradation of the system decoding capability.

In this report, the accuracy of azimuth measurement with the existing ATCRBS is outlined first. This is followed by a discussion of the possible applications of sum-difference techniques to the beacon system. These basically fall into two categories, i.e., beam-sharpening techniques and azimuth measurement. A detailed error analysis of the latter forms the bulk of the report. Next, based on the brief descriptions of the broadband and Common Digitizer systems contained in Appendices A and B, simple straw-man modifications are outlined that serve to illustrate the number and the technical complexity of new or modified components that are necessary to realize the monopulse capability in either system. Some cost considerations also are offered that lead, finally, to the conclusions and recommendations. Further appendices have been added to bring greater depth to certain arguments and analyses that are mentioned but briefly in the main body

of the report, in order to preserve the continuity of the discussion.

AZIMUTH ACCURACY AND RESOLUTION IN THE PRESENT ATCRBS

In weighing the advantages to be gained by adding a monopulse feature, it is important first to have a clear picture of the performance, both present and potential, of the existing beacon system.

This system has been and still is in a state of constant evolution, and very little measured data is available on the performance of each new version or modification.

What is termed the "current" ATCRBS in Reference 1, page 64 is in fact a system using some version of the ATC BI-3 interrogator set. This is sometimes also called the "manual" or the "broadband" system.

A brief functional description of this system is given in Appendix A. Although the width of a target slash (effective beamwidth) is typically four degrees, it is claimed that centermarking can achieve azimuth accuracies of 0.25 - 0.4 degrees. However, at present centermarking is not being used widely. The actual present operating accuracy therefore is in most cases less than the numbers quoted above. On the other hand, centermarking is rapidly coming into use as the new, computerized reply processing systems are being installed.

Generally, the accuracy of centermarking depends on the number of pulses per beamwidth (hits per target), which in turn depend on the pulse repetition frequency and the antenna scan rate. For example, with a four-degree effective beamwidth and a 360 per second interrogation rate, we find 16 hits per target for the terminal beacon system, scanning at 4 sec/rev, and 40 hits per target for the en route system, scanning at 10 sec/ rev. Another limitation on any azimuth measurement is the azimuth quantizing granularity. The azimuth pulse generator essentially resolves each antenna scan into 4096 equal increments of 0.088^{o} each, and clearly this implies a lower bound of $\pm 0.044^{o}$ on minimum achievable error. Other factors, such as boresight error, windloading, gearing errors, and mechanical alignment, are also present but are not considered serious (Ref. 1, App. E-5).

The four-degree effective beamwidth of the 28-foot beacon antenna limits the resolution between adjacent targets of identical range to approximately five degrees, or about twice the 3-dB beamwidth.

From the above discussion it is clear that the potential azimuth accuracy of the present beacon system has not been realized in the older installations that do not employ centermarking. Much better accuracy can be and has been realized by going to a different method of processing the target information which will now be described.

This system is currently being implemented at selected radar sites within the framework of the NAS En Route Stage A program which has been designed to provide a large degree of automation for Air Route Traffic Control Centers. Similarly, computerized systems are being installed at terminal sites, i.e., the ARTS III system and the TPX-42 equipment group.

In the NAS en route system, all processing of the received signal takes place within a subsystem termed the Common Digitizer (CD). A functional description of this system is given in Appendix B. The essential novelty here lies in the target detection logic. Unlike the manual system where each valid set of bracket pulses individually activates the PPI display to help generate the complete target track, the Common Digitizer consults a sophisticated sliding-window detection algorithm before a target is "declared," i.e., before a PPI display is generated. In this way it is possible to absorb occasional garbled or missed specimens in a run of replies, while still assigning a highly accurate azimuthal position to the target. The CD installations in NAS En Route Stage A as yet are not completely operational (1971), but preliminary field results are available, and these are also discussed in Appendix B.

Descriptive literature by the Burroughs Corporation (Ref. 6) lists the following performance claims. Azimuth accuracy is within ± 3 azimuth change pulses (± 0.26 degrees), and azimuth resolution is twice the 3dB beamwidth, or 5.6 degrees. The azimuth reference pulse is maintained within ± 0.02 degrees, and pulse-to-pulse jitter is held to ± 0.01 degrees, for an antenna scan rate of 5-6 rpm.

The field test data discussed in Appendix B confirm the claimed (single-site) azimuth accuracy performance of $\sigma = 3$ ACP's. The measured overall system accuracy was somewhat less because of registration errors between different radar sites. It is expected that these errors can be minimized as the system is progressively being "debugged."

No field test data on ARTS III were available at the time of writing (December 1971). Both manufacturer's test data and field test results are available, however, for the TPX-42 system. This is a somewhat smaller system consisting

of ground interrogator, beacon reply processor, and display units that the FAA intends to use for the terminal control of air traffic at small and intermediate sized airports. One installation is about to become operational at Binghamton, New York. A selected target track from the manufacturer's test data (Fig. 1) shows a 1σ azimuth error of less than 2 ACP's under the general conditions corresponding to terminal area surveillance. The FAA has also carried out field tests, and the results (Ref. 7) show that the azimuth accuracy for this system was dependent on the mode interlace ratio, the transponder reply mode, and the round reliability. A representative part of the test data implies 1σ limits on azimuth error of 2-4 ACP's, although sample runs with σ as low as 1 ACP or as high as 6 ACP's were also observed. By adjusting various internal threshold settings that control the sliding-window detection logic, the equipment was made to demonstrate an impressive capability to achieve target detection and decoding even in the presence of high fruit counts. It is reasonable to expect that similar performance will be realized eventually with the CD for the en route case.

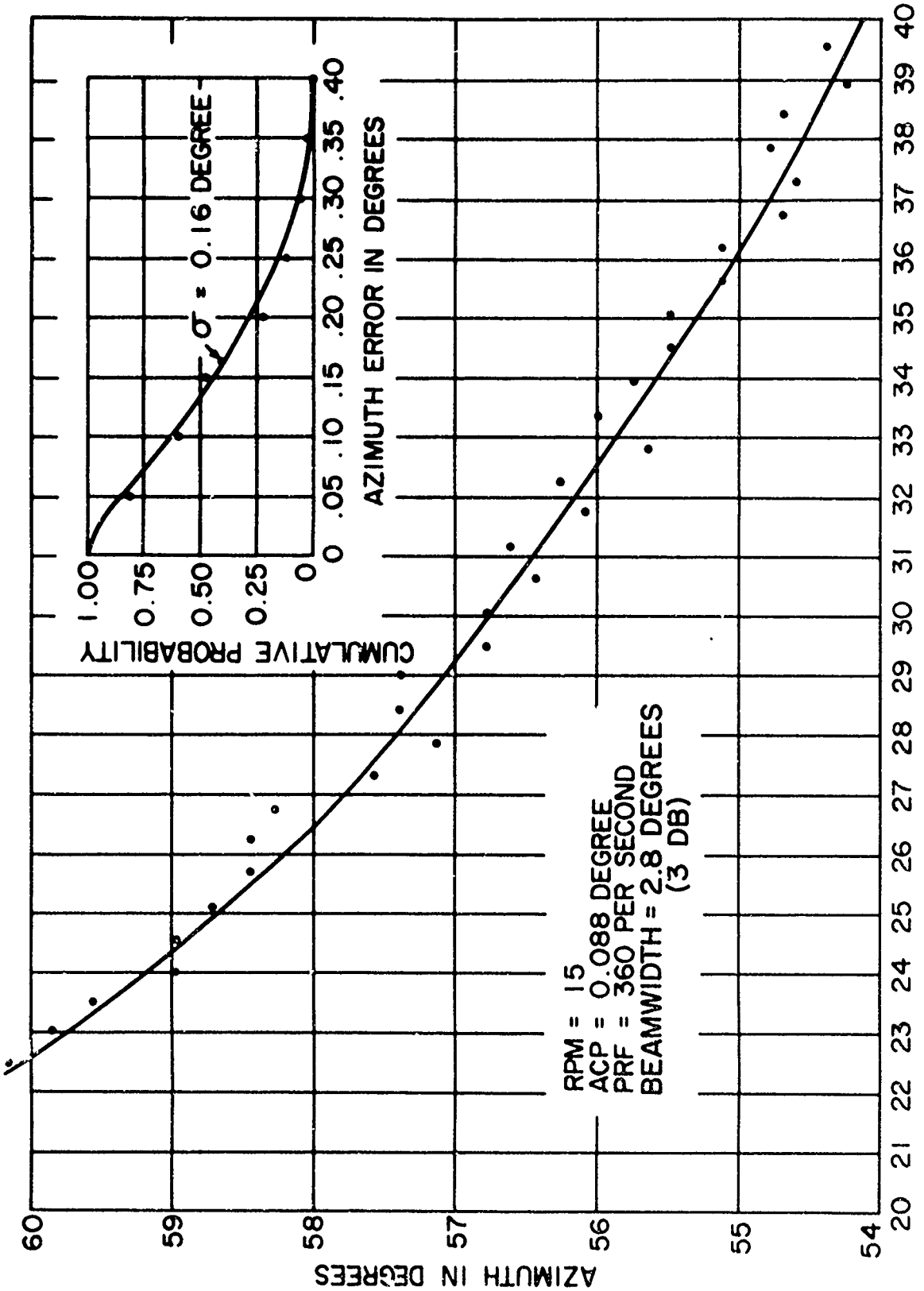

Figure 1. Measured Azimuth Accuracy With The TPX-42 Interrogator System

SUM-DIFFERENCE TECHNIQUES IN THE BEACON RADAR SYSTEM

The term "monopulse" is sometimes used in a broad sense to include any radar technique that makes use of both the sum and the difference patterns of an antenna. In this report, the term "sum-difference techniques" will be used generically, while "monopulse" will be reserved for use in the restricted sense of azimuth measurement by simultaneous lobing.

A recent demonstration of the application of sum-difference techniques to the ATC beacon system has been given by work at the MITRE Corporation (Ref. 3). Because of the cooperative nature of the beacon system, there is a sharp distinction between using these patterns for transmitting the interrogation pulse codes, and using them for receiving the reply signal from the airborne transponder. These applications will now be discussed.

INTERROGATOR SIDELOBE SUPPRESSION (ISLS)

The ability of a transponder to compare the amplitude of the P_1 and P_2 pulses forms the basis of conventional sidelobe suppression, where P_2 is transmitted over an omnidirectional pattern that swamps the sidelobe structure of the P_1 directional pattern. A possible transponder reply to a P_1-P_3 pulse combination received from an interrogator sidelobe will be suppressed when the (stronger) P_2 pulse is received via the omni pattern. However, as the suppression feature also operates on pulses received via the interrogator main lobe, a moderate amount of control can be exercised over the effective interrogation beamwidth, i.e., the angular sector over which transponder replies will be elicited, by adjusting the power level of the omnidirectional P_2 pulse.

Even better control is possible when the P_2 pulse is transmitted via the difference pattern. This is illustrated in Figure 2. Clearly, the interrogation beamwidth could vary from E-F to G-H, depending on whether the reply inhibit threshold of the transponder is set at $P_1 > P_2$ + 9dB or $P_1 > P_2$, respectively. Moreover, by increasing P_2 or decreasing P_1, the beamwidth can be made arbitrarily narrow. A smaller interrogation beamwidth results, of course, in a lesser number of replies from each target, but it also gives increased resolution between targets. The P_1/P_2 power ratio in practice would be adjusted as a compromise between the desired resolution, the desired range

(if P_2 is fixed, then P_1 must be varied) and the minimum number of replies necessary for reliable target detection and center-marking, where a statistical detector is used. A further constraint on the minimum effective beamwidth is the necessity to provide reliable decoding where modes are interlaced, i.e., where any one mode occupies only a fraction of the total run of beacon replies.

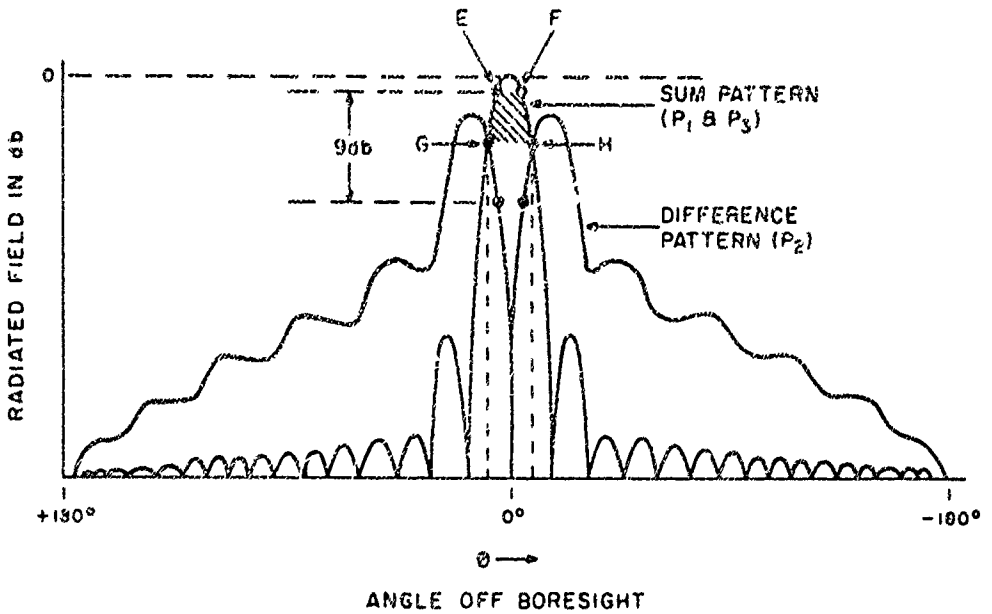

Figure 2. Interrogator Sidelobe Suppression by Transmitting P_2 Via the Difference Pattern (Ref. 2)

The chief drawback of beam sharpening by ISLS is the fact that it only works if the airborne transponder is SLS-equipped, with the inhibit thresholds properly adjusted. Under present conditions, a large portion of the military and general aviation traffic thus would be excluded from this type of system improvement. Other, less serious drawbacks are the reduction in maximum range if P_1 must be decreased and the possibility of a directional pattern sidelobe extending beyond the difference pattern amplitude. The latter problem can be remedied by transmitting P_2 both over the difference pattern and over an auxiliary omnipattern.

The advantages of beam sharpening by ISLS are improved resolution and a reduction of fruit and garble.

Figure 3 shows an example of RF circuitry that can be used to produce beam sharpening. The sum-and-difference characteristic of the 28-foot antenna is achieved by driving the right and left halves separately through a hybrid. This is only a stop-gap technique, however, as it produces very bad sidelobes through the sharp discontinuity in the center, and actually a completely new feed network must be used to optimize the aperture illumination. The purpose of the auxiliary omni-antenna is to compensate for the poor sidelobe characteristics. With a well-designed sum-difference antenna, the omni-pattern would not be used in the ISLS mode.

In Reference 3, actual PPI tracks are reproduced that demonstrate qualitatively the artificial beam narrowing that can be achieved by using ISLS in the configuration of Figure 3, with the FA 7202/AT 309 antenna. Further results on the effect of ISLS are given in Reference 4, which contains a comment on flight tests conducted by the Canadian DOT, using a Litton FA-7201 antenna. This antenna has a nominal 3dB beamwidth of 2.4 degrees. When used in a "sum only" mode, the average displayed target width was 5 degrees, but when used in a sum-difference (ISLS) mode, the displayed target width was reduced to 1.25 degrees, thus yielding a 4:1 improvement in target resolution. The aperture illumination used to produce the difference pattern in Reference 4 was not described, however.

While these field tests indicate the basic capabilities of beam sharpening by ISLS, little data is available so far that would illustrate operational acceptance and success of the ISLS. For example, beam-sharpening capability has been installed at selected sites by the U.S. Air Force and in certain ICAO countries, but it is not known to what extent this feature is actually being used, or what quantitative operational benefits are being realized.

In Reference 1, Appendix G-1, the peak airborne traffic distribution for 1968 has been listed as 10 percent commercial airlines, 27 percent military, and 63 percent general aviation. Many military transponders are not as yet equipped with SLS, and many general aviation craft possess no transponders at all, so that any improvement in overall surveillance due to the introduction of ISLS beam sharpening would not be effective on all aircraft at this time. However, if at some time in the future *all* airborne traffic can be made to carry SLS-equipped transponders, then ISLS may well become an effective tool for en route surveillance where the reduction in run length can be tolerated.

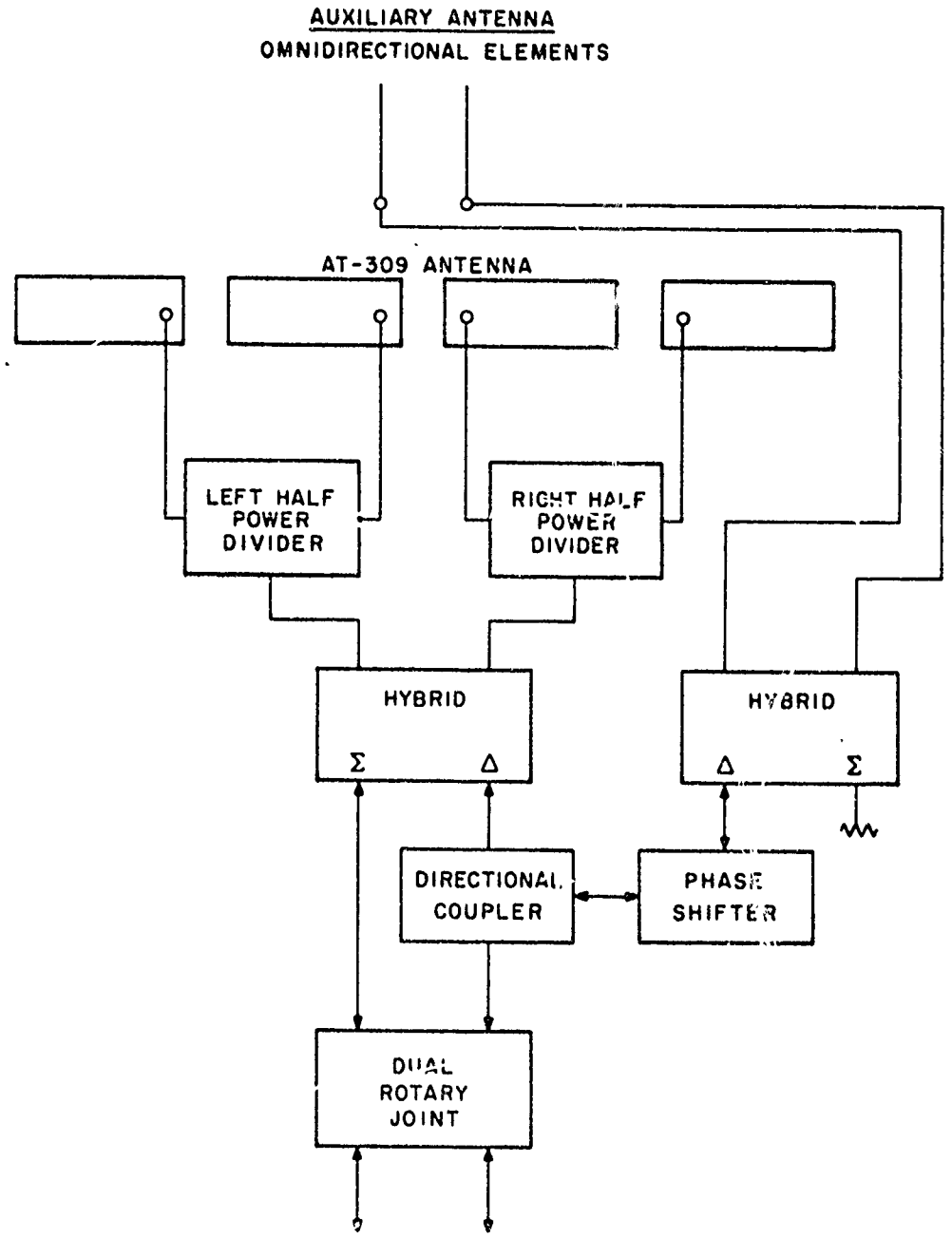

Figure 3. Modifications on the Beacon Antenna That Provide a Rudimentary Capability for Sum-Difference Operation (Ref. 3)

RECEIVER SIDELOBE SUPPRESSION (RSLS)

Beam sharpening can also be achieved by comparing the received sum and difference channel signals, and this method thus is independent of whether the airborne transponder is or is not equipped with an SLS feature. This approach can be understood by referring to Figure 2. Only those replies are accepted where the sum pattern return is stronger than the difference pattern signal. For a simple target, this limits the effective receiver beamwidth to the sector G-H, provided that the difference pattern sidelobe structure is everywhere higher than the sum pattern sidelobes, as shown. Only the main-lobe signals of the directional beam are passed.

A possible realization of RSLS is shown in Figure 4. This system requires careful gain matching and gain tracking of the sum and difference receiver channels over the required large dynamic range. In addition, careful attention must be paid to the sidelobe structure of both patterns in order to avoid any sum pattern "punch through." As the difference pattern sidelobes are relatively high, it is likely that the excessive fruit captured via these sidelobes would act to suppress a valid synchronous reply received in the main lobe of the directional pattern. That is, the broad difference pattern would intercept so many random pulses that the suppress gate could be triggered even for a valid reply.

Similarly, the effective beamwidth, which depends on a comparison of the Σ-Δ difference with a fixed threshold, could be jittered by interference signals in the difference channel, or the entire active beam sector could be shifted off-boresight by an asymmetry of the difference pattern lobes with respect to the main lobe of the sum pattern. Unfortunately, no analytical or measured data are available at this time that could serve to demonstrate just how serious any of these effects are. Despite these shortcomings, beam narrowing by RSLS has become a well-known technique. Either an ISLS or an RSLS scheme would almost certainly have to be used in support of a monopulse azimuth measurement, because for the (typical) case of multiple targets the inherently high sidelobe structure of the difference pattern otherwise would be troublesome. Generally, strong fruit returns via the sidelobe structure would add to the derived target return near boresight, thereby interfering with the single target azimuth measurement. By using RSLS, these fruit returns can be suppressed.

In work that has been described in Reference 2, an RSLS approach was carried one step further, in that a method was developed to derive a center mark for the beacon target from

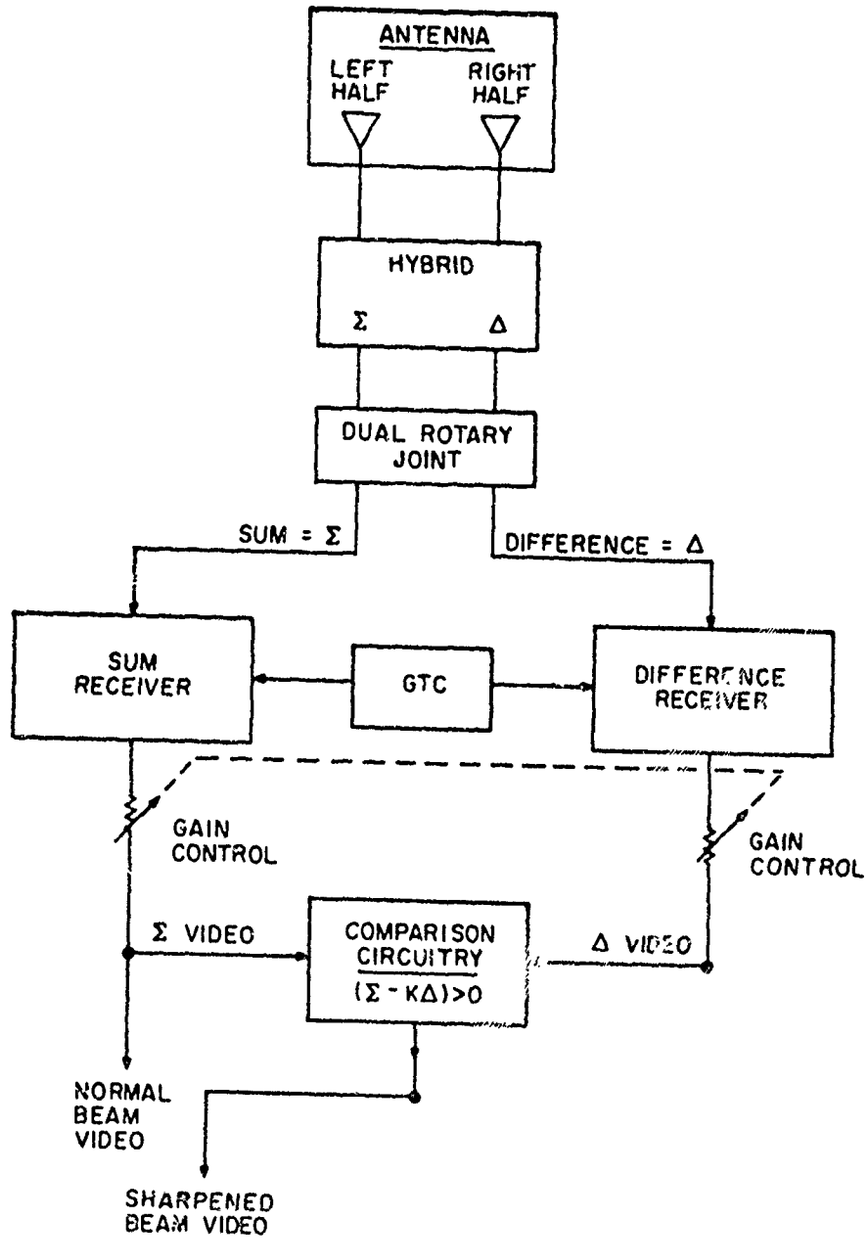

Figure 4. Receiver Connections for RSLS (Ref. 3)

a threshold-type comparison of the sum and difference channels. However, no data were given on the azimuth accuracy resulting from the use of this approach.

It should be mentioned that use can also be made of the omni pattern to produce artificial narrowing of the receiving beam. This is similar to the method used for ISLS that was briefly mentioned errlier; that is, a threshold comparison takes place between the two signals received via the sum pattern (main beam) and via the omni pattern.

A certain amount of confusion exists between "true" monopulse azimuth measurement and general sum-difference beam-sharpening techniques such as ISLS and RSLS. For example, the so-called monopulse on receive capability that has been provided in certain West German beacon interrogator stations of recent vintage actually is an RSLS scheme (Ref. 8).

MONOPULSE AZIMUTH MEASUREMENT

For the purposes of this report, the term monopulse will be reserved for the technique of azimuth measurement where a target is simultaneously illuminated by both main lobes of the difference pattern, and the normalized difference channel signal is evaluated on a continuous not a threshold basis. This technique is illustrated in Figure 5 (Ref. 9).

For a small angular range near boresight (about $\pm$ one-third of the beamwidth), the difference, or error, signal is a linear function of the target displacement from boresight, and this displacement can thus be measured with great accuracy. The processing of the monopulse signal differs depending on whether the signal return from the difference pattern is evaluated in terms of amplitude only, phase only, or both amplitude and phase. However, as all three sensing approaches can be shown to be mathematically equivalent, there is no inherent difference in achievable accuracy.

Phase comparison monopulse systems are basically adaptations of the short-baseline interferometer widely used in radio astronomy. Historically, the development of this type of system preceded the amplitude-comparison monopulse system, but current usage appears to strongly favor the latter.

The theory of monopulse measurement has been outlined by Rhodes (Ref. 10), and cogent discussions are available in standard handbooks (Refs. 9,11). The present discussion will therefore be confined to the application of amplitude-comparison monopulse methods to the ATC radar beacon system.

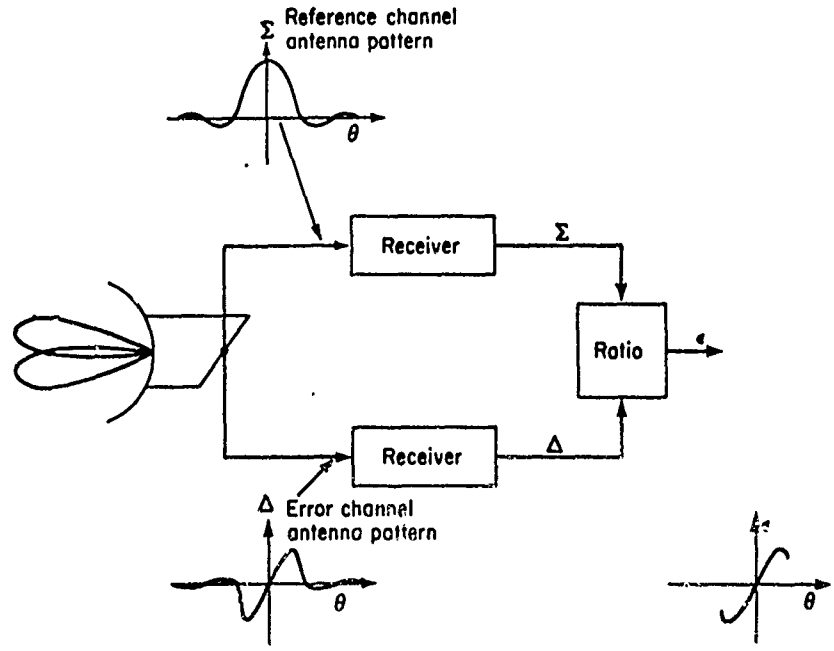

Figure 5. Monopulse Angle Measurement (Ref. 9)

A basic question is what improvement, if any, in accuracy can be achieved over the existing system. In subsequent sections, the individual error components that are expected to arise in a monopulse azimuth measurement will be calculated. The Model FA 7202 beacon antenna serves as a basis for these calculations, and the associated antenna patterns and performance parameters will be given first. Finally, an overall error budget will be presented which indicates that, under the assumptions specified earlier, no significant improvement in angular accuracy is expected by using monopulse methods. For the sake of completeness, however, specific straw-man modifications to existing hardware will be suggested to illustrate the cost and technical complexity involved in implementing a monopulse modification.

Antenna Parameters

As a basis for later calculations of monopulse measurement error, certain key parameters of the beacon antenna will now be established.

The interrogation antenna used by an Air Traffic Control Beacon Ground Station is a 28-foot, type FA 7202 unit. This

antenna consists of a horizontal array of 32, probe excited, resonant cavities that are used as radiators. The feeder network effects a tapered Dolph-Chebyshev current distribution that yields a low sidelobe level. The manufacturer lists the following set of antenna design parameters.

Gain	21 dB over an isotropic source
Horizontal aperture	27.3 ft
Horizontal beamwidth	2.35° at 3 dB below max.
Vertical beamwidth	50° at 3 dB below max.
Sidelobes	25 dB below max.
Back lobes	28 dB below max.
Input impedance	50 Ω

The optimal antenna gain is equal to

$$G_o = \frac{4\pi A}{\lambda^2} = \frac{4\pi(32)(0.81\lambda)(0.945\lambda)}{\lambda^2} = 307$$

where 0.81λ is the height, and 0.945λ the width of the radiating cavity. This indicates an antenna efficiency of

$$\eta_a = G_m/G_o = 0.41$$

The rms aperture width (for a uniform illumination) is

$$\mathcal{L}_o = \pi L/\sqrt{3} = 49.7 \text{ ft}$$

and with this one calculates the maximum value of K achievable with this aperture as

$$K_o = \mathcal{L}_o/\lambda = 55.1$$

Sum and difference antenna patterns applicable to the FA 7202 are presented in Figure 6. These patterns were measured by Litton Industries for the AT-309C, which is the military equivalent of the FA 7202 antenna. The military version employs the same aperture distribution as its civilian counterpart. However, it has been modified by the addition of a hybrid network into which signals from the two halves of the antenna are fed to produce the sum and difference voltages.

A plot of the ratio of the difference pattern to the sum pattern gain is given in Figure 7. In addition, Figure 8

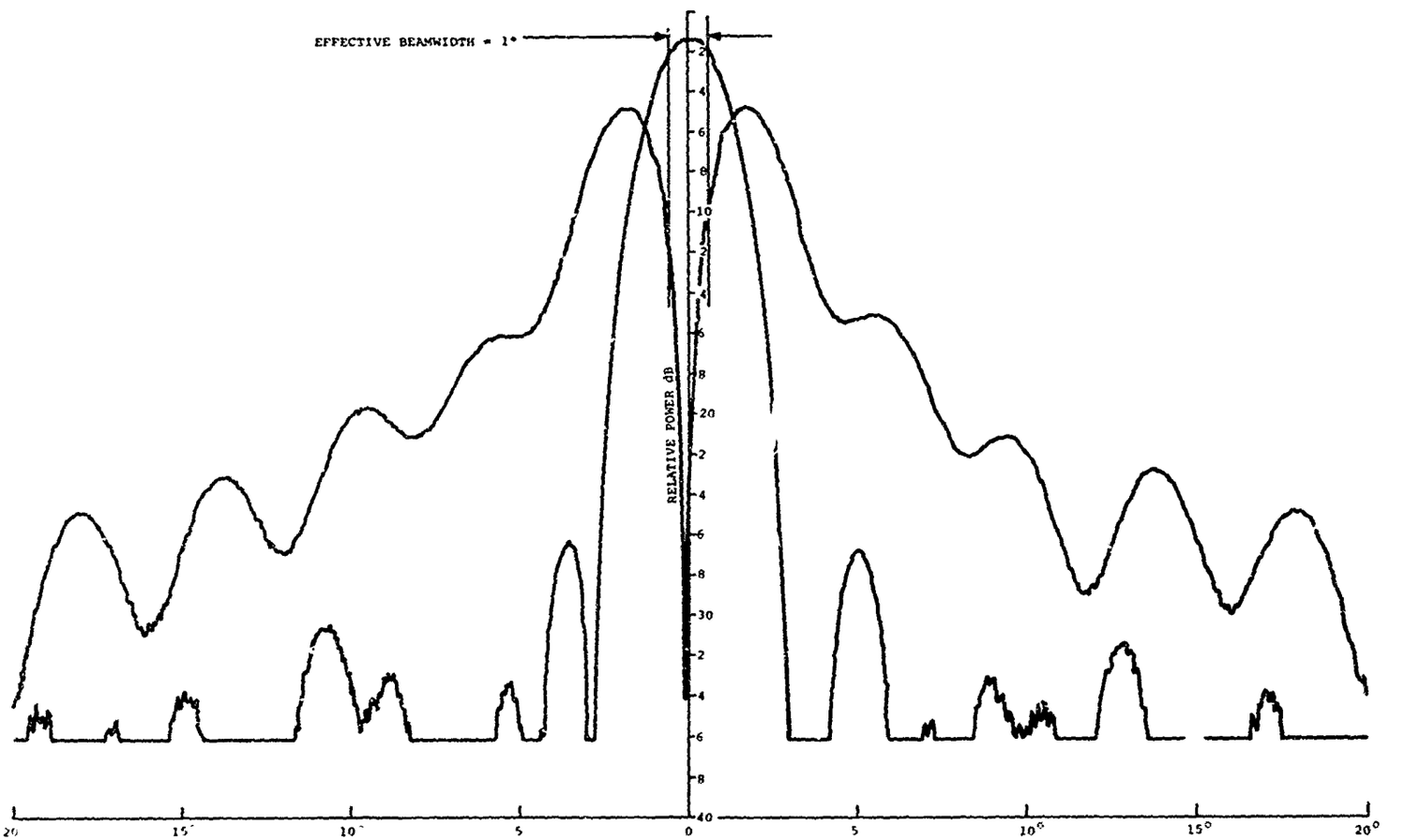

Figure 6. Sum and Difference Pattern,
FA 7202 Antenna with Modified Feed Network

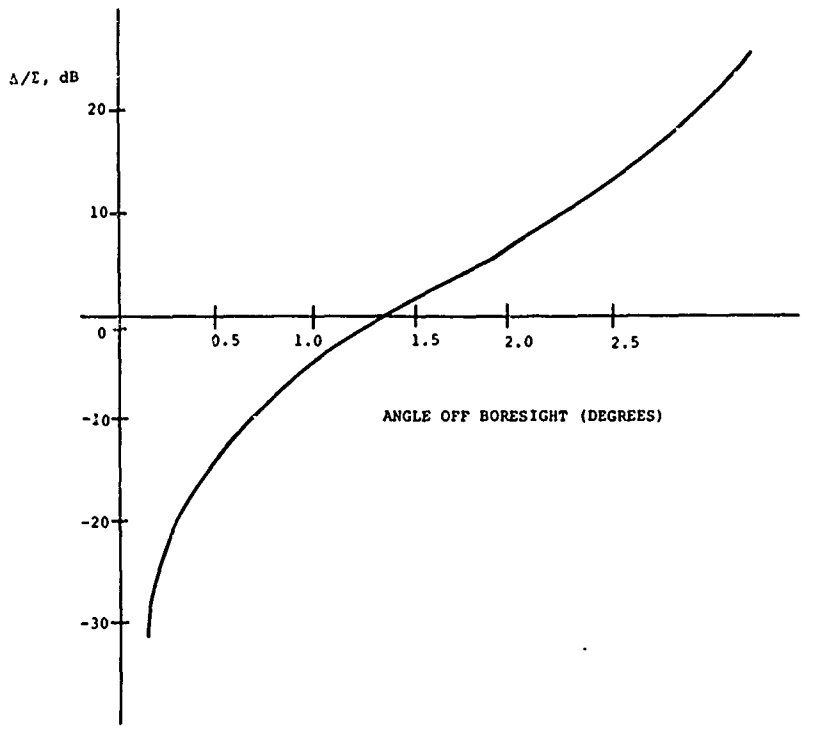

Figure 7. Power Ratio of Difference Pattern Gain to Sum Pattern Gain, FA 7202 Antenna with Modified Feed Network

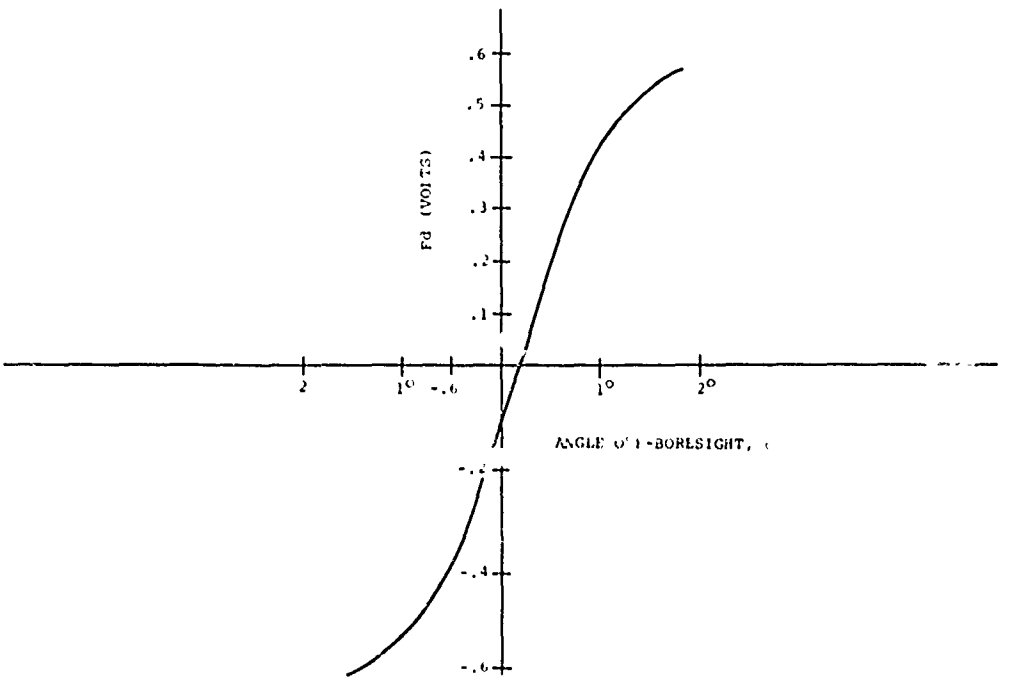

Figure 8. Difference Pattern Voltage Vs Angle Off Boresight, FA 7202 Antenna with Modified Feed Network

shows the difference pattern voltage $F_d(\theta)$, defined as the square root of the difference pattern power gain. From this curve is obtained the *normalized monopulse slope* for the antenna,

$$K_m = \frac{\theta_3}{\sqrt{G_m}} \left. \frac{\delta F_d}{\delta \theta} \right|_{\theta=0} = 1.52$$

The *relative difference slope* is given by

$$K = \frac{K_m \sqrt{\eta}}{\theta_3} = 23.7 \quad \text{(with } \theta_3 \text{ expressed in radians)}$$

and the *difference slope ratio* then is

$$K_R = K/K_o = 0.43$$

Finally, in Figure 9, the basic monopulse error curve is plotted, giving error signal vs angle off boresight. It is this curve which forms the basis of the actual monopulse azimuth measurement.

For convenience, the calculated antenna parameters are tabulated below.

TABLE 1. PARAMETERS FOR THE FA 7202 ANTENNA WITH MODIFIED FEED NETWORK

Parameter		Value
η_a	Antenna efficiency	0.41
K	Relative difference slope	23.7
K_r	Difference slope ratio	0.43
K_m	Normalized monopulse slope	1.52
G_o	Maximum achievable gain	24.9 dB

Sources of Error for a Monopulse Angle Measurement in the Beacon System

The monopulse method of angle measurement hitherto has only been applied to tracking radars using pencil beams, and an extension of these results in a scanning system using fan beams must be approached with caution. While extensive discussions of the different sources of angle error in tracking systems, including some measured data, can be found in the

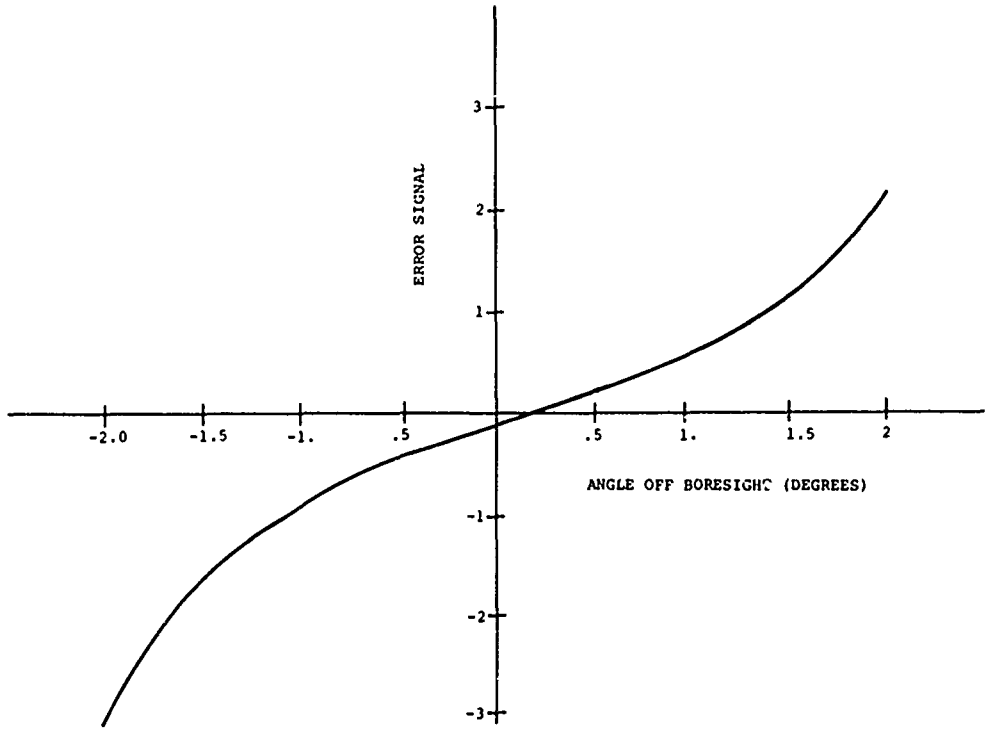

Figure 9. Monopulse Error Curve
FA 7202 Antenna with Modified Feed Network

books by Barton and Ward (Ref. 9) and Barton (Ref. 12), essentially no work has been done so far on scanning monopulse systems. However, some of the error sources carry over directly. These are thermal noise, monopulse network error, interference by undesired signals (garble, fruit, and multipath) and mechanical error. Other errors arise specifically from the nature of the antenna pattern (asymmetry of the fan beam) and from the fact that a scanning system must be capable of measuring target angles over a wider sector near boresight than a tracking system (off-boresight error).

Thermal Noise

In a primary radar system, thermal noise is one of the main factors limiting the performance, and a formidable body of literature exists on this topic. In fact, it was the desire to avoid this strong limitation by thermal noise which first led to the development of radar beacon systems, as these are, for practical purposes, unconstrained by this factor.

One can calculate the signal-to-noise ratio as a function

of range, and this has been done for the ATC beacon system, with the assumptions given in Table 2. These results were obtained using Equation (2-25) of Reference 13, reproduced below in consistent units,

$$(S/N) = P_b + G + G_b + 20\log\lambda - 20\log R - 10\log B - \overline{(NF_o)} - L_R + 77 \text{ dB} \quad (1)$$

where S/N = the signal-to-noise ratio, dB
P_b = transponder power, dBW
G = receiver antenna gain, dB
G_b = beacon antenna gain, dB
λ = wavelength, cm
R = target range, nm
B = receiver bandwidth (Hertz)
$\overline{NF_o}$ = the receiver noise figure, dB
L_R = return path loss, dB

The received signal-to-noise ratio is plotted as a function of range in Figure 10. As expected, the beacon system provides a very strong signal return, and even at the maximum operating range of 200 nautical miles an S/N ratio of 23 dB is obtained.

TABLE 2. ASSUMPTIONS MADE IN CALCULATING S/N RATIO FOR THE ATC BEACON SYSTEM

Transponder power	P_b = 500W
Transponder cable loss	L_c = 3 dB
Transponder antenna gain	G_b = 0 dB
Receiver antenna gain	G = 21 dB
Frequency	f = 1090 MHz
Return path loss	L_r = 2 dB
Receiver bandwidth	B = 10 MHz
Receiver noise figure	NF = 10 dB

The azimuth pointing error introduced by thermal noise is related to the S/N ratio by (Ref. 9, Equation 2.34)

$$\sigma_\theta = \frac{\theta 3}{K_m\sqrt{R_m}} \quad (2)$$

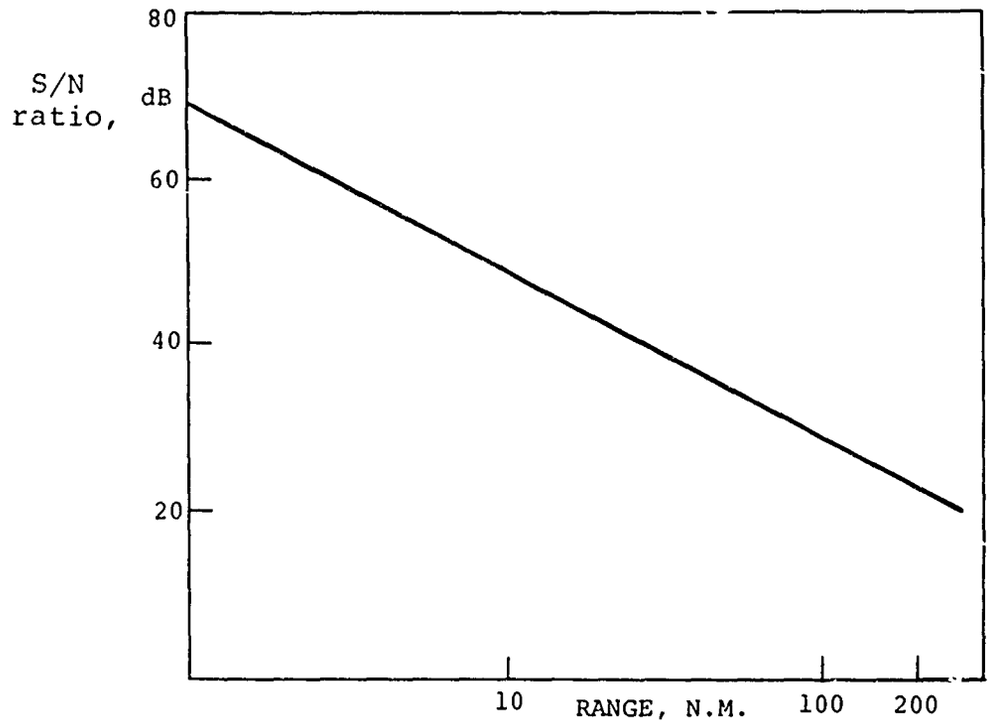

Figure 10. Calculated Signal-to-Noise Ratio Vs. Distance For the ATC Beacon System, With Parameters as in Table 2

where θ_3 is the 3 dB beamwidth, K_m is the normalized monopulse slope, and R_m is the on-axis energy ratio. This term is defined as

$$P_m = 2\eta\tau B(S/N) \qquad (3)$$

where B is the IF bandwidth, τ is the pulse duration time, and n is the number of reply pulses over which the signal is integrated.

The transponder reply format is shown in Figure 11. This consists of two framing pulses, 20.3 μsec apart, and a 12-bit information pulse sequence. Each reply pulse is nominally 450 nsec in duration, so that R is calculated with

$$\tau = 0.450 \times 10^{-6} \text{ sec}$$

In proceeding, we will assume that the monopulse processor extracts azimuth information only from one pair of bracket pulses, and therefore, n = 2.

Combining Equations (2) and (3) yields an expression for the tracking error in terms of the target range. The result

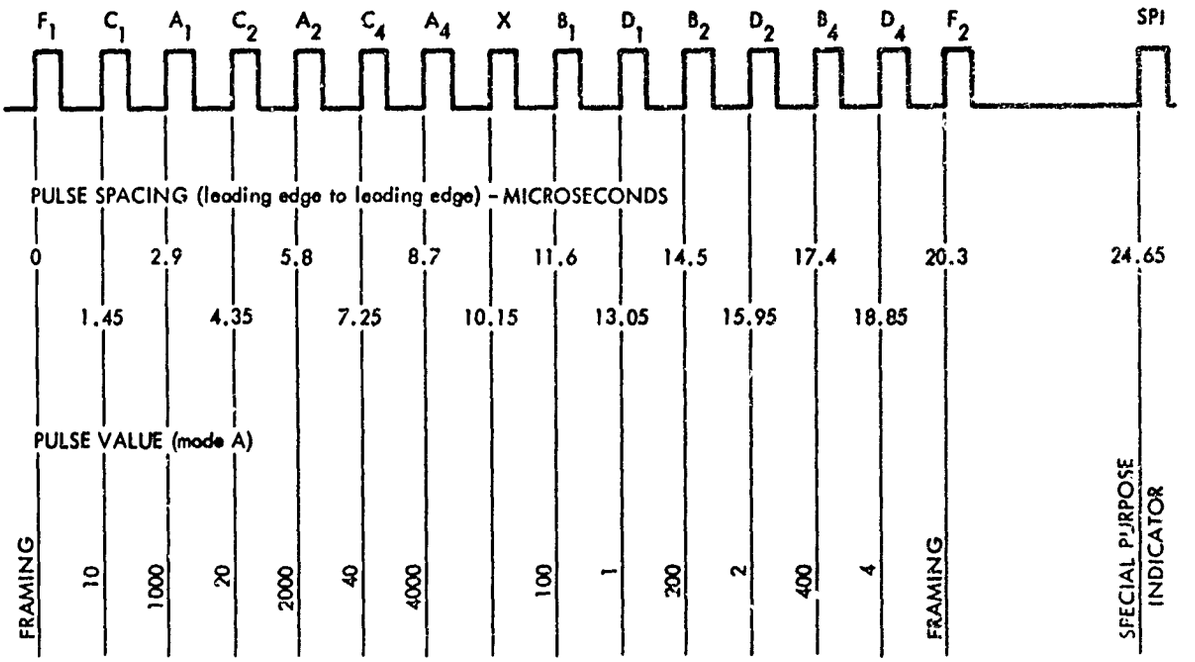

Figure 11. Transponder Reply Code Format (Ref. 1)

is shown in Figure 12. From this curve, the thermal noise error associated with a target 100 nm from the receiving antenna is $\sigma = 0.013^{o}$. The small magnitude of this error shows that in the beacon system the signal strength is so great that the impact of thermal noise is negligible.

It has been assumed here that the target essentially remains centered in the main beam. For off-boresight targets, the S/N ratio is smaller, and this results in a larger error. This case is analyzed in a later section.

It should also be recognized that the standard beacon target detection and decoding algorithms inherently are insensitive to AM (thermal) noise because they constitute digital processing of a pulse-code modulated signal. A monopulse azimuth measurement, however, is based on an amplitude comparison and therefore is highly sensitive to noise signals.

Monopulse Network Error

Monopulse network error can be understood in terms of Figure 13, which shows the basic elements of an amplitude-

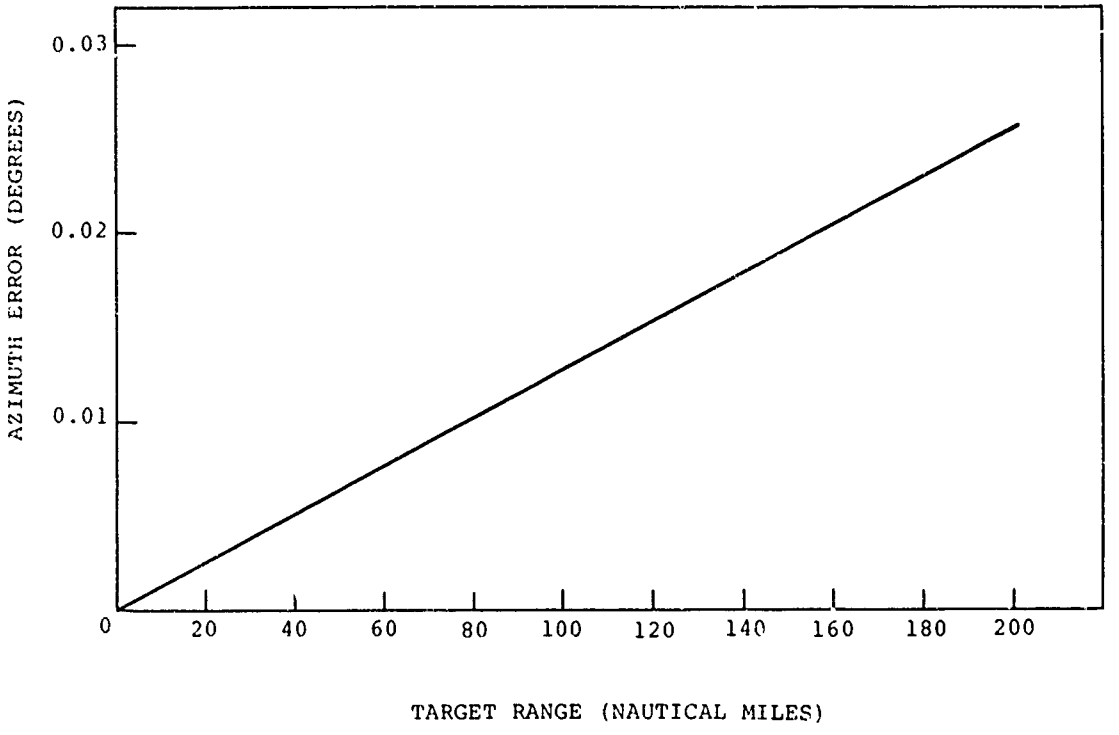

Figure 12. Azimuth Pointing Error Caused by Thermal Noise, Based on Signal Extraction From One Pair of Bracket Pulses

comparison monopulse system. The sum and difference channel signals are formed by suitably combining the signals from two or more antenna elements (segments) in the so-called comparator, which is generally a passive microwave feed network such as a hybrid or an array of hybrids (e.g., a Butler matrix). Precomparator error can arise from phase unbalance in the feed cables (caused, for example, by thermal expansion) or in the feed network itself, and generally this has the effect of causing a shift in the difference pattern null position, as well as a decrease in the null depth. As the precomparator error generally is fixed, it can in practice largely be eliminated by offsetting the feed or data system to center the "RF null" of the system, at least for a horn-fed tracking radar. For the case of an array antenna fed from a more complex passive microwave network, it should still be possible to correct for a null shift by introducing an electrical offset in the feed system. In order to give an idea of the error magnitudes likely to be involved, Figure 14 shows a calculated plot of the pointing error produced in a certain electronically scanned directive beam (Ref. 14) in response to a 22.5 degree phase change in two out of 24 beamsteering phase shifters, assigned symmetrically about beam center, as a function of the position of the

and insertion loss less than 0.1 ± 0.03 dB, with a between-channel isolation of 50 dB. These numbers are measured test values on production models, and the tolerances represent uncorrelated rotational variations.

The maximum imbalance of the VSWR's (between 1.06 and 1.10) corresponds to a difference of 0.006 dB in transmitted power, and as this is uncorrelated to the change in insertion loss it can be neglected. An additional error component arises from the phase shift differential between channels as the joint is rotated. In order to assess its possible impact, this error can be combined with the IF phase error that will next be discussed. Typical values of between-channel phaseshift are less than 10 degrees, with the deviation through 360 degrees rotation being less than one degree.

An important source of postcomparator error is the gain and phase variation in the sum and difference channel amplifiers which, in the beacon system, could be caused by IF detuning, change in signal power level at the receiver input, or temperature effects. Because the error detector in an amplitude comparison monopulse system is also sensitive to phase differences between the sum and difference channels, errors in phase "tracking" between the two channels will cause a boresight shift. Some discussion of this effect is given in Reference 11, pp. 337-339, and a detailed analysis is contained in Appendix E. As has been mentioned, the combined total error expected for a typical combination of pre- and postcomparator phase error is of the order of $\sigma = 0.03$ degrees, and this error is small, but not negligible.

It should be noted that with careful (if very costly) design, the monopulse network errors can be kept quite small. This is illustrated in Table 3 which lists the *total* angle error of a military instrumentation radar as 0.1 mil rms, or 0.006 degrees.

Another component of postcomparator error is the error due to transponder frequency shift.

The U.S. National Standard for the IFF Mark X ATCRBS specifies a frequency tolerance of ± 3 MHz around the transponder center frequency of 1090 MHz. Any offset of the transponder frequency from the nominal center frequency is equivalent to a tuning error in the receiver IF amplifier that generally results in an electrical boresight shift. The beacon system IF bandwidth is 10 MHz, however, so a ± 3 MHz frequency shift should *not* produce a significant error. Some pertinent data are available from measurements with the FPS-16 monopulse instrumentation radar (Ref. 12, Figs. 10, 11). With an 8-MHz IF bandwidth, a ± 3 MHz

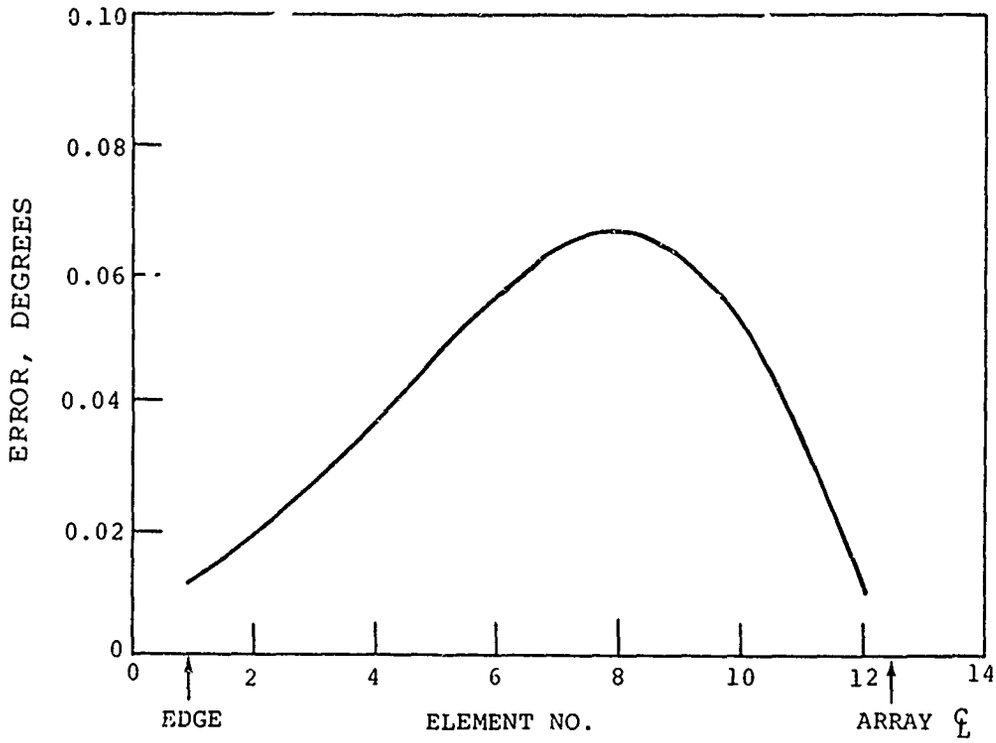

Figure 14. Calculated Beam Pointing Error For a 22.5° Phase Error in Two Symmetrically Placed Elements, Plotted Vs. Element Position. The circular array is designed for 4° beamwidth with 24 elements spaced evenly around a 60° active sector of radius 88.3 cm, with aperture illumination $\cos^2$ on 0.5 pedestal (Ref. 14)

disturbed antenna element. The array is designed to operate at 5.1 GHz, and the 3 dB beamwidth is four degrees. The maximum beam shift is 0.07 degrees, or 1.75 percent of the beamwidth. If a 10 degree random phase error is assumed, then linear scaling for the above beam would give a boresight shift of the order of 0.03 degrees, or nearly one percent of the beamwidth.

A detailed analysis of the sum-pattern pointing error due to phase errors in individual elements is given below and is applied directly to the case of the beacon antenna sum pattern.

The aperture illumination for the FA 7202 antenna is controlled by a feed network which establishes a Dolph-Chebychev distribution. This network is of the strip transmission line type and provides the excitations required by the 32 radiating elements.

It can be shown that for a linear array, the location of the beam center is perturbed by the phase errors in the following manner (Ref. 15):

$$\phi - \phi_c = \frac{\sum_{n=1}^{N} A_n \sin\varepsilon_n}{\frac{2\pi d}{\lambda} \sum_{n=1}^{N} A_n (n - N+1/2)} \qquad (4)$$

where ϕ is the location of the beam center
ϕ_c = the location of the boresight axis in the absence of feed network errors
A_n = the voltage weighting given to the nth radiating element
ε_n = the phase error in the nth feed path
d = spacing between radiating elements
N = total number of radiating elements

The phase errors encountered in the feed system are small, so Equation (4) may be linearized about the nominal values. This yields:

$$\Delta\phi_p = \frac{\sum_{n=1}^{N} A_n \varepsilon_n}{\frac{2\pi d}{\lambda} \sum_{n=1}^{N} A_n (n - N+1/2)} \qquad (5)$$

Assuming the errors in each path are randomly distributed, they may be characterized by a Gaussian density function with a zero mean and variance σ_p^2. The statistics of $\Delta\phi_p$ are then specified by:

$$E[\Delta\phi] = 0$$

$$\text{variance}\,[\Delta\phi] = \frac{\sigma_p^2 \sum_{n=1}^{N} A_n^2}{\left[2\pi d/\lambda \sum_{n=1}^{N} A_n (n - N+\tfrac{1}{2})\right]^2} \qquad (6)$$

Equation (6) was evaluated for the ATCRBS antenna sum pattern using the aperture weightings supplied in Reference (16). For an assumed phase error of $\sigma_p = 5^\circ$ in all elements, the shift in the center of the beam is described by

$$\sigma_{\Delta\phi} = 0.019^\circ$$

The pointing error is most sensitive to phase error in the most heavily weighted elements, i.e., in this case, the centrally located elements. To illustrate this, the pointing error was calculated for element No. 16 versus phase error, and the results are plotted in Figure 15.

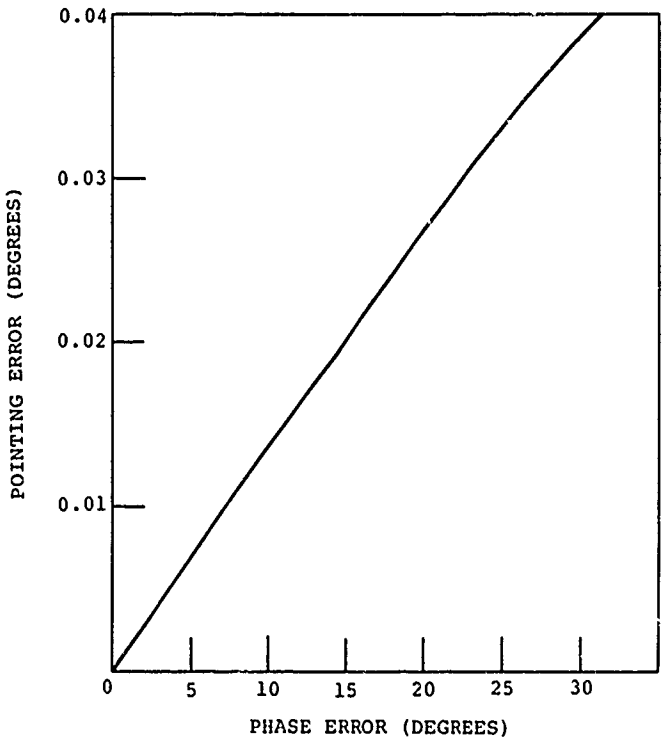

Figure 15. Pointing Error Induced by a Phase Error Associated with the Feed for a Centrally Located Element (FA 7202 Antenna, Sum Pattern)

An analysis of the difference pattern boresight error due to both pre- and postcomparator phase errors is contained in Appendix E. The results obtained there indicate that σ $\sigma = 0.03$ degrees is the correct order of magnitude for this type of pointing error, and this is about one percent of the beamwidth. No calculation has been made of the error due to gain variations between channels. It will be assumed that this error is comparable to the phase-tracking error, or $\sigma \approx 0.03$ degrees.

Postcomparator error is associated with the sum and difference channel signal paths through the dual rotary joint and the respective amplifiers. Representative performance for a modern rotary joint built for the frequency band 1030-1090 MHz is quoted by the manufacturer as VSWR≈1.08±0.02.

and insertion loss less than 0.1 ± 0.03 dB, with a between-channel isolation of 50 dB. These numbers are measured test values on production models, and the tolerances represent uncorrelated rotational variations.

The maximum imbalance of the VSWR's (between 1.06 and 1.10) corresponds to a difference of 0.006 dB in transmitted power, and as this is uncorrelated to the change in insertion loss it can be neglected. An additional error component arises from the phase shift differential between channels as the joint is rotated. In order to assess its possible impact, this error can be combined with the IF phase error that will next be discussed. Typical values of between-channel phaseshift are less than 10 degrees, with the deviation through 360 degrees rotation being less than one degree.

An important source of postcomparator error is the gain and phase variation in the sum and difference channel amplifiers which, in the beacon system, could be caused by IF detuning, change in signal power level at the receiver input, or temperature effects. Because the error detector in an amplitude comparison monopulse system is also sensitive to phase differences between the sum and difference channels, errors in phase "tracking" between the two channels will cause a boresight shift. Some discussion of this effect is given in Reference 11, pp. 337-339, and a detailed analysis is contained in Appendix E. As has been mentioned, the combined total error expected for a typical combination of pre- and postcomparator phase error is of the order of $\sigma = 0.03$ degrees, and this error is small, but not negligible.

It should be noted that with careful (if very costly) design, the monopulse network errors can be kept quite small. This is illustrated in Table 3 which lists the *total* angle error of a military instrumentation radar as 0.1 mil rms, or 0.006 degrees.

Another component of postcomparator error is the error due to transponder frequency shift.

The U.S. National Standard for the IFF Mark X ATCRBS specifies a frequency tolerance of ± 3 MHz around the transponder center frequency of 1090 MHz. Any offset of the transponder frequency from the nominal center frequency is equivalent to a tuning error in the receiver IF amplifier that generally results in an electrical boresight shift. The beacon system IF bandwidth is 10 MHz, however, so a ± 3 MHz frequency shift should *not* produce a significant error. Some pertinent data are available from measurements with the FPS-16 monopulse instrumentation radar (Ref. 12, Figs. 10, 11). With an 8-MHz IF bandwidth, a ± 3 MHz

TABLE 3. CHARACTERISTICS OF A MILITARY, MONOPULSE TRACKING RADAR, AN/FPS 16. (Ref. 12, p. 343)

Frequency	5400 to 5900mc
Pulse widths	0.25, 0.5, and 1.0μsec
Repetition rates	160 to 1707 pps
Antenna size	12-ft diameter reflector
Antenna gain	44.5 dB
Beamwidth	1.1°
Monopulse feed type	4-horn, amplitude comparison
Receiver noise factor	11 dB maximum
Receiver bandwidths	1.6 and 8.0 mc
Coverage	Azimuth 360° Elevation -10° to 85° Range 500 to 400,000 yd
Detection range ($1.0m^2$)	150 n miles
Accurate tracking range ($1.0m^2$)	75 n miles
Angle error (bias)	0.1 mil rms } COMPARATOR ERROR
(noise)	0.1 mil rms }
Range error (total)	10 yd rms

tuning error results in boresight errors of the order of 0.1-0.2 milliradians, or 0.006 to 0.012 degrees. This is an insignificant error compared to other errors with the beacon system.

Mechanical Errors

For the uniformly rotating beacon antenna, mechanical boresight shifts can arise from mechanical deflections (including load stresses, windloading, and solar heating effects), gear backlash, and bearing wobble. Errors that normally arise with a servo-driven tracking antenna are absent, but for completeness these are summarized in Table 4. In the terminal area, mechanical deflection is caused primarily by windloading on the ASR antenna that acts as a supporting structure for the beacon antenna, and this obviously is eliminated once the entire structure is housed inside a radome, such as is the case with the en route beacon antennas. For exposed antennas, windloading can be a serious problem, especially when low-frequency structural oscillations are set up by the wind forces. The mechanical engineering aspects of windloading and of gear errors are discussed thoroughly in Reference 17. Graphs of wind forces on standard antennas are given in Reference 18. Extensive wind tunnel testing of scaled-down steerable reflectors has been done at the Jet Propulsion Laboratory, for example (Ref. 19). While no work seems to have been done on establishing a general relationship between mechanical deflections and the

TABLE 4. SOURCES OF ANGLE ERROR IN A PRECISION TRACKING RADAR

CLASS OF ERROR	TYPE OF ERROR		REMARKS
	SYSTEMATIC	RANDOM	
Tracking Independent	Wind	Wind Gusts	Errors developed by a steady wind are a function of antenna position relative to wind direction. Variations in wind loading (gusts) will cause variable deflections and servo errors.
	Gravity	Gravity Anomalies	Errors are developed by variable deflections and torques caused by the force of gravity on the structural components. The deflection error is, in general, a cosine function of elevation pointing angle. Gravity anomalies exist as a result of the effect of sun, moon, and planets on earth's gravity.
	Temperature Gradient	Temperature Anomalies	Errors due to temperature gradients are a result of uneven expansion of the structural members. This may result from solar heating or ambient temperature.
	Azimuth Alignment	Unknown Migration of Earth's Pole	The deviation from true north (or south) of the zero azimuth position is considered an error. The accuracy of the survey will determine the extent to which this error can be considered correctable.
	Leveling		Misleveling of the antenna produces both azimuth and elevation errors. The azimuth error varies as a function of the sine of the azimuth angle times the tangent of the elevation

TABLE 4. SOURCES OF ANGLE ERROR IN A PRECISION TRACKING RADAR (CONT.)

CLASS OF ERROR	TYPE OF ERROR		REMARKS
	SYSTEMATIC	RANDOM	
			angle, and the elevation error is a function of the cosine of that angle.
	Orthogonality		Non-orthogonality between the axes produces an azimuth error proportional to the target tangent of the elevation angle, but a negligible elevation error.
		Bearing Wobble	Errors produced by bearing wobble are similar to those produced by misleveling and orthogonality except that they are considered random because of the tolerance on the rolling elements.
	Boresight Axis Setting and Drift		Any errors in the collimation process as well as subsequent drifts and deviations in the electrical axis appear as boresight errors. These errors are primarily a function of the depth of null achieved by the hybrid and the receiver phase stability.
	Servo Dead Zone, Unbalance and Drift	Servo Noise	Nonlinearities in the servo components can introduce an unbalance which produces a beam shift. The servo amplifiers, drive system, and tachometer produce a random noise error within the servo pass band.

TABLE 4. SOURCES OF ANGLE ERROR IN A PRECISION TRACKING RADAR (CONT.)

CLASS OF ERROR	TYPE OF ERROR		REMARKS
	SYSTEMATIC	RANDOM	
	Backlash & Friction	Backlash & Friction	The effects of backlash and friction are most evident at low tracking velocities where the starting friction considerably exceeds the running friction, causing discontinuous motion.
	Antenna Unbalance		Errors due to antenna unbalance result from the fact that the unbalanced forces are taken through the drive pinion into the pedestal and base, thus causing structural deflections, which vary in magnitude as a function of the elevation angle.
	Data Gearing	Data Gear Nonlinearity & Backlash	Random errors are produced by nonlinearity and backlash, while systematic errors are errors introduced by "wind-up" of the shafts and backlash.
	Encoder Misalignment	Data Takeoff Nonlinearity and Granularity	Random errors are produced by the nonlinearity and resolution inherent to the encoder construction; misalignment of the encoder with the antenna axis causes an unequal loading on the encoder shaft bearing and a consequent local increase in friction causing a bias error.
Tracking Dependent	Dynamic Lag	Dynamic Lag Variations	The servo lag error in tracking a source is determined by the values of the error constants and by the real and apparent velocity, acceleration, and higher derivatives of

TABLE 4. SOURCES OF ANGLE ERROR IN A PRECISION TRACKING RADAR (CONT.)

CLASS OF ERROR	TYPE OF ERROR		REMARKS
	SYSTEMATIC	RANDOM	
			source angles as viewed by the receiver.
	Torque Error		Disturbance signals enter the servo at various points between the sectional divisions defined by the open loop transfer function. Throughout the bandwidth of the servo a disturbance signal is attenuated to an equivalent error which is the disturbance divided by the loop gain preceding the disturbances entering point.
		Deflections of Antenna and Pedestal Caused by Acceleration	Tracking errors are developed by variable deflections and torques caused by the accelerations introduced to the antenna in order to follow the source path.
	Servo Hunting	Servo Hunting	Hunting or tracking loop transient errors are determined by the time response characteristics of the servo loop and the spectral density spectrum of the various input target motions and disturbances.
	Atmospheric Reradiation	Irregularities in Atmospheric Reradiation	The atmosphere not only absorbs radiation, but also in accordance with Kirchoff's radiation law, reradiates at its temperature proportional to the absorption along the path. Because of the layered atmosphere construction geometry this

TABLE 4. SOURCES OF ANGLE ERROR IN A PRECISION TRACKING RADAR (CONT.)

CLASS OF ERROR	TYPE OF ERROR		REMARKS
	SYSTEMATIC	RANDOM	
			can introduce a bias error in a lobe-comparison angle sensing system. The scattering and reflection of radio waves by the associated condensation and precipitation products may also be of concern at shorter wavelengths.
	Galactic Background Radiation		For lower frequencies (Longer Wavelengths) the radiation from the general galactic plane is observable. This background radiation field displays a distribution on the celestial sphere which concentrates itself toward the plane of the Milky Way. It reaches maximum intensity in the Sagittarius region which contains the nucleus of our galaxy.
	Ground Radiation	Multipath	Ground reflections are considered a component of the angle-dependent antenna noise temperature in the derivation of the angle error tracking equation. These noises can introduce a bias error at small elevation angles which would tend to be in the opposite direction to the refractive error. Further target signals can be reflected from the surface of the earth, and enter the receiver with an amplitude which depends upon the off-axis response of the antenna. The relatively narrow beams used in tracking and the lack of time coherence associated with the radiation from the radio star tend to reduce multipath errors to negligible values.

resultant boresight error, it appears that good design can make these errors negligibly small. On page 617, Reference 13, the total mechanical error for a modern monopulse tracker is listed as 0.04 mils (bias) and 0.025 mils (noise). For a scanning radar, the mechanical error in principle should be even smaller, because the antenna simply rotates about a vertical axis. Mechanical error therefore can be neglected in the beacon system, provided a radome is used.

Error Due to Pattern Asymmetry

Azimuth measurement with amplitude monopulse depends on a comparison of the amplitude of the signal received by each of the two main lobes of the difference pattern. It is evident that the method assumes perfect symmetry between these lobes. Such symmetry is difficult to achieve, however, as Figure 15 illustrates, which shows a fairly typical sum-difference pattern. Moreover, as the asymmetry is caused by ground interference with the vertical pattern, it will change as the antenna is scanned around, depending on the nearby terrain, as well as on the elevation angle at which the pattern cut is taken. A certain amount of degradation of the accuracy of the monopulse measurement would no doubt result from this asymmetry, though for measurements very close to boresight this might not be serious.

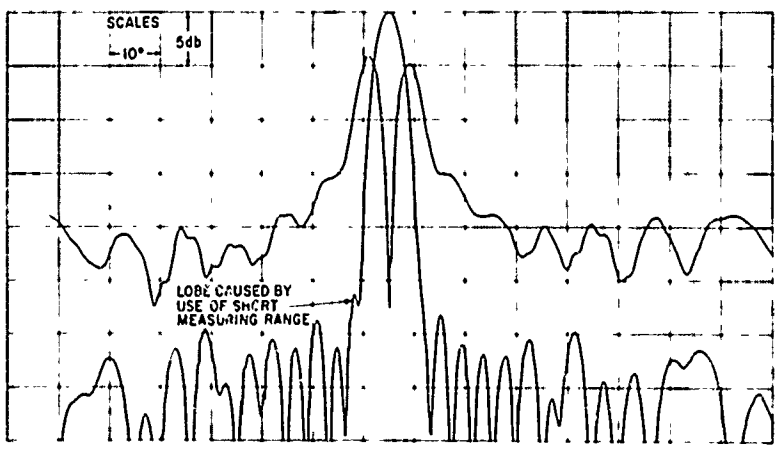

Figure 16. Measured H-Plane Pattern for AN/GPA-123 and AN/GPA-128 Antennas (Ref. 5)

A rigorous analysis of this error must include the operation of the multiplicative detector on the combined signals in order to arrive at the total error. Work on such an analysis is in progress (at TSC), but no results are available at the time of this writing.

More important, probably, is the effect of the difference-pattern asymmetry on the operation of the interrogator or receiver sidelobe suppression, because these depend on the intersection of the sum and difference patterns, as shown previously in Figure 2. It is evident how the active beam sector can be shifted to either side by a difference pattern asymmetry, thereby causing an error in centermaking the true beam.

Off-Boresight Error

When a monopulse measurement is made on a target that is not centered on the antenna boresight, error components may arise from two separate and unrelated causes. First, because the signal strength received from a target decreases with the antenna gain, while the thermal noise contributions remain constant, the S/N ratio decreases, and hence σ increases. An analytical expression has been derived by Sharenson (Ref. 20) that describes the increase in σ away from boresight. In slightly simplified notation, it reads

$$\frac{\sigma(\theta)}{\sigma(o)} = \sqrt{L_\theta \left[1 + \left(K_m \frac{\theta}{\theta_3} \right)^2 \right]} \quad , \theta < \frac{\theta_3}{2} \qquad (7)$$

where

$L_\theta = \frac{G(o)}{G(\theta)}$, the off-boresight gain reduction factor

k_m = normalized monopulse error slope

θ_3 = 3 dB beamwidth

θ = off-boresight angle

Equation (7) has been plotted in Figure 17.

It is seen, for example, that for targets three-tenths of a beamwidth away from boresight, σ already is 15 percent greater than it would be for an on-boresight measurement. However, $\sigma(o)$, due to noise, is negligibly small in the beacon system, as has been shown, and remains small even with a 15 percent increase.

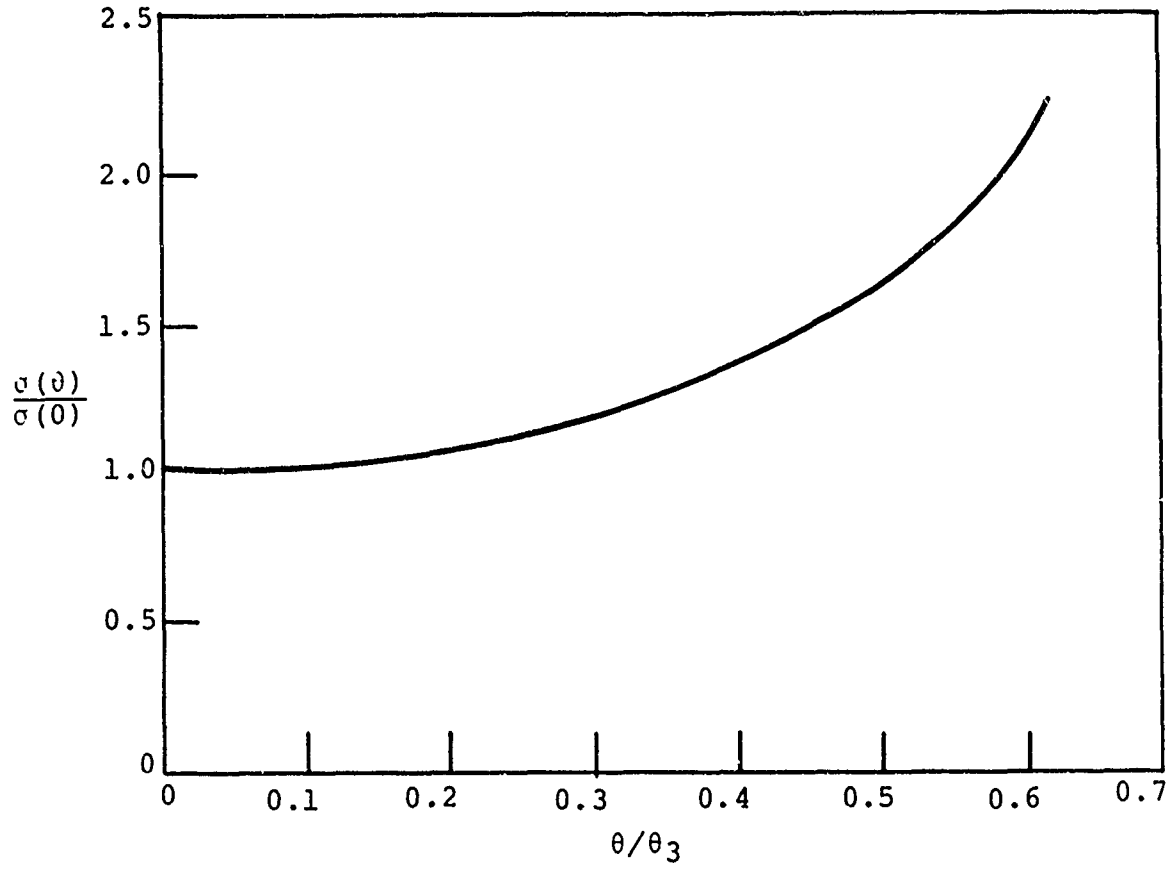

Figure 17. Normalized Increase of σ with Angle Off-Boresight, due to Decreasing S/N Ratio

A more serious error is introduced as shown in Figure 18. Because the nonlinear monopulse error characteristic is being approximated as a straight line, the indicated target azimuth for a given error voltage will be increasingly different from the true azimuth, as the target departs from an on-boresight position. This error, which is a bias error, has been calculated for a monopulse measurement based on the sum-difference pattern of the FA 7202 antenna (Fig. 6) and is plotted in Figure 19. Clearly, the bias error becomes significant for off-boresight target positions beyond about one degree, that is, beyond forty percent of the 3 dB beamwidth, where it already amounts to as much as 0.2 degrees.

However, as the bias error is a known function of the off-boresight angle, it can in principle be removed from the measurement. For example, let $\hat{\theta}_L$ be the azimuth estimate produced by the monopulse processor, where the subscript indicates that the estimate is derived under linear assumptions. From the error curve, the correct estimate $\hat{\theta}_C$ can be expresses as a functio

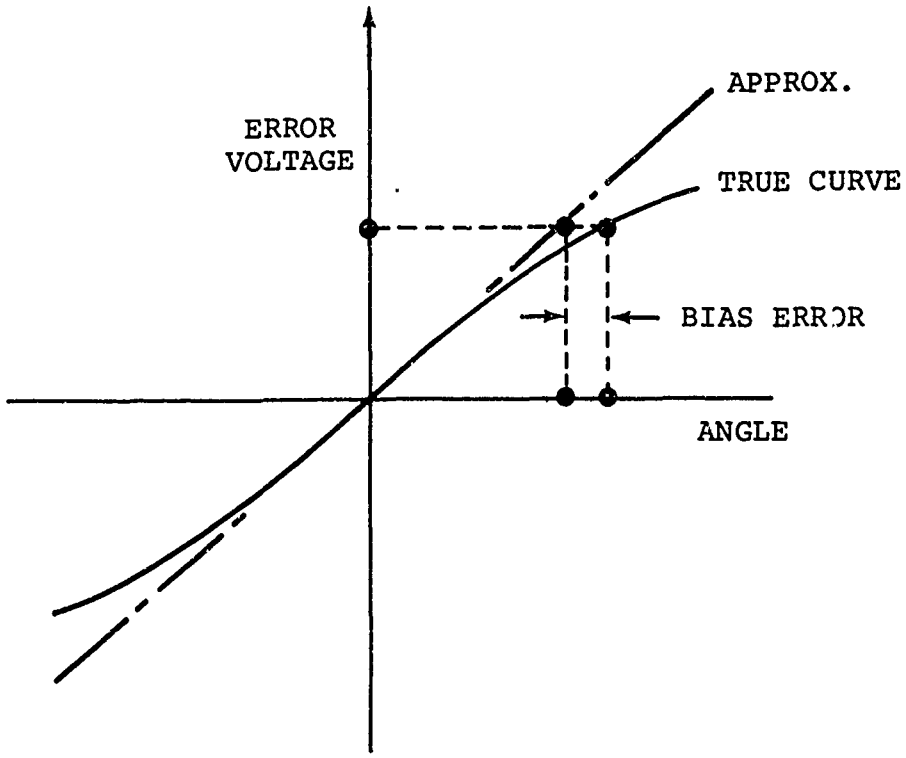

Figure 18. Illustrating the Bias Error that Arises from an Off-Boresight Monopulse Measurement

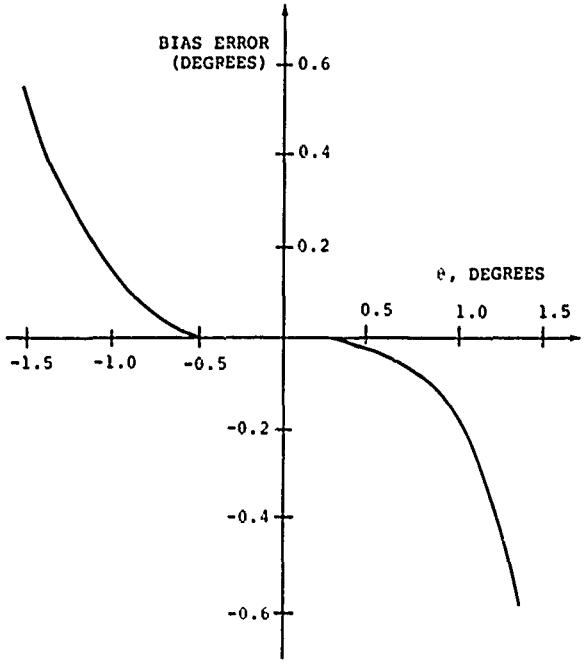

Figure 19. Bias Error Associated With an Off-Boresight Measurement, Using the Sum-Difference Patterns of Fig. 6

$$\hat{\theta}_C = f(\hat{\theta}_L) \qquad (8)$$

of $\hat{\theta}_L$, and a correction on $\hat{\theta}_L$ can thus be generated from a knowledge of the nonlinear curve. Presumably, this would be done on a threshold basis, i.e., only for θ_L exceeding a certain threshold would the correction be applied, whereas for smaller values of $\hat{\theta}_L$ the approximation $\hat{\theta}_C \simeq \hat{\theta}_L$ would be accepted as valid. For large angles off-boresight, the difference between the true and the linear characteristics becomes as large as the error voltage itself, and accurate cancellation would be difficult.

In summary, it has been shown that monopulse azimuth measurement on off-boresight targets is subject to accuracy degradation primarily because of the nonlinearity of the monopulse error characteristic. In the case of the rudimentary sum-difference pattern generated with a modified FA 7202 beacon antenna, the nonlinearity error becomes significant at an off-boresight angle of about forty percent of the 3 dB beamwidth. With a correction algorithm built in, the useful range can be extended.

Error Due to Interfering Targets

The customary application of monopulse azimuth measurement is in precision tracking radars where a single target is being held on or near boresight by moving the antenna to follow the target. However, in the multitarget environment of the air traffic control surveillance system, replies from more than a single target generally will be received, and when individual replies interfere with each other, the accuracy will be degraded.

Interfering replies may be synchronous when two or more targets are interrogated by the same beam, or they may be asynchronous (i.e., fruit) when one ground station intercepts a reply that has been elicited by a different ground station. The code train of an interfering reply may become interleaved with the desired pulse train without actually overlapping individual pulses, and in this case, the code validation algorithms of the receiver system will still extract the desired target information. However, when pulse overlap (garble) occurs, the reply train generally cannot be decoded and hence is rejected. It may be noted that beacon signals are processed digitally, whereas monopulse angle information is inherently analog in character. The latter therefore must be extracted before the beacon reply train is amplitude-limited and digitally validated. This could be done, for example, by measuring the framing pulse amplitude of each reply before processing.

The interference situation postulated here is illustrated in Figure 20, which shows the bracket pulses of the desired target superimposed on a background of interfering pulses.

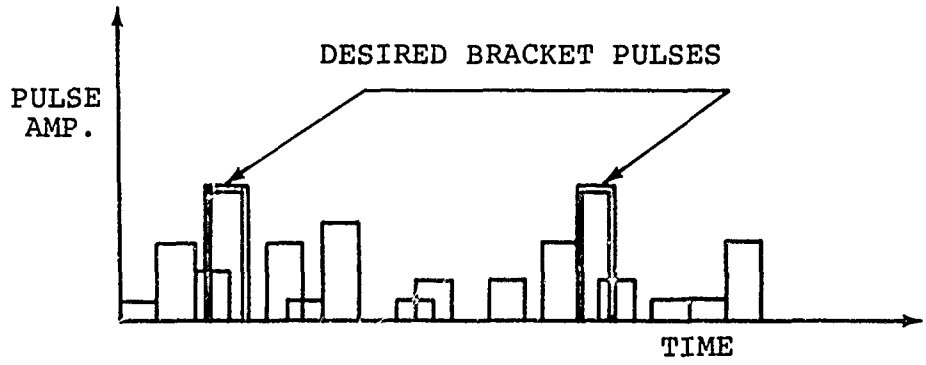

Figure 20. Assumed Typical Interference (Fruit) Background Monopulse Measurement When the Sidelobe Level is High

The following discussion applies to the case where there is direct overlap between the framing pulses of the desired target reply and *any* pulses received from interfering targets. The most obvious method of minimizing interference from undesired replies is to reduce their amplitude at the receiving antenna by narrowing the main beam and by minimizing the sidelobe level, especially for the difference pattern.

Measured difference patterns with optimally designed aperature illuminations for the 28-foot beacon antenna were not available at the time of this writing. Patterns are given in Reference 4 for a number of beacon antennas that are, however, intended for use with ISLS, where the difference pattern sidelobe structure must everywhere be *above* the sum pattern sidelobes. All patterns indicate sum pattern sidelobes that are down 28-30 dB, while the difference beam sidelobes typically are 10 dB or more above the sum pattern sidelobe structure, independent of the width of the sum beam. Moreover, the first shoulder of the difference pattern generally is only about 10 dB from the difference pattern peak.

It is conceivable that difference patterns can be designed that have a much lower sidelobe structure, and such patterns will be an important ingredient in any beacon monopulse measurement. Some analytical work toward the design optimization of sum-difference antennas has been done by Bayliss (Ref. 21).

The use of receiver sidelobe suppression (RSLS) has been suggested to produce artificial narrowing of the receiving beam, i.e., to eliminate sidelobe interference. However, RSLS depends on a comparison of the sum and difference channel returns, with fixed thresholds that determine the effective beamwidth. Any interference added to the difference channel will reduce the effectiveness of this threshold logic, and thus RSLS is subject to a type of degradation quite similar to that of the azimuth angle measurement. That is, an undesired signal from the sidelobes would add randomly to the main beam signal and would cause a random fluctuation of the effective beamwidth around the fixed thresholds.

As it appears difficult to achieve sum-difference antenna patterns that reduce interference from undesired targets to a negligible level, it is necessary to assess the magnitude of the expected error when such interference is present. This will be done both for the case when only a single interfering target exists and for the general multiple-target case.

Adjacent Target Interference. The case of a single, adjacent, interfering target is illustrated in Figure 21. The desired target A is assumed to be near boresight, at an angle α, and the interfering target B is located at an angle β, but still in the main beam. The error curve which forms the basis of monopulse angle measurement is generally approximately linear only over a range of $\pm$ one-third beamwidth near boresight.

If it is assumed that the off-boresight displacement of both targets is within the linear range, then the angular estimate $\hat{\theta}$ for either target is simply proportional to the sum-difference signal ratio,

$$\hat{\theta} = \frac{1}{C_m} \frac{D}{S} \qquad (9)$$

where C_m is a constant. The sum and the difference signals will either be in phase or 180 degrees out of phase, depending on where the target is located with respect to the boresight axis.

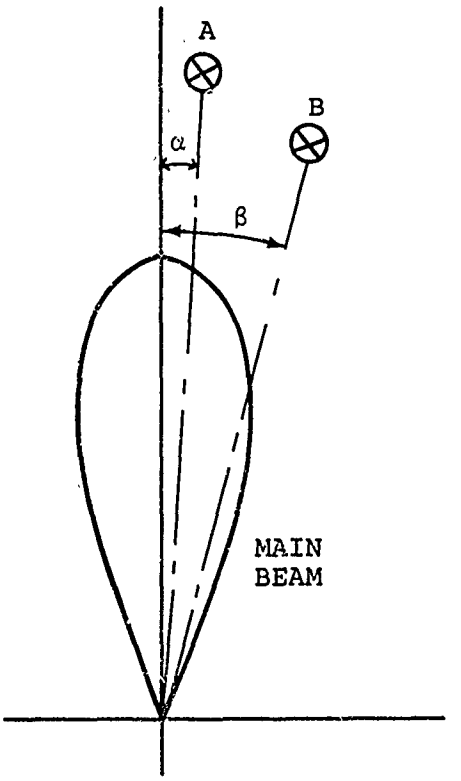

Figure 21. Target Geometry for Single-Target Interference Close to Boresight

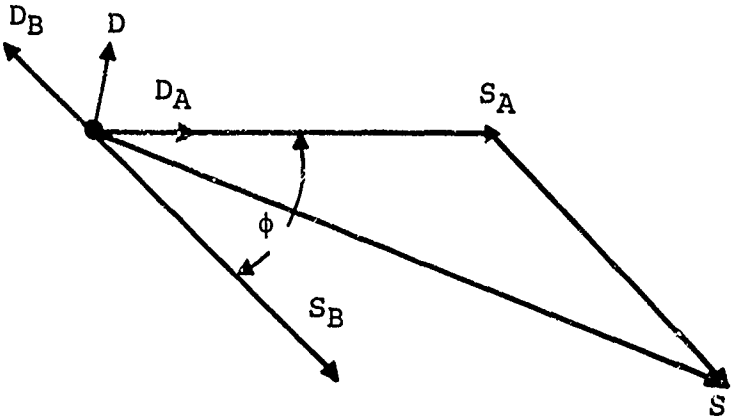

Figure 22. Composite Sum and Difference Signals Generated by Two Targets

When both targets are replying together, the composite sum and difference signals will be generated as the sum of the individual phasors, as shown in Figure 22, and they will no longer be in phase alignment. The composite angle estimate then is

$$\hat{\theta} = \frac{1}{C_m} \frac{\vec{D}_A + \vec{D}_B}{\vec{S}_A + \vec{S}_B} \tag{10}$$

or, representing the difference signals by their equivalent angular displacements,

$$\hat{\theta} = \frac{\alpha\vec{S}_A + \beta\vec{S}_B}{\vec{S}_A + \vec{S}_B} \tag{11}$$

If we let $\vec{S}_B/\vec{S}_A = ge^{j\phi}$, then

$$\hat{\theta} = \frac{\alpha + \beta ge^{j\phi}}{1 + ge^{j\phi}} \tag{12}$$

A family of curves for $\hat{\theta}$ as a function of g and ϕ, with fixed α and β, is presented in Figure 23 which was taken from Reference 22. It is seen that as the phase angle ϕ varies over $[0, 360^{\circ}]$, the estimate $\hat{\theta}$ traces out a circle in the complex plane.

The commonly used multiplicative monopulse processor will measure that part of the difference signal which is in phase or 180 degrees out of phase with the sum signal, i.e., the real part of the complex angle $\hat{\theta}$. As $\hat{\theta}$ traces out a circle in the complex plane, its real part moves along a diameter. The expected value of $\hat{\theta}$ therefore corresponds to the center of the circle, and the random component is proportional to the radius R. The expressions are

$$\hat{\theta} = \frac{\alpha - \beta g^2}{1 - g^2} \tag{13}$$

and

$$\sigma = \frac{R}{\sqrt{2}} = \frac{g(\beta - \alpha)}{\sqrt{2}\ (1-g^2)} \tag{14}$$

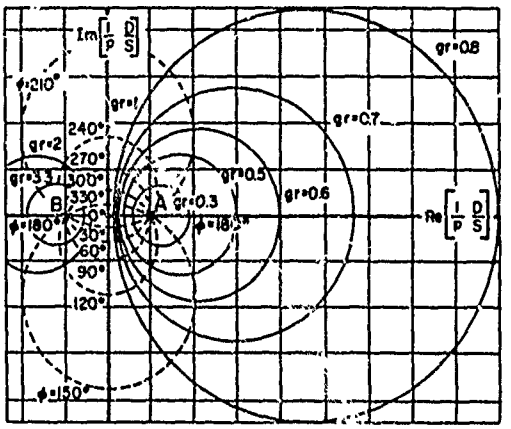

Figure 23. Complex Indicated Angle in One Coordinate (The first target is at angle A, the second target at angle B. Amplitude ratio and phase of the second target relative to the first are gr and ϕ, respectively. The figure is normalized so that the origin is at midpoint of A and B, and unit distance is (A-B)/2.) (Ref. 22)

For the case where the first target is located on-boresight and the ratio of interfering to desired signal power is small, i.e. α=o, and $g^2 \equiv I/S<<1$, we have

$$\hat{\theta} = -\left(\frac{I}{S}\right)\beta \qquad (15)$$

and

$$\sigma = \beta\sqrt{\frac{I}{2S}} \qquad (16)$$

Equation (16) is identical to Equation (5.4), Reference 9,for the case where just one observation is taken.

In the linear approximation, therefore, both the bias and the random error components increase with the off-boresight angle of the interfering target, but this increase is balanced in part by the corresponding decrease in received interfering power level. The nonlinear Equations (13) and (14) are plotted in Figures 24A and B, where $\hat{\theta}$ and σ have been derived on the basis of the sum-difference pattern of Figure 6. It may be noted that

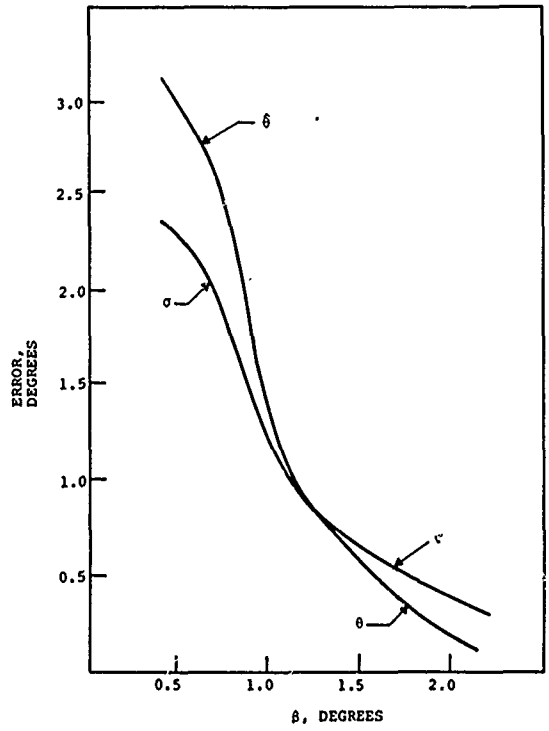

Figure 24A. Bias and Random Errors Due to a Single Adjacent Interfering Target at Angle B (Calculations are based on the antenna pattern of Figure 16, with the two targets at identical range)

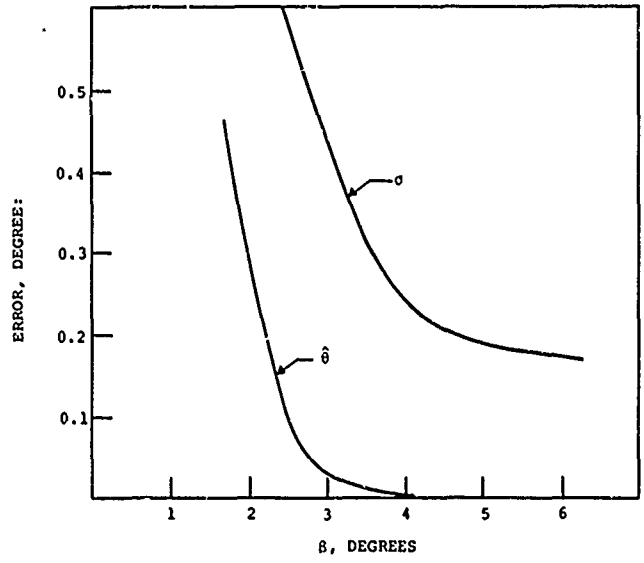

Figure 24B. Extension of Figure 23A for Large Off-Boresight Angles

for this pattern, the assumption of a linear error curve is essentially correct out to $\beta = 1.0$ degree. Beyond this angular range, the nonlinearity of the error curve must be taken into account. From Figure 24A, it is seen that interference by a second target in the main beam leads to very large errors in the monopulse measurement, of the order of 0.5 - 3 degrees for two targets that are separated by less than two degrees in azimuth. The rapid increase of the error with decreasing target separation illustrates the relatively poor resolution properties of a simple monopulse measurement due to the broad shoulders of the difference pattern.

Typical azimuth separation of targets at identical range is greater than two degrees, however. In fact, the operational minima for aircraft separation are rigidly governed by FAA standards. Under radar surveillance, current standards permit en route longitudinal separation as low as 3 - 5 miles and lateral separation (route width) of 3 - 8 miles, depending on local conditions. For an azimuth separation of 3 miles at a 60-mile range, the angle subtended is 3 degrees. From the extended plot in Figure 24B, this corresponds to a random error of $\sigma = 0.44^{\circ}$ and $\theta = 0.30^{\circ}$. Clearly, the random error dominates and is rather large. For greater off-boresight angles, the error appears to level off near 0.18 degrees.

This completes the discussion of interference by a single, second target in the main beam. The case where interference comes from the sidelobes is best discussed in terms of an interference *background* representing the multiple-target environment. This will be done in the next section.

Sidelobe Target Interference. The error caused by the interference of nearby point targets has been calculated for the case of a primary, tracking monopulse radar in Reference 9, Chapter 5, and certain parts of this analysis carry over to the beacon system. In particular, Equation (5.3) is useful, which gives the angle error σ introduced by interference from a foreign target, as

$$\sigma = \frac{\sqrt{\eta}}{K\sqrt{2n_e(S/I_\Delta)}} \qquad (17)$$

where η = sum-channel antenna efficiency = 0.41
K = error slope of the difference pattern = 23.7/degree
S = signal power in the sum channel
I_Δ = interference power in the difference channel
n_e = number of observations = 2

The values of K and η were calculated previously in the section "Antenna Parameters." It is assumed that only one set of bracket pulses is observed, so that $n_e = 2$.

In calculating the ratio S/I_Δ, it is convenient to assume two targets that are widely separated in azimuth but have equal range and elevation. The exact position of the interfering target cannot usually be predicted, and it is often more meaningful to characterize the difference pattern by an average sidelobe level over the region of expected interference. If the desired target is assumed to be at the peak of the sum pattern, and if both targets have identical transponders, then S/I_Δ simply becomes a ratio read from the antenna pattern. For the (non-optimized) pattern of Figure 6, for example, the ratio of the sum pattern peak to the difference pattern sidelobe peaks is 14dB, 20dB, 22dB, etc., depending on the assumed position of the interfering target. For complete analysis in the beacon context, one would assume a distribution of many interfering targets and assign a value of S/I_Δ to each target, depending on the average sidelobe level in the target area. The total error would then amount to the rss sum of the individual errors. Here, we shall merely characterize the problem, and this is done in Figure 25 which plots the angle error on a single reply, caused by interference from a single sidelobe target, as a function of the ratio of sum pattern peak to difference pattern sidelobe level at the interfering target azimuth. For a 22dB sidelobe level, for example, this error would be σ=0.06 degrees, and if the uncorrelated errors of, say, 20 targets were added in rss fashion, the total error would be σ=0.27 degrees. Although this error can be reduced by taking a larger number of observations, as is shown through the inverse-square root dependence on n_e in Equation (17), it is clear that sidelobe interference is another important source of error for the monopulse azimuth measurement.

As will be evident from the error summary to be presented in a later section, the error due to interfering targets contributes almost 75 percent of the total random error. If either ISLS or RSLS were used to artificially narrow the beam, then the interfering replies from adjacent or sidelobe targets would either be inhibited at the source (ISLS) or else would be suppressed at the receiver (RSLS). For the en route case, an effective beamwidth of 1.5 degrees is sufficient to elicit 15 replies per sweep, and as this corresponds to the number of replies that characterize terminal area surveillance, it is evidently adequate for decoding purposes. Either ISLS or RSLS therefore could be used to eliminate foreign-target interference, subject to the drawbacks of these approaches that have been discussed previously.

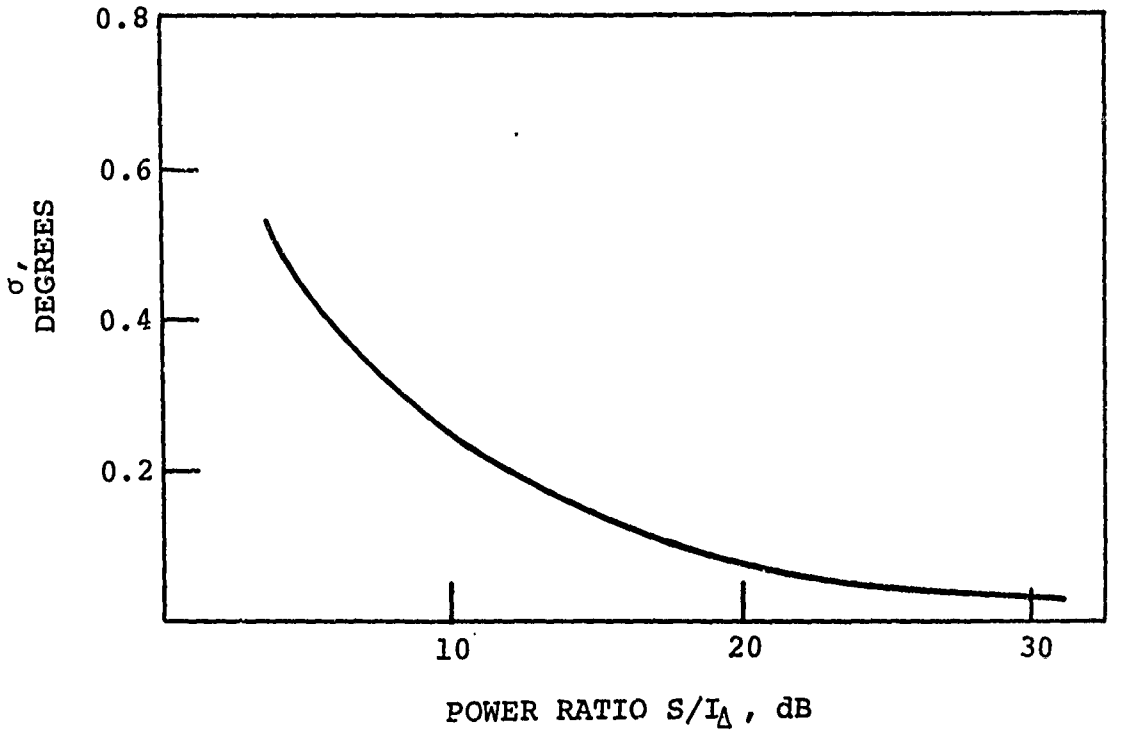

Figure 25. Single-Reply Angle Error Caused by Single Interfering Target, Not Adjacent, Plotted vs the Power Ratio of the Sum Pattern Peak to the Difference Pattern Sidelobe Level at the Interfering Target Azimuth. The modified FA 7202 antenna is assumed.

Multipath Error

Multipath error is defined as that error which arises when an echo from the desired target is received over a propagation path other than the most direct path between the target and the radar (Ref. 9). While such errors can appear in any of the four radar coordinates (azimuth, elevation, range, and range rate), only the azimuth error is of interest here. Multipath signals that cause azimuth error can arise by reflection from rough ground or sea surfaces, or by reflection from a vertical structure, such as a high-rise hotel near an airport. Generally, signal paths in arbitrary planes can arise by reflection from inclined surfaces or from rough surfaces at any angle. In the ATC beacon radar system, multipath signals can cause the appearance of false targets, such as illustrated in Figure 26 which is taken from Reference 23. However, no data is available that could serve as a measure of "graceful" degradation of beacon system accuracy due to multipath, i.e., of the magnitude of the small multipath errors that do not fall into the "catastrophic" category where a false target appears tens of miles away. In the

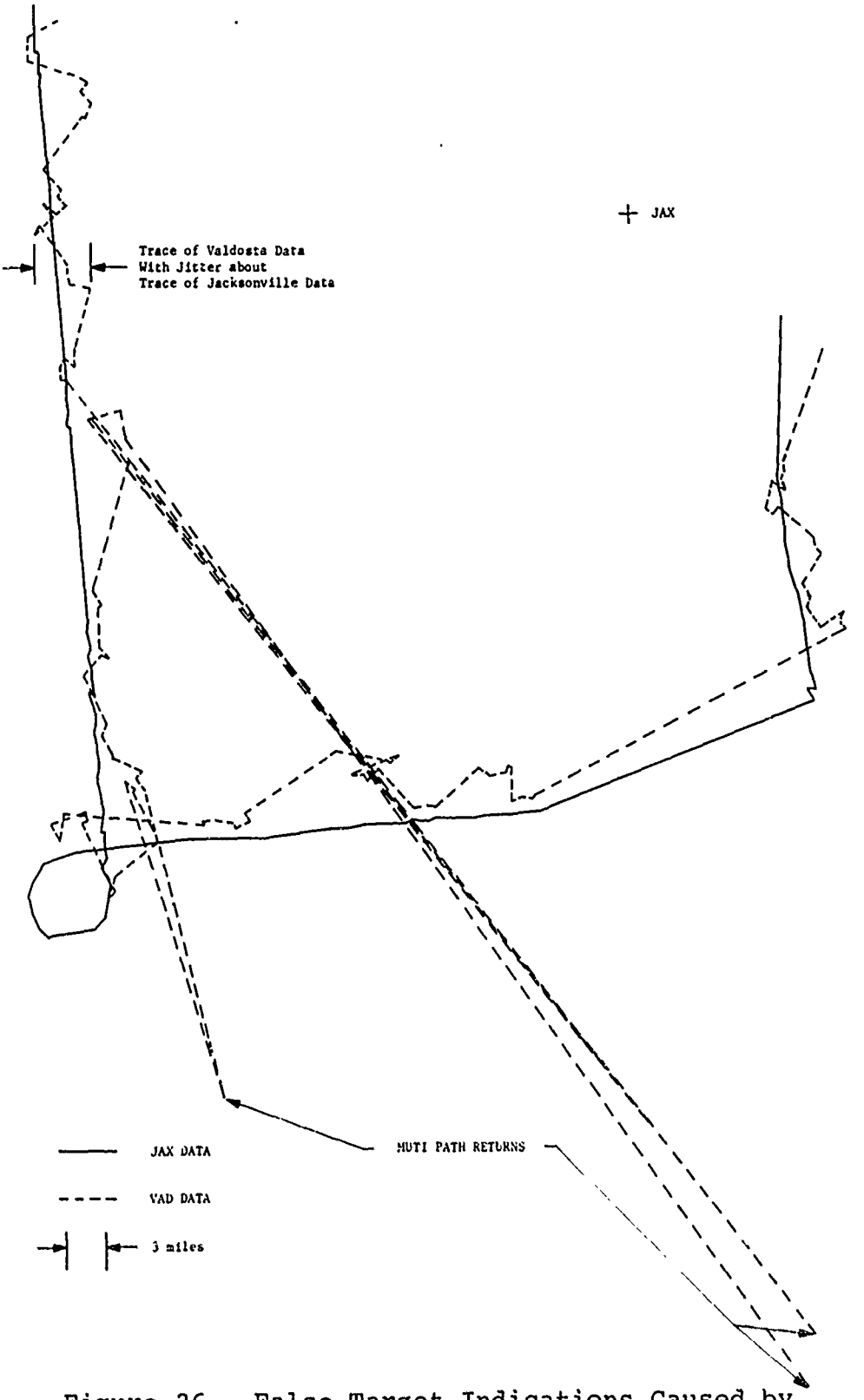

Figure 26. False Target Indications Caused by Multipath Returns (Ref. 23)

context of the monopulse error analysis, only the accuracy *degradation* due to multipath is of interest.

While pertinent field data cannot be given here, one would expect a much smaller incidence of multipath signals than of general fruit signals. However, the probability of garbling (pulse overlap) is bound to be much higher for the multipath interference because of the near equality of the path length. Depending on the site configuration, the presence of multipath garble therefore could add significantly to the general interference background and hence to the measurement error.

A detailed analysis of multipath error, valid for surface reflections, is given in Appendix F. Under quite reasonable conditions, the calculated error can be as great as σ=0.12 degrees for a target at 10 degrees elevation over wooded terrain, and clearly this error is not negligible. Multipath reflections from tall buildings are considered in Appendix G, and these are seen to cause errors on the order of σ=0.08 degrees.

Summary of Error Contributions

In this section, the typical contributions to the total error in a monopulse azimuth measurement with the beacon antenna are summarized. Signal extraction from a single beacon reply is assumed. These error components are uncorrelated and must be added in a root-sum-of-squares fashion to derive the total error. However, as the interfering target error has been derived only for an on-boresight position of the desired target, the bias error that is incurred when the desired target itself moves off-boresight will not be included in the error summation. This implies that only the on-boresight beacon replies will be used for the monopulse azimuth measurement, and the resulting error estimate therefore is slightly optimistic. The error budget then is as follows.

a. Thermal-noise error at 100 n.m. range, σ=0.013 degrees.

b. Network error
   - Phaseshift error: $\simeq$ 0.03 degrees
   - Amplitude error: $\simeq$ 0.03 degrees
   - Frequency shift error: $\simeq$ 0.01 degrees

c. Mechanical errors (with radome): negligible

d. Pattern asymmetry: see (b)

e. Off-boresight error (for target 1 degree off-boresight)
   - S/N related: negligible
   - Nonlinearity related: bias = 0.19 degrees

f. Interfering targets

Adjacent target at 3 degrees off-boresight: σ=0.44 degrees

Sidelobe targets (20 assumed): σ=0.27 degrees

g. Multipath error, due to reflections from

1. moderate sea, at elev. 18 degrees: σ=0.12 degrees
2. wooded terrain, at elev. 10 degrees: σ=0.07 degrees
3. tall structures: σ=0.8 degrees
   (derived for a single building 50 feet wide and 75 feet high, situated 1/2 mile from site)

Assumed total multipath error = 0.13 degrees.

Total random error from causes other than interfering targets:

$$\sigma \approx 0.14 \text{ degrees}$$

Total random error: $\sigma \approx 0.53$ degrees
Off-boresight bias error: $\varepsilon \approx 0.19$ degrees

From these numbers it is clear that the interference from undesired targets causes the dominant error, and that this reduces the single-reply monopulse accuracy below that of the existing ATCRBS when equipped with sliding-window target detection.

However, with the use of either ISLS or RSLS for beam sharpening, the interfering-target error would essentially be eliminated, so that the total random error would be reduced to σ=0.14 degrees, or equivalently σ=2 ACP's, based on the detection of a single reply. This represents a slight improvement over the existing system accuracy which is σ=3 ACP's, based on the detection of a complete target run.

The following remarks may serve to clarify the assumptions made for calculating the individual error components.

The thermal noise calculations are based on a perfectly omnidirectional target radiator placed at the boresight of the interrogator antenna. For less ideal conditions, i.e., with aircraft antenna nulls and with nulls in the vertical lobing pattern of the ground antenna, thermal noise error can become significant, but such conditions are not considered here.

The mechanical errors can be made negligible by appropriate design. For the existing terminal beacon antenna, windloading of the ASR sail would cause the dominant mechanical error. No windloading exists for the radome-enclosed ARSR sails that support the en route beacon antenna.

The dominant components of random error, i.e., interfering-target and multipath error, all decrease as $1/\sqrt{n}$, where n is the number of beacon replies (bracket pulse pairs) observed for the monopulse measurement. For example, if nine replies near boresight are evaluated, the total random errors become $\sigma=0.18$ degrees without beam sharpening, and $\sigma=0.05$ degrees with beam sharpening, or 2 ACP's and 1 ACP, respectively. For the en route system, 10 replies would occupy no more than an angular sector of ± 0.5 degrees near boresight, and thus the average bias error due to nonlinearity is negligible for this case. The realization of such accuracy would constitute a significant improvement over the present performance of the NAS en route system. In the terminal area, a one-degree beam sector would intercept only four replies, and the improvement would not be as great. Quite generally, it should also be remembered that the quoted monopulse accuracies are calculated estimates that are still subject to confirmation by experiment, whereas the $\sigma=3$ ACP accuracy of the existing system represents a measured quantity and is therefore more reliable.

Application to the NAS En Route System with the Common Digitizer

Ideally, a monopulse angle measurement can be made on the basis of just a single beacon reply, and the implication is that the present accuracy of azimuth measurement can thus be matched or improved upon with fewer interrogations per sweep. The error analysis of the previous sections shows this to be true only if ISLS or RSLS is used, due to the presence of interfering targets in the beacon system. The ISLS approach only involves the transmission of the P_2 pulse over the difference pattern, and no modifications to the receiver are necessary. As RSLS is based on a threshold comparison of the sum and difference channel signals, only the logic circuits to do this comparison are required to implement it (see Figure 4), because the other components are shared with the azimuth measurement function. In Figure 27 below, a straw-man modification kit has been outlined that would expand the Common Digitizer to include a monopulse azimuth capability. An RSLS mode of operation is assumed. The general approach here is to generate a vernier correction on the azimuth angle of the beam centermark, as the latter already is derived with considerable accuracy by the present Common Digitizer. Referring to Figure 27, the monopulse measurement circuitry is triggered by the RSLS threshold logic circuit. After analog-to-digital conversion, the monopulse data are stored in a buffer memory for the remainder of the target duration. When the CD centermark has been formed, the contents of the buffer memory are added to form a new, corrected centermark. All this assumes, of course, that the monopulse correction is much more accurate than the original centermark. The single-reply monopulse error is about two-thirds of the azimuth error of

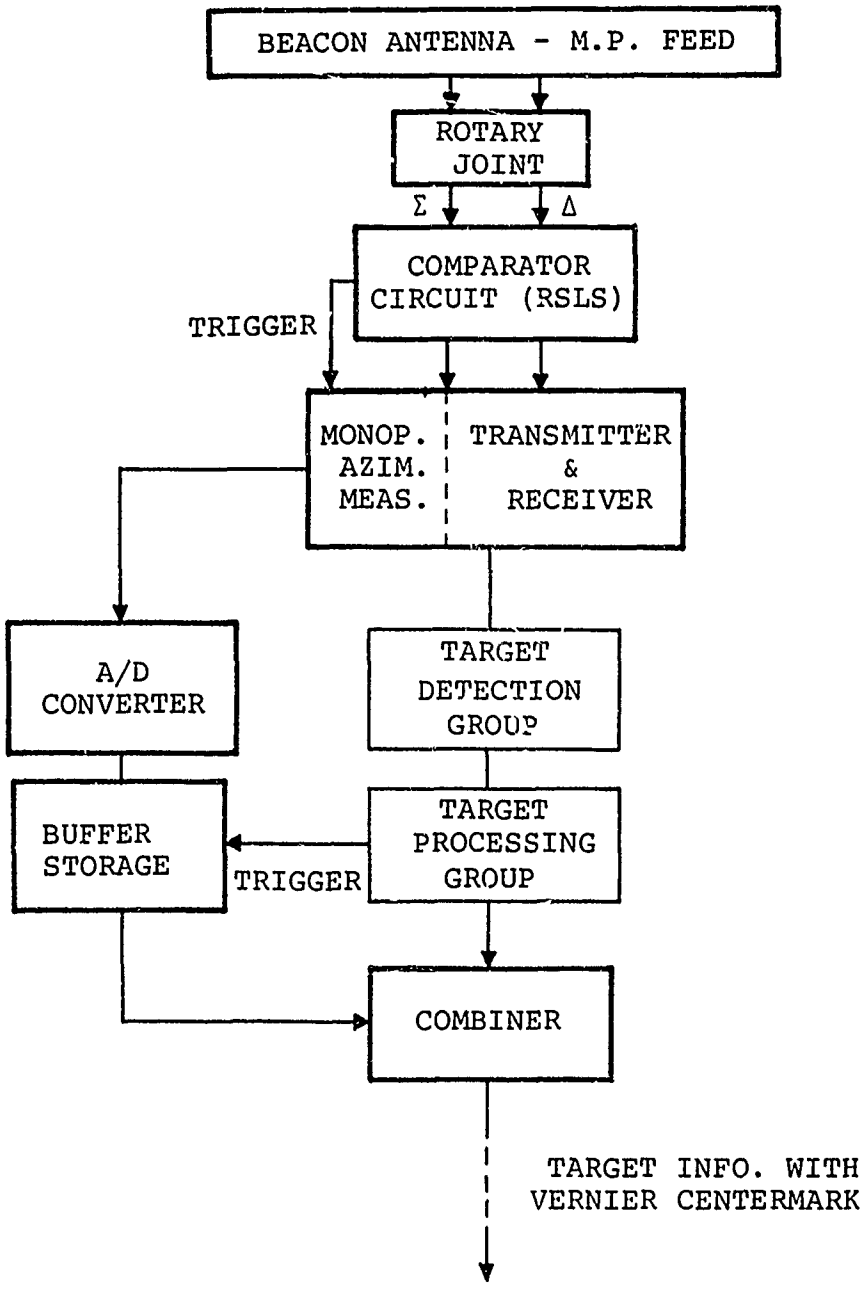

Figure 27. Monopulse Vernier Azimuth Capability Added to the Common Digitizer. The required new system components are shown with heavy lines.

the nominal CD centermark, but if the monopulse information is integrated over a series of replies, errors as small as one ACP could in principle be realized. In either case, the introduction of a monopulse measurement results in a considerable increase in system complexity and cost that may or may not be justified, depending on how great an azimuth error can be tolerated in a particular application.

Application to the En Route Manual System

It has been indicated that the addition of a monopulse feature to the NAS en route system would only bring marginal benefits because the CD already is capable of highly accurate azimuth determination. The en route manual system, on the other hand, does not now use centermarking and thus might benefit more from a monopulse capability. In effect, the function of the monopulse measurement would be to generate an accurate centermark either in conjunction with or as a substitute for the present PPI slash marks that indicate a beacon target. One possible modification of this type has been designed in detail elsewhere (Ref. 2), and the block diagram is reproduced in Figure 28. The centermark is generated by threshold logic applied to the sum and difference channel signals. That is, whenever the sum channel signal is 10-20 dB above the difference channel, depending on the target range, the beacon replies are gated to a separate video amplifier chain that is connected parallel with the usual video processor channel. An AND gate for the centermark pulses allows sharing the defruiting function of the regular defruiter. The centermark pulse trains are then bracket-decoded in a separate decoder, and the decoder output pulses are connected to a pulse stretcher that produces centermarks of controllable length. The output of the pulse stretcher goes directly to the PPI scope. Further details can be found in Reference 2.

It will be realized that the method described above is a threshold-logic approach that is subject to similar errors as the monopulse azimuth measurement. Still, as the destination of this data is not a tracking computer but only the visual display on the PPI scope, the accuracy available from reading the (approximate) centermark is probably as great as can usefully be employed for this system. It is questionable, however, whether the increased complexity and added cost of the modified system shown in Figure 28 can be justified merely by the capability of generating an approximate centermark. Certainly, the replacement of entire ATCBI-3 systems with the Common Digitizer appears to be a sounder solution technically.

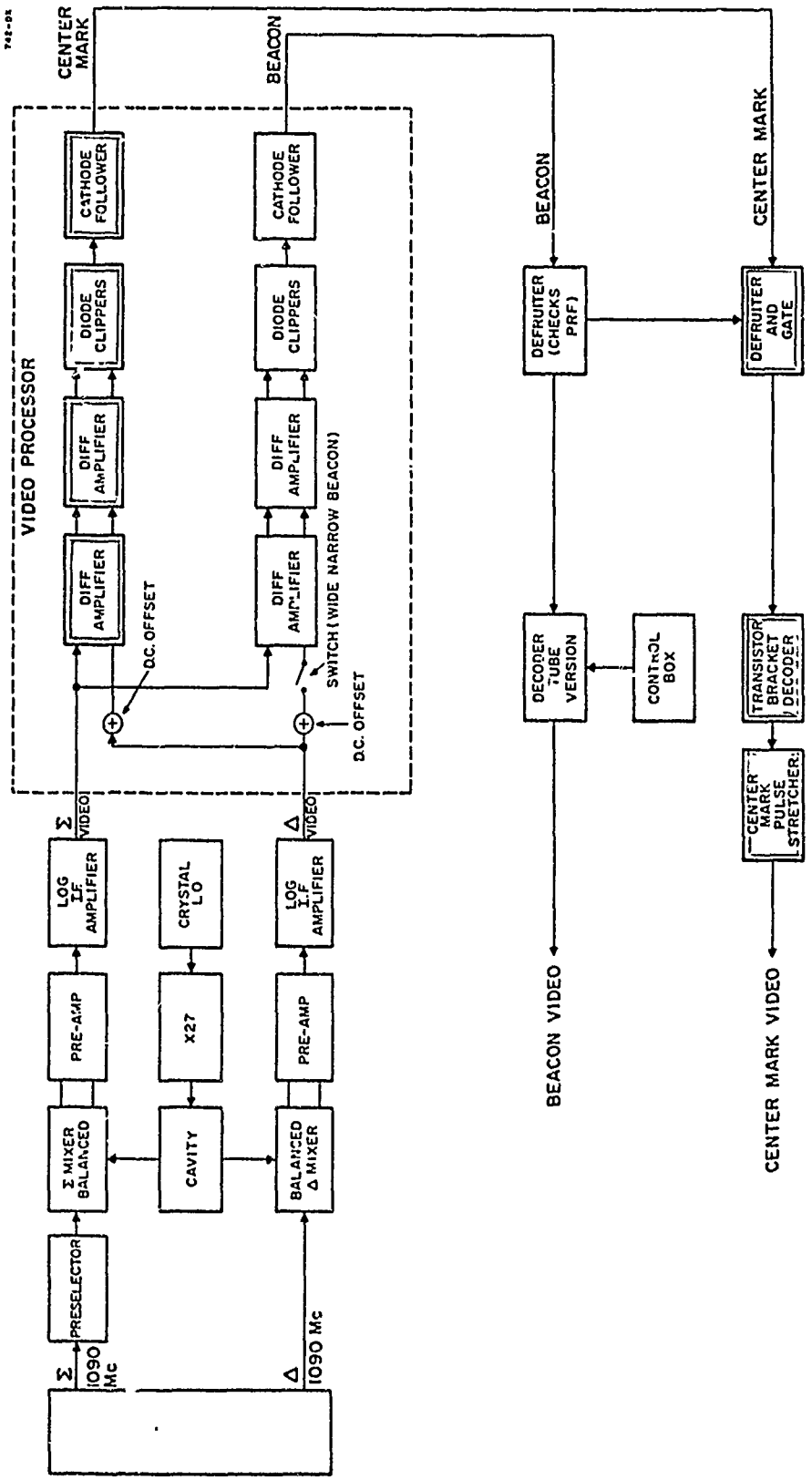

Figure 28. A Method of Generating a Centermark in the Manual Beacon System. New equipment required is shown in double lines. (Ref. 2)

CONCLUSIONS AND RECOMMENDATIONS

The purpose of this report has been to investigate the feasibility of and, implicitly, any advantages accruing from a modification of the existing ATC Radar Beacon System. The modification would consist of providing the existing antenna with a sum-difference capability by means of a new feed network and then deriving synthetic beam-narrowing and/or monopulse azimuth measurements from this pattern.

Azimuth measurement by sum-difference techniques, i.e., "monopulse," has deservedly acquired a reputation for being very accurate, based on its use in precision radar tracking applications. An application of this technique to target azimuth determination in the ATC beacon environment clearly is technically possible. However, for a number of reasons that have been discussed in this report, the accuracy in this new environment is not expected to be as good as in the single-target tracking case, unless methods of artificial beam sharpening are used. Even if such methods are used, the gain in accuracy over the present NAS en route system is marginal.

A detailed cost analysis of a monopulse option therefore becomes a rather academic exercise, because even a small improvement in accuracy would have to be bought at a considerable price in added system complexity. This has been indicated in Figures 27 and 28, in terms of the number of modified system components required. It must also be remembered that whereas in the simple broadband system standard IF amplifiers with AGC are adequate, the monopulse receivers must maintain both gain and phase tracking over a wide dynamic range, and this also adds complexity and expense.

A few remarks may be in order on the general nature of the beacon azimuth measurement, both with and without the monopulse modification. The ATCRBS is a pulse amplitude modulated system where target detection and code validation are based on purely digital signal processing techniqess using statistical methods in the more recent versions. The fact that the replies are not target echoes as in primary radar, but are beacon replies, insures essentially complete freedom from thermal noise problems, so that the received pulses can easily be clipped and shaped for subsequent decoding. On the other hand, the fact that the system is beacon based can cause a great amount of self-interference in the form of garbling of received pulse trains by overlapping replies from unwanted targets (fruit). This self-interference can be reduced greatly by eliminating redundant interrogations and redundant replies, and the residual interference can be suppressed at the receiver by digital filtering (defruiting) techniques. By statistical processing of the remaining good

replies, it is still possible to achieve very good accuracy.

In contrast to this, the monopulse measurement is inherently analog in nature. Its information is contained in terms of the received pulse amplitude, and thus it is highly sensitive to interference from the superimposed signals of undesired targets. The problem of multi-target interference is made worse by the fact that the antenna difference patterns which are the basic sensors for the monopulse error signal tend to have a high sidelobe level. Azimuth measurement by the monopulse method, though technically feasible, therefore is essentially incompatible with the present ATCRBS. However, if multi-target interference can be eliminated, such as in a roll-call mode of interrogation where each target only replies when discretely addressed, the fact that a single monopulse measurement in principle is capable of locating a target with great accuracy could be used to reduce the necessary dwell time of the antenna beam and thereby to improve the system performance.

This study has been addressed only toward a modification of the present en route surveillance system, represented by the old manual system and by NAS En Route Stage A with the Common Digitizer. The ARTS III terminal surveillance system has not been addressed explicitly, but it is not believed that its inclusion in the tradeoff would change the overall conclusions. These are as follows.

The addition of a sum-difference antenna capability is evidently feasible. The use of artificial beam narrowing that employs the SLS feature of airborne transponders in principle can be effective in reducing the fruit rate. However, other methods, such as improved interrogator management, may be adequate as well as more cost-effective. The use of a single-reply monopulse azimuth measurement in conjunction with the present ATCRBS is not expected to improve the accuracy of the existing system, unless beam sharpening is used simultaneously, and even then the improvement is marginal, with σ going from 3 Azimuth Change Pulses (ACP's) to 2 ACP's. If monopulse information from more than one beacon reply is utilized, the error in principle can be reduced to σ=1 ACP. For the NAS en route system, the corresponding estimated improvement in site accuracy may justify the increased system complexity and cost, depending on the site requirements. For the broadband (manual) system, the monopulse information could be used to generate an accurate centermark. Again, this would require a series of complex and costly system modifications, with relatively high technical risk. On the other hand, the Common Digitizer delivers known accuracy at a known price and therefore appears preferable where an improvement on the broadband system is considered.

As has been pointed out, the quoted errors for a monopulse azimuth measurement are only calculated estimates. It is recommended, therefore, that a series of measurements be made that will provide a solid data base to confirm these error estimates. These would include measurements of monopulse azimuth accuracy, both with and without beam sharpening; direct measurement of the signal-to-interference power ratio; isolation and measurement of multipath error; and measurement of the monopulse network error. Data of the effect of short run lengths on sliding-window detector performance would also be of interest. Finally, a combined analytical/experimental effort should be launched to improve the difference pattern of the 28-foot beacon antenna.

APPENDEX A

THE MANUAL BEACON SYSTEM

The beacon radar system currently being used (1971) is based on the ATC BI-3 interrogator/signal processor. The essential parts of this system are sketched in Figure A1. A brief description of the signal flow in the receive mode follows (Ref. A-1).

Incoming reply code trains, at the receiver frequency, are passed from the antenna through a diplexer to the receiver circuits of the transmitter/receiver.

Provision is made for dynamically increasing the gain of the receiver with increasing range (STC) so that the amplitude of the signals at the output of the receiver will be more nearly constant. The video output signals from the receiver are routed through the video defruiter before being sent via broadband microwave link to the indicator site, i.e., the air traffic control center. The defruiter rejects all extraneous signals (fruit) that are not synchronous with the local interrogation rate.

At the indicator site, individual pulses are reshaped to compensate for any degradation introduced by the remoting circuits, and the pulse trains are then decoded. Several decoding options are available on demand for display at individual controller positions. Generally, any reply containing two framing pulses spaced by 20.3 μsec will produce a single response, i.e., a dot for display on the controller's PPI scope. As the interrogator beam sweeps across the target, a series of 10-40 such "hits" typically will be produced, and these will combine to generate the familiar slash marks that to the controller represent a beacon target.

References

A-1. ATC Radar Beacon Interrogator, ATC BI-3, Theory of Operation, FAA Manual FR-527-1, FAA Aeronautical Center, Oklahoma City, Oklahoma, June 1970.

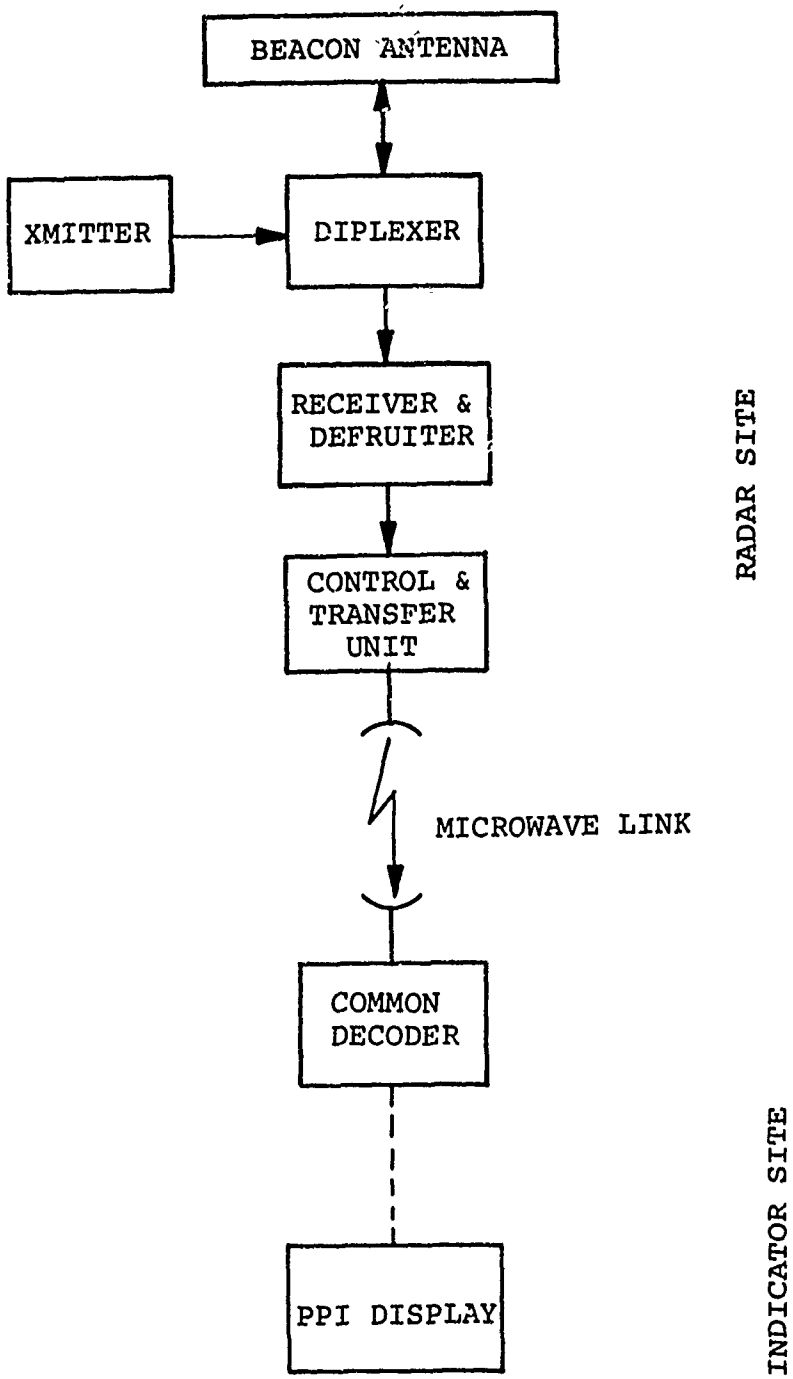

Figure A1. "Current ATCRBS" Data Acquisition and Transfer System

The purpose of this Appendix is to give a brief description of the NAS En Route System, Stage A, Model 1 and to list those performance measures and test results germane to the question of a monopulse modification for this system.

The NAS En Route Stage A program is designed to provide a large degree of automation for Air Route Traffic Control Centers (ARTCC's). The necessary hardware and software are already being installed at selected sites. A set of general performance tests that were conducted at the Jacksonville, Florida ARTCC has been described (Ref. B-1), and the results have been published (Refs. B-2, B-3).

Before addressing these test results, a brief description of the basic system is in order. The heart of the NAS en route system is the Common Digitizer (CD). This is an equipment group that carries out digital processing of the inputs it receives from the NAS surveillance radars. The Common Digitizer determines both whether a *bona fide* target exists and the range and azimuth of the target, if one is declared, with respect to the radar site. This processing is done directly at the transmitter site, which simplifies data transmission to the indicator site (control center). As all video information is converted to digital form, wideband microwave links are not required, and all data transmission takes place via modems and narrowband lines. For this reason, the CD-equipped NAS en route system is sometimes called "the narrowband system." A block diagram of the basic system is shown in Figure B1, and a functional description follows (Refs. B-4, B-5).

Incoming reply code trains at the receiver frequency are suitably amplified and passed to the *beacon reply group* which detects and processes valid reply code trains. Further reply code processing is conditional on the detection of bracket pulses by the beacon reply group.

Garble sensing logic detects when the relative positions of two replies are such that they garble each other; that is, one or more pulses of one reply appear at pulse positions of the other reply. Such replies are flagged as "garbled." Closely spaced and interleaved replies are correctly processed, however.

The pulse quantizer, which is a part of the beacon reply group, checks each code pulse for minimum width and minimum amplitude. If the pulses are below the minimum width or amplitude, they are rejected. In this manner video noise pulses are eliminated and an output of beacon video replies without noise is provided. It may be noted that in the

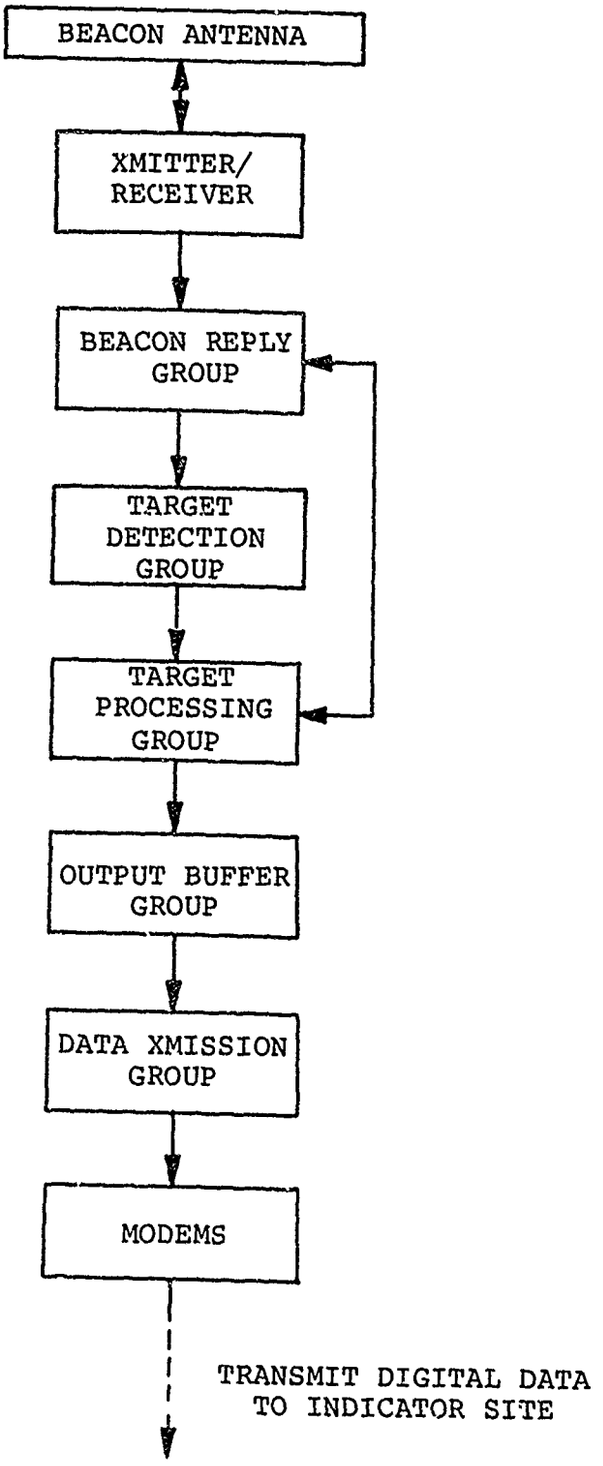

Figure B1. Received Signal Flow in the Common Digitizer

beacon system, "noise" essentially is present only in the sense of garbled pulse trains, and *not* as thermal noise or clutter. The detection process does not extract pulses from noise (as in the radar case), but merely checks for garble or distortion. The pulse train is assumed to be there once the bracket pulses have been detected, and thereafter routine decoding and garble detection is done by standard logic circuits.

The beacon reply group supplies those bracket detections containing a mode 3/A (identity) reply to the *target detection group*. Target detection is achieved by using an 11-bit, sliding-window, statistical detector that examines the beacon return history for each range cell (Ref. B-6). The technique of sliding-window detection will be examined in greater detail in Appendix C. Basically, this technique yields improved accuracy and reliability by looking at a set of recent beacon returns simultaneously rather than serially, as is done in the older broadband system. Detection is accomplished by counting the number of hits occurring in a particular range cell and comparing this hit count with various criteria to determine leading and trailing edges for a target. When the number of returns equals the leading edge threshold of a detector, the detector declares leading edge. When the number of returns decreases to the trailing edge threshold, trailing edge is declared. The leading and trailing edge thresholds are determined by internal leading and trailing edge criteria switches. The setting of these switches is done empirically for best results in any given traffic environment. When a target is declared, target azimuth and range are entered in the target processing memory.

The *target processing group* performs centermarking, run length determination and discrimination, beacon code validation, Mode C conversion and target status record keeping and control.

Centermarking (beam splitting) is the process by which the target center azimuth is determined. Run length is the angle through which the target is detected. The run length must fall between maximum and minimum limits for the information to be further processed as a target. This "run length discrimination" is an important feature that helps to eliminate false targets.

The target processing group receives beacon code replies directly from the beacon reply group, when a target has been declared by the target detection group. Beacon code replies are temporarily stored in the beacon reply group where they are checked for garbled and interfering

conditions. Upon completion of these checks, the code replies are ready for transfer to the target processing memory. A third threshold level, beacon validate threshold (B_V), is used to initiate the code reply transfer from the beacon reply group to the target processing gouup. The number of mode 3/A framing pulses contained in the sliding window is compared to a manually adjusted B_V level. When the number of framing pulses in the sliding window exceeds the B_V setting, the reply code is transferred to the target processing memory.

Code validation requires that two successive reply codes in response to the same mode from the same aircraft be identical. Therefore, when a second code is received, the first code reply is removed from the target processing memory and compared against the second code reply. If the two codes are identical, the code is replaced in memory along with the fact that it is a valid code. The reception of a valid code stops the storage and comparing of additional code replies from the particular aircraft. If the received code reply does not match the stored code reply, the code reply is said to be non-valid, and the received code reply is stored for comparison with the next received code reply. This process of storage and comparison continues until a valid code is received or target trailing edge is obtained.

When the beacon reply group detects a garbled or interfering code reply, the framing pulses are placed in the sliding window, but the code information is destroyed. Information indicating a garbled code reply is placed in the target processing memory with the target range and azimuth. From this information a beacon message is generated without code information.

Contained in the target processing memory will be leading edge azimuth, trailing edge azimuth, range, target type (beacon), code information, mode information, code validity, garbled or interfering code information and military emergency information. From this information a target message is generated.

The *output buffer group* accepts the completed target messages from the target processing group and passes them, properly formatted, to the *data transmission group* for transmission to the indicator site.

This completes the functional description of the Common Digitizer. It may be noted (Ref. B-7) that the differences between narrowband and broadband radar data are *not* with respect to accuracy. The new narrowband system can be no more accurate than the video information provided to it.

The difference between the two is in the precision with which target position is reported. The broadband video information tells the region in which the target is located, whereas the digitizer processes the video information to determine exactly where in this region the target is located to centermark the beam. That is, the digitizer uses the *target start* and *target stop* azimuth information from the detection process to declare the target location (in azimuth) to be midway between the two. Consequently, broadband and narrowband accuracy are comparable, but the narrowband data is much more precise.

In this Appendix, different performance parameters will be considered both at the controller level, with the controllers equipped with measuring rules to aid their visual observation, and at the operational program level, for the case of the narrowband (CD) system, where the target information is available in numerical form.

The Jacksonville test results to be discussed here are designated "Area C 40" where the object was to optimize the surveillance (as opposed to tracking) performance of the NAS en route system, using a number of FPS-16 precision tracking radars (see Table B1) as a standard for range and azimuth measurements. The actual data were recorded at the Jacksonville, Florida, ARTCC and were later evaluated at NAFEC, Atlantic City. Heavy emphasis was placed on optimizing the operating parameters of the Common Digitizer (CD) during the early stages of testing. The test results for individual system parameters will now be discussed. Besides material taken from References B-2 and B-3, some comments made in Ref. B-7 will be paraphrased.

SYSTEM DETECTION CAPABILITY

The number of radar returns received from a target is determined by the pulse repetition frequency of the radar, the scan rate of the antenna, and the effective beamwidth of the antenna. Given this information for a specific radar, it is possible to determine the number of returns that the CD should look for to declare a target. However, the process is complicated by the fact that not every pulse transmitted by the radar produces a countable return for the CD. This is due to radar propagation anomalies, mode interlace on beacon radar, and the unstable behavior of aircraft as radar targets.

For target detection, the CD first sorts out radar returns in range bins. The size of the bins is 1/2nm or 1/4nm,

TABLE B1. PERFORMANCE SUMMARY FOR
FPS-16 PRECISION TRACKING RADAR (REF. B-1)

Technical Description: C-band monopulse precision tracking radar, either skin or beacon mode of operation.

Data Output: Range, elevation and azimuth from potentiometers and synchros and digital encoders.

Display at Operator's Console: Dual A-scope monitor
Repeater dial
Digital output

Performance Data

Azimuth: Continuous 360°

Elevation: -10° to +85°; 200° modification available

Digital Output: Up to 100 samples/sec

Dynamic Tracking Accuracy: Azimuth and elevation: 0.10 to 0.4 mils rms, depending on signal-to-noise
Slant range: 5 to 6 yd rms

Tracking Rates: Range - Up to 10,000 yd/sec on six radars
Up to 20,000 yd/sec on two radars

Azimuth - Up to 40°/sec

Elevation - Up to 30°/sec

Antenna: Five radars with 12-ft parabolic, gain 44.5dB, beamwidth 1.1° dumpable
Three radars with 16-ft parabolic, gain 46.5dB, beamwidth 0.82°

Transmitter power: 1 MW, fixed frequency, 250 kW tunable
PRF 320 to 1707 pps (200-NM radar)
PRF 160 to 1346 pps (500-NM radar)
PRF 80 to 1707 pps (1000-NM radar)
PRF 80 to 1707 pps (infinite-mile radar)

Pulse Width: 0.25, 0.5 and 1.0 μsec

depending upon the radar pulse width. The *width* of the range bin that the CD inspects for radar returns at any given time is 11-17 pulse repetition periods for primary radar and 11 pulse repetition periods for secondary (beacon) radar. A count is maintained of the number of "hits" found in this "window." When the number of hits *equals* or *exceeds* a threshold value, a target start azimuth is declared.

It should be noted that the CD must process targets within the same range cell sequentially. That is, it must complete the detection process on one target before it can begin detection on another. This will have some bearing on target spacing in the narrowband system just as it does in the broadband (manual) system.

Since the narrowband system performs additional processing on video information that the broadband system simply displays, it can be expected that there will be some differences in the detection characteristics of the two systems. The narrowband system attempts to eliminate noise and clutter returns from the broadband video while maintaining a comparable probability of detection on *bona fide* targets.

Indeed, from the measured statistics given in Reference B-2, Section 4, the probability of beacon detection turns out to be about the same for the (old) broadband system and the (CD) narrowband system, with average, clear-weather blip/scan ratios of 0.97 and 0.96, respectively. (No fruit count was made.) These numbers correspond to single-site observations, and by using the NAS Stage A Operational Program to switch between the outputs from more than one site, the system blip/scan ratio can be expected to increase further. However, it was not actually possible to demonstrate such improvement during the tests, due to various system imperfections, i.e., "bugs." The practice in NAS Stage A of deriving a given target track by automatically switching between simultaneous inputs from different sensors also creates other problems such as registration errors. These will be discussed in later paragraphs.

SYSTEM POSITION ACCURACY

The system position accuracy is concerned with a mapping measurement, i.e., the establishment of the true geographical target position. The system position error is a composite error. By direct comparison of the CD data produced at each beacon radar site with data from the FPS-16 precision radar, the beacon subsystem azimuth error component was found to be $\sigma = 3$ ACP's. As the system tracking logic utilizes two types

of data (beacon and primary radar) from a number of radar sites (preferred and supplementary), errors in target position also arise as a result of an occasional exchange of data type (collimation errors) and of data source (registration and site location errors). Total system accuracy was not actually measured because of problems that were found to exist with the individual sites. However, the mean collimation error is estimated to be 2 ACP's. Site registration errors are intended to be cancelled automatically by the real time quality control (RTQC) function of the operational program. The efficacy of this mechanism could not be tested either, however, so that no data are available on what residual site registration error remains after cancellation (Ref. B-2, Section 4.5.2.4).

SYSTEM RESOLUTION

Resolution is a measure of the CD's ability to detect and properly position closely spaced targets. For the C-40 tests, two measures of resolution were defined:

1. The distance between two proximate aircraft when the separation between the aircraft can no longer be determined by the operational program.

2. The distance between two proximate aircraft when the separation between the aircraft can no longer be determined from the display.

An instructive discussion of the problem of resolution in general is contained in Reference B-7, as follows:

> "(Fig. B-2) depicts three pairs of targets that can be used in illustrating the concept of resolution in the CD. All three pairs of targets are separated by the same distance. Recalling the manner in which the CD detects and positions targets, it can be seen that the targets at "A" will probably turn up in the same range cell and likewise for the targets at "B". Conversely, the targets at "C" will be in different range cells. The angular region θ is intended to represent the azimuthal separation required between targets in order for the CD to differentiate between targets that are in the same range cell (about 1° for search and 10° for beacon). The limiting factor here is the beam structure associated with the surveillance radar. The beam width will determine how many "hits" are received from a target. This is important for targets in the same range cell, since the

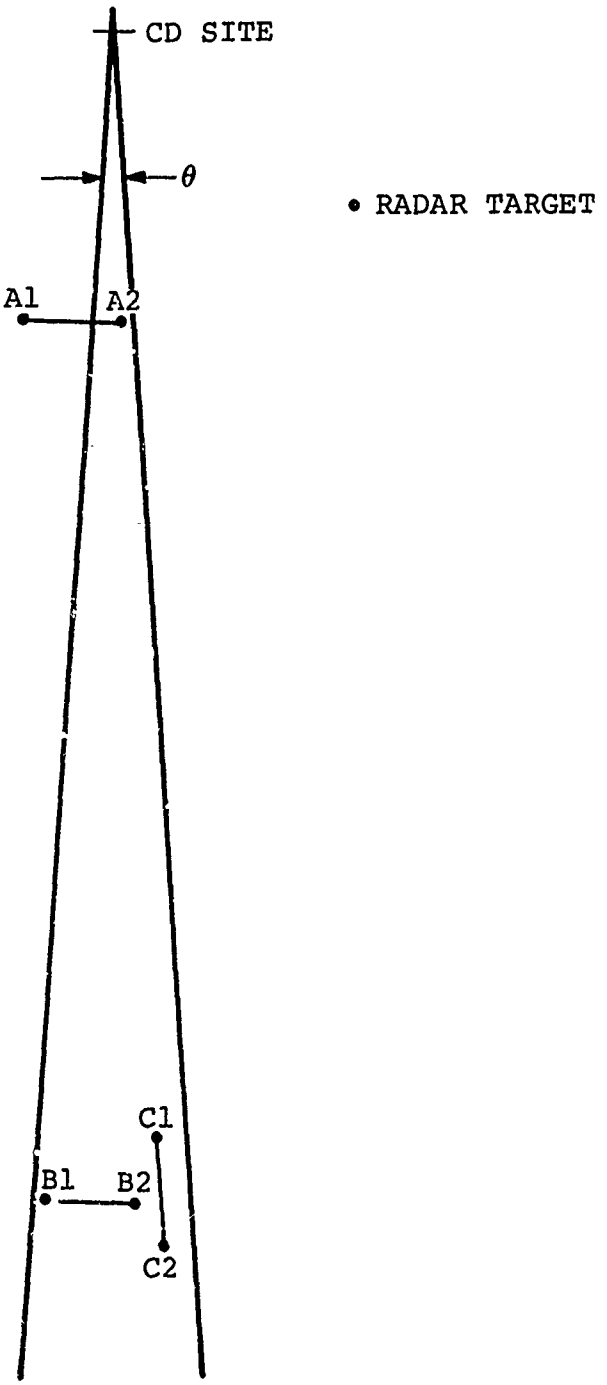

Figure B2. Target Orientation Considerations In Resolution (Ref. B-7)

CD must process "hits" from one target before it is ready to process "hits" from a second target. For example (see Figure B-2), the CD would be finished processing "hits" from A2 before it would have to process "hits" from A1. On the other hand, the CD would be getting "hits" from B2, then B1 and B2 simultaneously, and then B1, resulting in a continuous and extended run of "hits" in the same range cell from B1 and B2. The "hits" from C1 and C2 would also be overlapping in arrival time at the CD, but they would be sorted into different range bins and would not pose a target processing problem in the CD. Of the three cases considered, then, only the "B" case poses a problem with respect to separating aircraft in the CD....In the presence of a resolution problem ...the narrowband receiver declares a single target. The video information from the broadband receiver provides no clear definition of where one target ends and the other begins...."

Resolution was measured by comparing the indicated separation distance with the separation distance obtained from the FPS-16 precision radars, for both the operational program and the observer displays. Range and azimuth separations are not differentiated. The results are shown in Figures B3 and B4. Typical errors appear to be 0.5nm for the operational program, and 1.0nm for the observers; i.e., the use of the display system in effect doubles the resolution error that exists at the output of the operational program. No significant differences were noted between the resolution performance of the NAS Stage A Model 1 system and the broadband (manual) system at the observer level.

SUMMARY

In this Appendix, a functional description has been given of the Common Digitizer (CD) equipment group which forms the heart of the NAS En Route Stage A, Model 1, radar beacon system. Some results of early operational tests have been summarized. While considerable "debugging" of this system clearly is still required before firm performance data can be stated, the following conclusions have already emerged.

On the basis of clear-weather tests, the beacon target detection probability is about the same for the CD as it is for the broadband (manual) system. The target separation error, referenced to the FPS-16 precision tracking radar, is of the order of 1nm, as seen by the controller, and this is

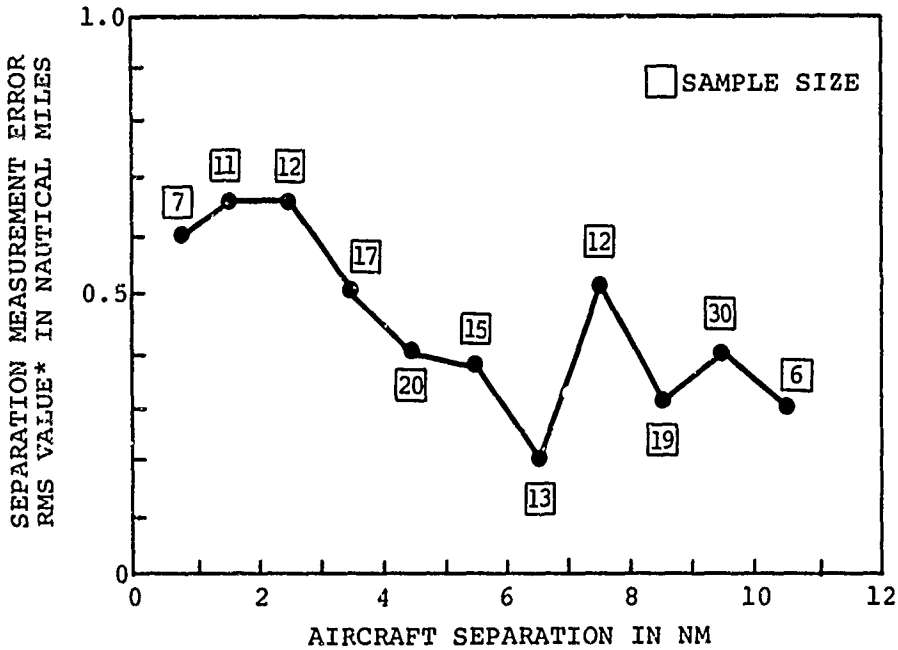

* RMS VALUE OVER THE INDICATED ONE NM INCREMENT

$$\text{RMS ERROR} = \left\{ \frac{1}{\eta} \left(\varepsilon_1^2 + \varepsilon_2^2 + \cdots \varepsilon_\eta^2 \right) \right\}^{\frac{1}{2}} \left[\bar{\varepsilon}^2 + \sigma^2 \right]^{\frac{1}{2}}$$

$\varepsilon_1, \varepsilon_2 \cdots \varepsilon_\eta$ = SEPARATION MEASUREMENT ERRORS

$\bar{\varepsilon}$ = MEAN ERROR

σ = STANDARD DEVIATION

Figure B3. Separation Measurement Errors for NAS Operational Program Data vs FPS-16 Radar Data

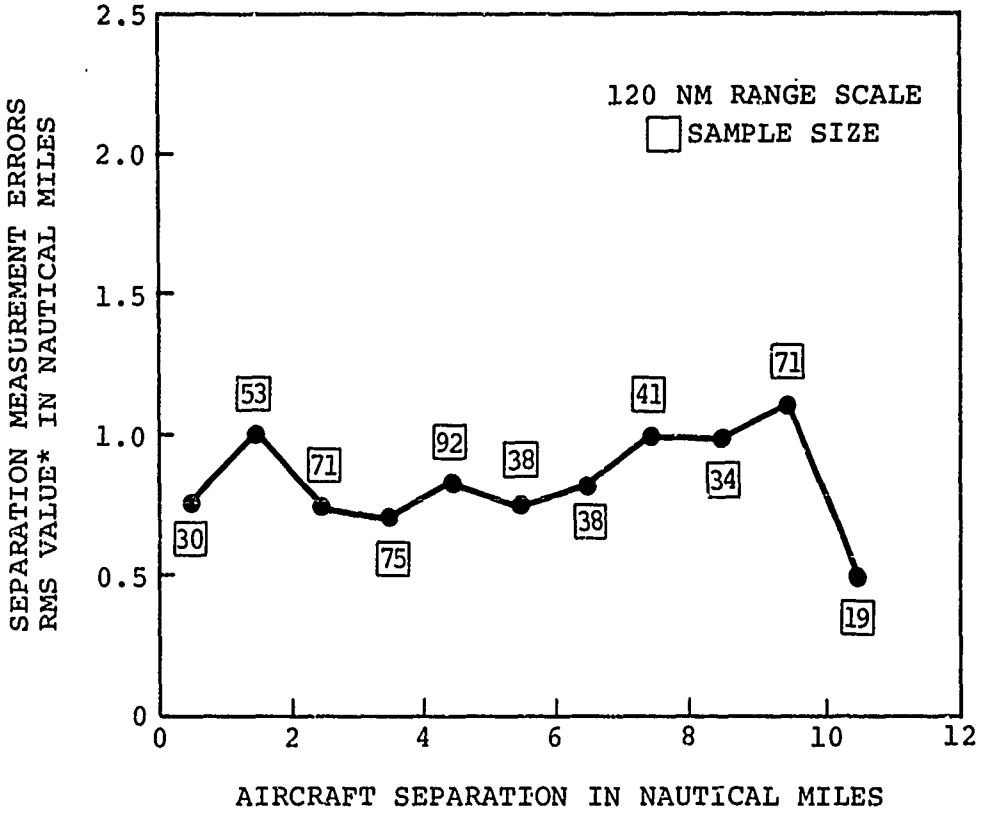

* RMS VALUE OVER THE INDICATED ONE NM INCREMENT

$$\text{RMS ERROR} = \left\{ \frac{1}{\eta} \left(\varepsilon_1^2 + \varepsilon_2^2 + \cdots \varepsilon_\eta^2 \right) \right\}^{\frac{1}{2}} = \left[\bar{\varepsilon}^2 + \sigma^2 \right]^{\frac{1}{2}}$$

$\varepsilon_1, \varepsilon_2 \cdots \varepsilon_\eta$ = SEPARATION MEASUREMENT ERRORS

$\bar{\varepsilon}$ = MEAN ERROR

σ = STANDARD DEVIATION

Figure B4. Separation Measurement Errors for Controllers vs FPS-16

a measure of the system resolution as well. Again, no significant differences were noted between the resolution performance of the manual and the automatic (CD) system. The total system position accuracy was not measured, but two important components of the position error were. These are the beacon subsystem error (σ = 3 ACP's) and the collimation error (σ = 2 ACP's). The residual site registration error was not measured. The beacon subsystem and collimation errors together are of the same order of magnitude as the 0.25-0.4-degree azimuth accuracy quoted in the ATCAC Report for the manual system if centermarking were used. If the automatic cancellation of site registration errors within the CD can be made to operate as intended, then the total system accuracy will be within these limits as well.

References

B-1. System Shakedown, NAS En Route Stage A, Model 1, Surveillance Optimization, Areas C40/C50, Test Specifications; Report NTR-1208, The MITRE Corp., Atlantic City, New Jersey, Nov. 1968.

B-2. C40 Final Test Report, MTR 4414, The MITRE Corp., Washington, DC, March 23, 1970.

B-3. C50 Final Test Report, MTR 4415, The MITRE Corp., Washington, DC, April 8, 1970.

B-4. System Description, National Airspace System, En Route Stage A, Report SPO-109, DOT/FAA, Washington, DC, Part II, Chapter I, May 1968.

B-5. Introduction to the Common Digitizer, (AN/FYQ 47, 49) Manual FRD-410, Vol. 2, pp. 3-23ff, FAA Aeronautical Center, Oklahoma City, Oklahoma, March 1970.

B-6. AN/FYQ 47, 48, 49 Common Digitizer, Report No. D-774A, Burroughs Corporation, July 1968.

B-7. E. P. Carrigan, Final Report on System Errors Related to Separation Standards for NAS Stage A, Model 1 (TOS, No. 19) MTR No. 4417, The MITRE Corp., Washington, DC, April 8, 1970.

B-8. E. P. Carrigan, Preliminary Analysis of NAS Stage A Model 1 System Errors Relating to Separation Standards, MTR No. 4407, The MITRE Corp., Washington, DC, 1 December 1969.

APPENDIX C

SLIDING-WINDOW TARGET DETECTION

The class of binary statistical detectors, of which the sliding-window detector represe a special case, is discussed thoroughly in Reference C-1, and no attempt will be made here to deal with the formidable body of literature on automatic-detection theory that has sprung up during the 1960's. However, a recent paper by Weinstein (Ref. C-2) is directly addressed to target detection in the beacon system, and this paper will be drawn upon directly.

In the sliding-window detector, the "window" is a sequence of n consecutive observations, with the oldest observation being dropped when a new one is obtained. An observation consists of a binary 1 or 0 depending on whether or not a valid reply to a given interrogation has been received. A typical sample thus may look like this - (000100111111) - which one might intuitively recognize as the beginning of a target indication. Actually, definite statistical criteria can be established for determining the leading and the trailing edge of a beacon target. Following the target end, the center-mark is determined by averaging the leading and the trailing edge positions and adding a bias which is a function of the target detection parameters.

The most important measures of target detector performance are the false alarm rate, the probability of detection, and the azimuth accuracy. These characteristics are intimately related in a manner best illustrated by Figure C1. Of particular interest here is the common dependence on the detection criteria, i.e., the method of weighting target hits in counting toward a threshold and the setting of the threshold itself. For example, there is a tradeoff between false alarm rate and azimuth accuracy, as raising the leading-edge threshold will decrease both characteristics at the same time. For the purpose of this report, the most important implication of the close interrelationship between the azimuth accuracy and the other parameters of the detection process is that with a sliding-window detector, the run length (number of target observations per sweep) cannot be reduced arbitrarily without degrading the detector performance. Any form of synthetic beam narrowing, either on transmit or on receive, will of course reduce the number of replies per sweep. The improvement in the accuracy of determining target azimuth with a monopulse measurement over a reduced number of hits, may well be lost again by the adverse effect of a reduced run length on the detector performance.

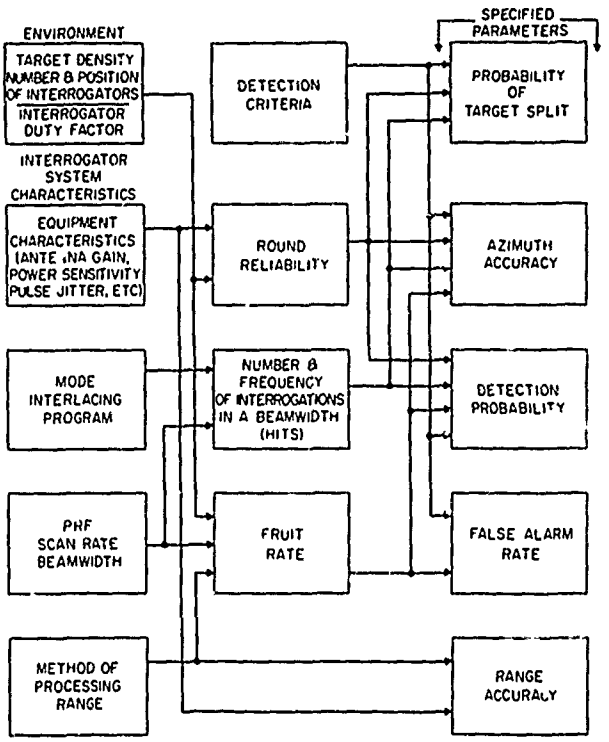

Figure C1. Interrelationship of Parameters for Sliding-Window Detection in the Beacon System (Ref. C-2)

References

C-1. J. W. Caspers, Automatic-Detection Theory, in Radar Handbook, M. Skolnik, ed., McGraw-Hill, New York, NY, ch. 15, 1970.

C-2. S. M. Weinstein, Beacon Target Processing for Air Traffic Control, Proc. IEEE, Vol. 58, pp. 408-412, March 1970.

APPENDIX D

DESIGN AND ANALYSIS OF MONOPULSE PRIMARY RADAR SYSTEMS

INTRODUCTION

Historically, monopulse techniques were first developed during World War II in order to meet the need for more accurate tracking of primary radar targets. The earlier method of target tracking by sequential lobing was essentially a beam-switching technique and as such was subject to accuracy degradation because of target scintillation, i.e., random, rapid changes in the radar cross section of the target. Because the monopulse method made use of the signals from several beams simultaneously, target scintillation was no longer a problem.

Modern radar trackers still are based on the monopulse principle, and the large body of literature that has been generated on the subject is dominated by primary radar tracking applications where the radar is continually focussed upon the target, and the error signal is employed in a feedback loop to move the beam and keep the target near boresight. The radar target-tracking problem is characterized by

1. Uncooperative targets

2. Low signal-to-noise levels

3. On-boresight targets

Under these conditions, receiver noise is the limiting factor in estimating the angle of arrival, and intricate signal processing schemes are required to extract the signal parameters from the noise background.

The problem of estimating the angle of arrival of a beacon signal in the context of the air traffic control environment is markedly different. The signal-to-noise ratio here generally is large, so that the impact of receiver noise is negligible, and the angle of arrival of an isolated target thus can be estimated to a very high degree of accuracy. However, the large return signal strengths also have the disadvantage that interference from other targets and multipath phenomena become more important.

Nevertheless, certain results from the analysis of the tracking radar case carry over to the beacon case, and it is the purpose of this Appendix to give a brief survey of some important papers on the subject of monopulse tracking radars.

A BRIEF LITERATURE SURVEY OF MONOPULSE TRACKING RADARS

No discussion of monopulse techniques is complete without a reference to the classic monograph by Rhodes (Ref. D-1) which

summarizes the early work in the field.

One of the first works dealing with the accuracy of radar measurements in general is that of Manasse (Ref. D-2), where it is shown that the achievable accuracy with which the angle of arrival of a signal can be estimated is a function of the antenna aperture size and the signal-to-noise ratio. Manasse assumed that the received waveform contained the desired signal corrupted by additive white noise and employed the method of maximum likelihood to derive the optimum estimate for angular location. For on-boresight targets, the minimum angular error is equal to

$$\sigma_{\hat{\theta}} = \left| \frac{\lambda}{\mathfrak{L}\sqrt{R_o}} \right| \qquad \text{(D.1)}$$

where

$\sigma_{\hat{\theta}}$ is the rms error in estimating the azimuth angle of arrival, θ.

λ is the wavelength of the received signal.

R_o is the peak signal-to-noise energy ratio available at the output of a matched filter. This parameter characterizes the detectability of the signal.

$\mathfrak{L}$ is the rms length of the aperture.

For a rectangular aperture of length L, $\mathfrak{L}$ is given by $\mathfrak{L}=\pi L/\sqrt{3}$, and the optimum angular error equals

$$\sigma_{\hat{\theta}} = \frac{0.73\lambda}{\sqrt{R_o}\, L}$$

Kirkpatrick (Ref. D-3) had shown previously that in order to maximize monopulse accuracy the sum channel must have uniform illumination, and the difference channel must have a linear-odd illumination function.

The subject of monopulse accuracy in the search mode has been discussed by Sharenson (Ref. D-4) for amplitude monopulse. In this work he focussed attention on off-axis targets and derived relations for the mean and the variance of the angle estimate. His analysis showed that the resulting estimate was unbiased, and that its variance increased as the target moved off boresight.

Sharenson considered the case of a strong signal return (SNR > 12 dB), and he assumed Gaussian receiver noise to be present in the sum and difference channels. He defined an

expression for the error voltage

$$V = \frac{\Delta + n_1}{\Sigma + n_2} \tag{D.2}$$

where n_1 and n_2 are the in-phase components of the noise voltage in channels one and two, respectively. These terms are completely characterized by a variance σ^2, and a correlation ρ between the sum and difference channels.

Sharenson expanded the above expression and neglected second order terms, as justified by the high S/N ratio. Then, by assuming a linear monopulse error curve and employing an approximate relation between the slope and half-power beamwidth, θ_3, he obtained the following expression for the mean and the variance of the measured variable $\hat{\theta}$,

$$\begin{cases} E[\hat{\theta}] = \theta, \text{ the true angle} \\ \sigma_{\hat{\theta}} = \dfrac{\theta_3}{2\sqrt{2S/N}} \left[L_\theta \left(1 + \dfrac{4\theta^2}{\theta_3{}^2} \right) \right]^{1/2} \end{cases} \tag{D.3}$$

where L_θ accounts for the reduced signal from the offset target.

These equations specify the tracking performance of the monopulse radar in terms of the beamwidth, the signal-to-noise ratio, and the off-boresight angle.

Berger (Ref. D-5) later refined the above results by employing a more accurate value for the error slope. He assumed that the antenna pattern was composed of two pencil beams which were described by either Gaussian or sin x/x shapes. For example, for the case of the Gaussian beam the exact value of the error slope at the origin is $C = 1.19/\theta_3$. The modified equations are

$$E(\hat{\theta}) = \theta$$

$$\sigma_{\hat{\theta}} = \frac{0.84\theta_3}{\sqrt{S/N}} \sqrt{L_\theta \left(1 + 1.41 \frac{\theta^2}{\theta_3{}^2} \right)} \tag{D.4}$$

The previous papers dealt with the question of angular estimation accuracy where the processing scheme consists of simple sum and difference channel comparison. Several recent publications have also considered the more general problem of parameter estimation accuracy where the processing scheme is arbitrary, but where the measurements are still obtained as before from an amplitude comparison monopulse radar. These studies employed a generalized likelihood ratio function, which was maximized to give the optimum estimation strategy.

Explicit expressions for this strategy have been derived for a number of special cases, and the resulting bias error and variance of the estimate have been computed. Among the efforts in this area are the works by Hofstetter and Delong (Ref. D-6), Urkowitz (Ref. D-7), Mosca (Ref. D-8), and McGinn (Ref. D-9).

Regardless of the method of parameter estimation, the accuracy of monopulse angle measurement depends strongly on the antenna patterns from which the sum and difference signals are derived. The optimum design of these patterns will be discussed next.

OPTIMUM DESIGN OF MONOPULSE ANTENNAS

A number of different criteria for optimizing the design of (amplitude) monopulse antennas have been suggested. Kinsey (Ref. D-10) has defined two possible figures of merit, as follows.

First, the *angular sensitivity* of a monopulse antenna is characterized by the slope of the difference pattern at boresight, $\Delta'(o)$, normalized by the maximum theoretical angular sensitivity.

Second, the *difference mode gain* of the difference pattern is defined as the maximum gain of the difference pattern, normalized by the maximum theoretical gain. This theoretical limit is achieved using a uniform, equiphased illumination (Ref. D-11).

Of these two performance criteria, the angular sensitivity provides the more sensitive indicator of antenna performance for the tapered aperture illuminations encountered in practice.

The angular sensitivity can be readily determined from the measured antenna characteristics of the sum pattern gain, the normalized sensitivity, and the aperture size. For beacon tracking this figure of merit is (Ref. D-10)

$$20 \log \frac{K}{K_o} = 20 \log \frac{K/\sqrt{G}}{K_o/\sqrt{G_o}} + 10 \log \frac{G}{G_o} \qquad \text{(D.5)}$$

where

$K/\sqrt{G}$ is the normalized angular sensitivity obtained from the sum and difference patterns.

G/G_o is the antenna gain factor.

K_o/G_o is a system parameter (equal to $1/\sqrt{3}$ for a rectangular aperture).

A different design criterion has been suggested by Rhodes (Ref. D-1), i.e., the *slope-sum product* at boresight, $\Delta'(o)\Sigma(o)$. This criterion of optimality is preferred because maximizing the slope alone does not insure a strong return. Indeed, maximizing the on-boresight sensitivity, $\Delta'(o)/\Sigma(o)$, leads to the following dilemma. As the squint angle increases, the slope factor $\Delta'(o)$ increases, but $\Sigma(o)$ decreases at a greater rate. Their ratio is therefore a monotonically increasing function which has no maximum within the main beam. On the other hand, since the strength of the received signal is proportional to the sum pattern gain, a logical optimality criterion is the product of the two functions, $\Delta'(o)\Sigma(o)$. Rhodes (Ref. D-1) also showed that choosing the squint angle as half the 3dB beamwidth maximizes the slope-sum product $\Delta'(o)\Sigma(o)$.

References

D-1. D. R. Rhodes, Introduction to Monopulse, McGraw Hill, New York, 1959.

D-2. R. Manasse, "Summary of Maximum Theoretical Accuracy of Radar Measurements," Mitre Report SR-11, April 1960.

D-3. G. M. Kirkpatrick, "Aperture Illuminations for Radar Angle of Arrival Measurements," IRE Trans. on Aeronautical & Navigational Electronics, vol. AE-9, pp. 20-27, Sept. 1953.

D-4. S. Sharenson, "Angle Estimation Accuracy with a Monopulse Radar in the Search Mode," IRE Transactions on Aerospace & Navigational Electronics", vol. ANE-9, pp. 175-179, Sept. 1962.

D-5. H. Berger, "Angular Accuracy of Amplitude Monopulse Off-Boresight Radar," Proc. IEEE Trans. Information Theory, vol. IT-17, pp. 411-412, March 1971.

D-6. E. Hofstetter and D. F. Delong, Jr., "Detection and Parameter Estimation in an Amplitude-Comparison Monopulse Radar," IEEE Trans. Information Theory, vol. IT-15, Jan. 1969, pp. 22-30.

D-7. H. Urkowitz, "The Accuracy of Maximum Likelihood Angle Estimates in Radar & Sonar," IEEE Trans. on Military Electronics, pp. 39-45, Jan. 1964.

D-8. E. Mosca, "Angle Estimation in Amplitude Comparison Monopulse Systems," IEEE Trans. Aerospace & Electronic Systems, vol. AES-5, March 1969, pp. 208-212.

D-9. J. W. McGinn, Jr., "Thermal Noise in Amplitude Comparison Monopulse Systems," IEEE Trans. Aerospace & Electronic Systems, vol. AES-2, Sept. 1966, pp. 550-556.

D-10. R. R. Kinsey, "Monopulse Difference Slope and Gain Standards," IRE Trans. on Antennas & Propagation, vol. AP-10, pp. 545-546, May 1962.

D-11. P. W. Hannan, "Maximum Gain in Monopulse Difference Mode," IRE Trans. on Antennas and Propagation, vol. AP-9, pp. 314-315, May 1961.

APPENDIX E

BORESIGHT SHIFT DUE TO RF AND IF PHASE ERRORS

An important source of error in a monopulse azimuth measurement is the difference in phaseshift that arises, for various reasons, between IF signals from the right-hand and left-hand lobe of the difference pattern, and between the sum and difference channels after passage through the hybrid network. These phase errors carry through to the multiplicative detector and are there combined to yield an overall boresight error. An analysis of this effect has been carried out in Reference E-1 for a four-feed, amplitude monopulse tracking system, and this analysis will be paraphrased and expanded below.

The effect of phase errors on the tracking boresight will be analyzed in the azimuth plane only. The error detector multiplies the sum and difference signals appearing at the output of the IF amplifiers. These signals are originally derived in azimuth by Hybrid 1 of Figure E1. This hybrid takes the sum and difference of the signals from the left and right half of the monopulse feed. The signals will be in phase, but their amplitudes will vary as the antenna azimuth pointing angle ϕ_o moves through the target, such that they are equal when ϕ_o is equal to the target angle ϕ_t. Assuming the error curve can be considered linear in the region where $(\phi_o - \phi_t)$ is small, the signals in the left pair of feeds, e_L, and the right pair of feeds, e_R, can be described

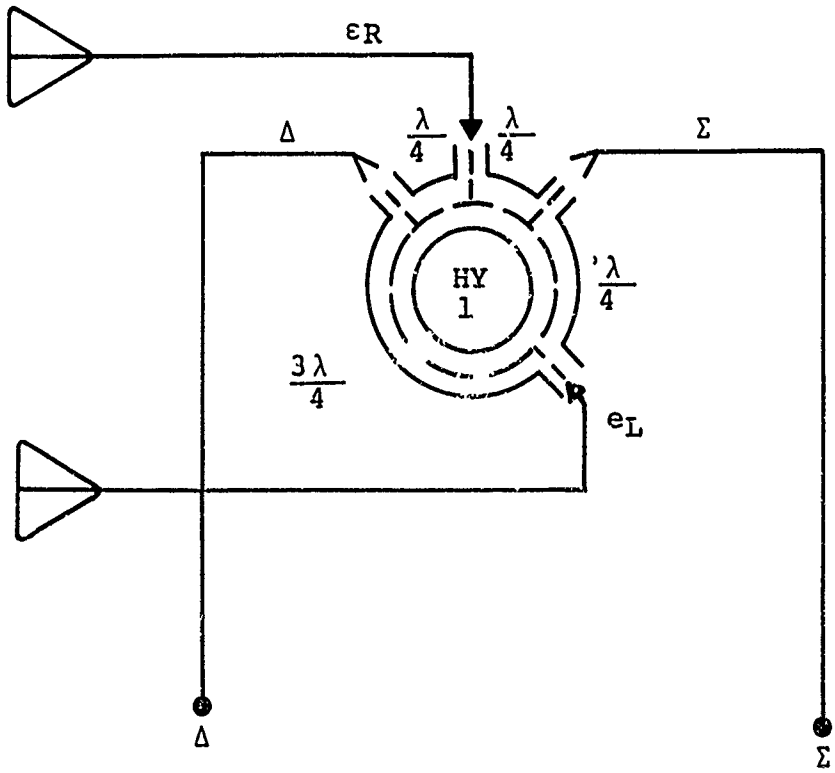

Figure E1. Hybrid Bridge Circuit for Tracking Feed

by the functions:

$$e_L = A[1 - K(\phi_o - \phi_t)]\cos\omega t \qquad (E.1)$$

$$e_R = A[1 + K(\phi_o - \phi_t)]\cos\omega t \qquad (E.2)$$

where A is the signal amplitude of the feed pairs when the antenna is on target, ω is the RF frequency, and K is an antenna gain constant. For the case where the feeds are spaced a beamwidth apart, K is equal to the reciprocal of the antenna beamwidth.

First, the effect of a phase error τ added to the argument of e_L will be considered. This represents a phase error occurring before the difference network. Also, for simplicity, ϕ_t will be set to zero so that when ϕ_o is zero, the antenna is pointing at the target. Hybrid 1 has a sum output e_S and a difference output e_D which represent the sum and difference of e_L and e_R such that:

$$e_S = A(1+K\phi_o)\cos\omega t + A(1-K\phi_o)\cos(\omega t+\tau) \qquad (E.3)$$

$$e_D = A(1+K\phi_o)\cos\omega t - A(1-K\phi_o)\cos(\omega t+\tau) \qquad (E.4)$$

Performing the phasor addition, one finds

$$e_S = \sqrt{2}\,A\left[1 + K^2\phi_o^2 + (1-K^2\phi_o^2)\cos\tau\right]^{1/2} \cdot\cos\left[\omega t + \tan^{-1}\frac{(1-K\phi_o)\sin\tau}{(1+K\phi_o) + (1-K\phi_o)\cos\tau}\right] \qquad (E.5)$$

$$e_D = \sqrt{2}\,A\left[1 + K^2\phi_o^2 - (1-K^2\phi_o^2)\cos\tau\right]^{1/2} \cos\left[\omega t + \tan^{-1}\frac{(K\phi_o-1)\sin\tau}{(1+K\phi_o) - (1-K\phi_o)\cos\tau}\right] \qquad (E.6)$$

and this shows how e_S and e_D reflect the phase error τ.

Second, a phase error η can occur at RF or IF between hybrid 1 and the product detector. This phase error is added to the argument of e_D. The smoothed output of the product detector becomes the dc voltage signal

$$e_o = A^2\left[1 + 2K^2\phi_o^2 + K^4\phi_o^4 - (1-K^2\phi_o^2)^2\cos^2\tau\right]^{1/2} \cdot\cos\left[-\eta + \tan^{-1}\frac{(1+K\phi_o)\sin\tau}{(1+K\phi_o) + (1-K\phi_o)\cos\tau} + \tan^{-1}\left\{\frac{(1-K\phi_o)\sin\tau}{(1+K\phi_o) - (1-K\phi_o)\cos\tau}\right\}\right] \qquad (E.7)$$

where Equation (E.7) now incorporates both τ and η. For the condition where there are no phase errors ($\eta=\tau=0$), Equation (E.7) reduces to:

$$e_o = 2A^2K\phi_o \tag{E.8}$$

As expected, there is no boresight error in this case; that is, $e_o = 0$ when $\phi_o = 0$. The condition where $\tau = 0$ and η is finite gives:

$$e_o = 2A^2K\phi_o\cos\eta \qquad (\tau=0) \tag{E.9}$$

This condition also shows no boresight error, but only a loss of sensitivity for finite values of η.

When both η and τ are finite, the error voltage is given by Equation (E.7). It is seen that the condition $e_o = 0$ occurs only when the argument of the cosine function is $\pm\pi/2$, i.e., when

$$-\eta + \tan^{-1}\left\{\frac{(1+K\phi_o)\sin\tau}{(1+K\phi_o) + (1-K\phi_o)\cos\tau}\right\} + \tan^{-1}\left\{\frac{(1-K\phi_o)\sin\tau}{(1+K\phi_o) - (1-K\phi_o)\cos\tau}\right\} = \pi/2 \tag{E.10}$$

The trigonometric relationships for this condition are illustrated in Figure E2 where:

$$\tan\alpha = a/b \tag{E.11}$$

$$\tan(\beta-\eta) = b/a \tag{E.12}$$

$$\tan(\beta-\eta) = 1/\tan\alpha \tag{E.13}$$

$$\tan\alpha\tan(\beta-\eta) = 1 \tag{E.14}$$

With these relationships and using the identity

$$\tan(\beta-\eta) = \frac{\tan\beta-\tan\eta}{1+\tan\beta\tan\eta} \tag{E.15}$$

Equation (E.10) reduces to

$$\left[\frac{(1-K\phi_o)\sin\tau}{(1+K\phi_o) - (1-K\phi_o)\cos\tau}\right]\left[\frac{\dfrac{(1+K\phi_o)\sin\tau}{(1+K\phi_o) + (1-K\phi_o)\cos\tau} - \tan\eta}{1 + \dfrac{(1+K\phi_o)\sin\tau\tan\eta}{(1+K\phi_o) + (1-K\phi_o)\cos\tau}}\right] = 1 \tag{E.16}$$

After some algebra, one arrives at the expression of Dunn and Howard (Ref. E-1) which is:

$$\phi_o = \frac{1}{K}\left[\frac{-1 + \sqrt{\sin^2\tau\tan^2\eta + 1}}{\sin\tau\tan\eta}\right] \qquad (E.17)$$

Equation (E.17) describes the measured boresight angle ϕ_o for the case when the output of the product detector is zero, in the presence of phase errors τ and η. Thus, ϕ_o becomes the total pointing error due to τ and η.

For the usual case where τ is small, we have

$$\sqrt{\sin^2\tau\tan^2\eta+1} \approx \frac{\sin^2\tau\tan^2\eta}{2} + 1 \qquad (E.18)$$

and

$$\phi_o \simeq \left(\frac{1}{K}\right)\left(\frac{\tau\tan\eta}{2}\right) \qquad (E.19)$$

Actually, this relationship for small τ can be derived directly by making the appropriate approximations in the original identity; i.e., $\cos\tau\simeq 1$, $\sin\tau\simeq\tau$, and $K\phi_o<1$. Thus,

$$\frac{\tau}{2K\phi_o}\left[\frac{\tau/2 - \tan\eta}{1 + \frac{\tau\tan\eta}{2}}\right] = 1 \qquad (E.20)$$

or

$$K\phi_o \simeq \frac{\tau^2-\tau\tan\eta}{2+\tau\tan\eta} \simeq \frac{\tau\tan\eta}{2} \qquad (E.21)$$

so, again $\phi_o \simeq \frac{\tau\tan\eta}{2K}$ as before. (E.22)

A family of curves for the total pointing error, Equation (E.17), has been plotted in Figure E3. If it is assumed that both η and τ are of the order of 10 degrees a small but not negligible pointing error of 0.03 degrees results.

An interesting relationship between the phase error τ and the null depth of the difference pattern can be derived. Consider the difference signal as previously derived,

$$e_D = \sqrt{2A}\left[1+K^2\phi_o{}^2 - (1-K^2\phi_o{}^2)\cos\tau\right]^{1/2}\cos(\omega t+\alpha) \qquad (E.23)$$

where:

$$\alpha = \tan^{-1}\left\{\frac{-(1-K\phi_o)\sin\tau}{(1+K\phi_o) - (1-K\phi_o)\cos\tau}\right\} \qquad (E.24)$$

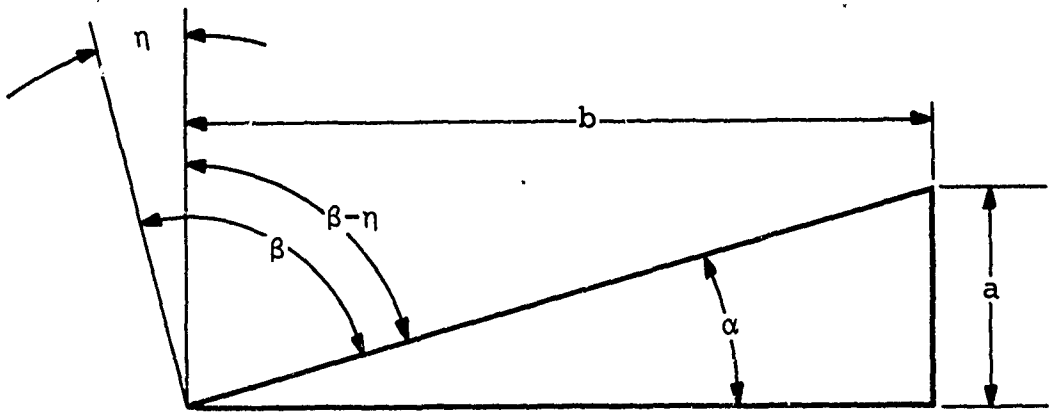

Figure E2. Trigonometric Relationships for the Condition $\alpha+B-\eta \approx \pi/2$

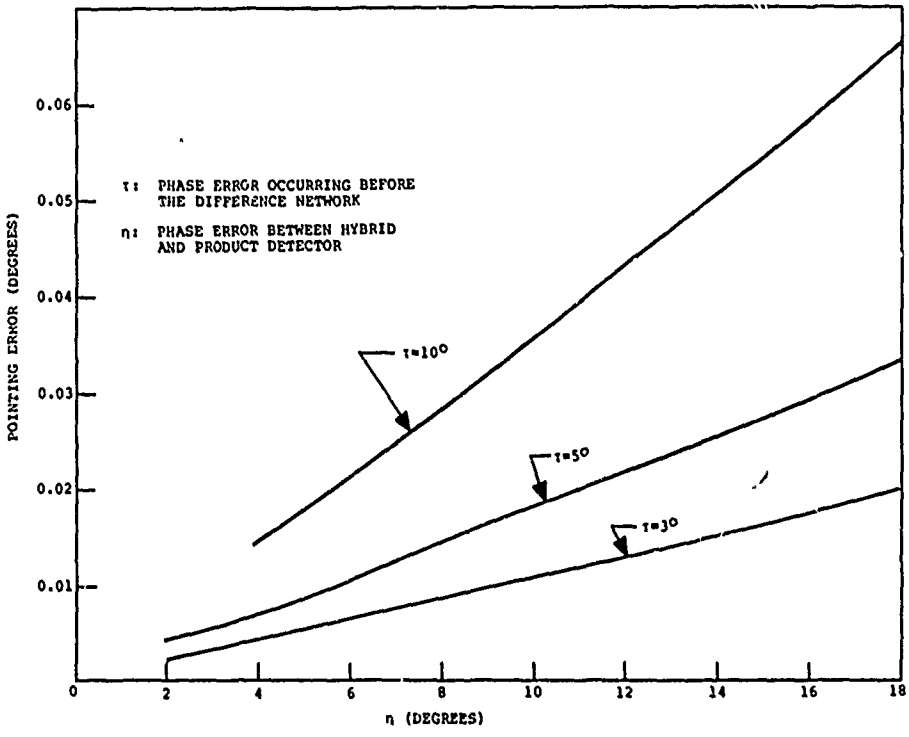

Figure E3. Azimuth Pointing Error Due to RF and IF Phase Errors

The squared function is

$$(e_D)^2 = 2A^2\left[1+K^2\phi_o{}^2 - (1-K^2\phi_o{}^2)\cos\tau\right]\cos^2(\omega t+\alpha) \qquad (E.25)$$

Now at boresight $\phi_o = 0$, and the amplitude becomes

$$(e_D)_o^2 = 2A^2\left[1-\cos\tau\right] \qquad (E.26)$$

or

$$(e_D)_o^2 = 4A^2\sin^2(\tau/2) \qquad (E.27)$$

For small values of τ this leads to

$$\frac{(e_D)_o}{A} \simeq \tau \qquad (E.28)$$

That is, the normalized voltage amplitude at null is equal to the RF phase error τ. The difference pattern null depth therefore becomes a readily available measure of this phase error.

References

E-1. J. H. Dunn and D. D. Howard, "Precision Tracking with Monopulse Radar," Electronics, vol. 35, no. 17, pp. 51-56, April 22, 1960.

APPENDIX F

SOURCES OF MULTIPATH ERROR

In this Appendix, a summary will be presented of certain analytical relationships of multipath error that are germane to the beacon system. The equations will be applied and extended where necessary. Specifically, multipath errors will be analyzed according to whether they arise by signal reflection from ground or sea surfaces. Reflections from tall buildings near the radar site will be considered in Appendix G.

MULTIPATH ERRORS ARISING FROM SURFACE REFLECTIONS

A major source of multipath error arises from ground reflections as shown in Figure F1.

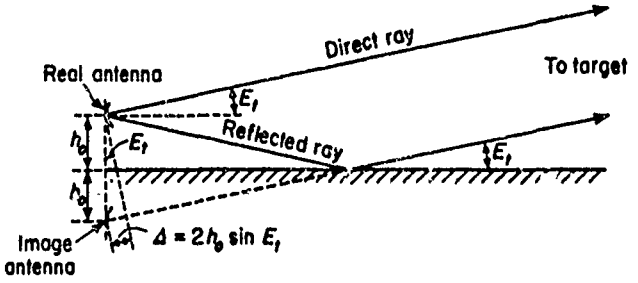

Figure F1. Geometry of Surface-Reflected Multipath Interference (Ref. F-1)

In addition to the direct reply received from an elevation angle E_T, a reflected reply arrives at an angle $-E_T$ relative to the horizon. The effect of this phenomenon is to cause the radar to perform as if there were two targets, the primary aircraft and its image. For tracking radars, this introduces a serious error into elevation measurements, the magnitude of which is given by

$$\sigma = \frac{\rho}{C_M \sqrt{2 G_{SE} n_e}} \qquad \text{(F.1)}$$

where ρ is the surface reflection coefficient, G_{SE} is the main lobe to side lobe gain ratio evaluated at the elevation angle E_T, n_e is the effective number of independent samples, and C_M is the monopulse error slope.

When the reflecting surface is smooth and horizontal, ground reflections will not introduce error into an azimuth measurement. However, if the ground is inclined, a component of the multipath disturbance is introduced into the azimuth determination. The magnitude of this error equals the

elevation multipath error (Eq. F.1) multiplied by $\sin\alpha$, where α is the angle of ground inclination. This is the case of interest in the beacon system.

The surface reflection properties of various materials have been studied by several authors (Refs. F-2, F-3). The reflection coefficient of the earth may be readily determined from knowledge of its electromagnetic parameters. This relation is (Ref. F-2, pg. 398)

$$\Gamma_v = \rho_v e^{i\phi_v} = \frac{\sqrt{e_c}\sin E_T - 1}{\sqrt{e_c}\sin E_T + 1} \qquad (F.2)$$

where Γ_v is the reflection coefficient for a vertically polarized incident plane wave, with ρ_v and ϕ_v representing the associated magnitude and phase delay. The parameter e_c is the complex dielectric constant. This coefficient is empirically related to the conductivity σ and the dielectric constant ε by

$$e_c = \varepsilon - i60\lambda\sigma \qquad (F.3)$$

Data on the earth's constitutive parameters for various types of terrain are presented in Table F1.

TABLE F1. ELECTROMAGNETIC PARAMETERS FOR VARIOUS SURFACE TYPES

Terrain	Conductivity σ (mhos/meter)	Dielectric Constant ε (electrostatic units)
Sea water	5	80
Fresh water	8×10^{-3}	80
Dry, sandy, flat coastal land	2×10^{-3}	10
Marshy, forested flat land	8×10^{-3}	12
Rich agricultural land, low hills	1×10^{-2}	15
Pastoral land, medium hills and forestation	5×10^{-3}	13
Rocky land, steep hills	2×10^{-3}	10
Mountainous (hills up to 3000 feet)	1×10^{-3}	5
Cities, residential areas	2×10^{-3}	5
Cities, industrial areas	1×10^{-4}	3

This information is taken from Reference F-4, pg. 26-3. Additional data can be found in Reference F-2, pg. 398.

With the values listed in Table F1, the complex reflection coefficient of a smooth surface can be computed for various angles of incidence. This information has been calculated for the beacon frequency (Ref. F-5). A typical set of curves is reproduced in Figure F2, which illustrates the dependence on the terrain characteristic of the angle where ρ approaches zero. The variation of the reflection coefficient with frequency is indicated in the curves of Figure F3, taken from Reference F-3.

The preceding discussion applies to reflections from a smooth surface. When the reradiating surface is irregular, the amount of specular reflection is decreased and a component of diffuse scattering is introduced. Under these conditions the coefficient of *specular* reflection, ρ, is given by

$$\rho = \rho_o \rho_s \qquad \text{(F.4)}$$

where ρ_o is the reflection coefficient characterizing a smooth surface of the same material, and ρ_s is the specular scattering factor. This parameter is given in terms of the rms deviation in surface height, σ_h, the incident angle E_t, and the wavelength λ by (Ref. F-3, pg. 246)

$$\overline{\rho_s^2} = \exp\left\{-\left(\frac{4\pi\sigma_h \sin E_t}{\lambda}\right)^2\right\}, \qquad \text{(F.5)}$$

assuming that the flat-earth approximation is valid. Similarly, the coefficient of *diffuse* reflection is given by

$$\rho = \rho_o \rho_d \qquad \text{(F.6)}$$

where ρ_d is the diffuse scattering coefficient.

The diffuse and specular scattering coefficients are plotted as a function of the *roughness factor*, $\sigma_h \sin E_T/\lambda$, in Figure F4. The critical angle γ_c where $\overline{\rho_s^2}$ equals one-half is considered the transition point between a smooth and a rough surface. Above this elevation angle, diffuse scattering plays an important role, whereas below it, specular reflection dominates.

The effect of surface irregularities is to scatter the received energy over a region surrounding the image point (Fig. F5). This area, with boundaries that are functions of the elevation angle and of the rms slope of the rough surface, σ_α, has been designated the *glistening surface* (Ref. F-3), and this is illustrated in Figure F5.

Sample calculations of the azimuth error introduced by

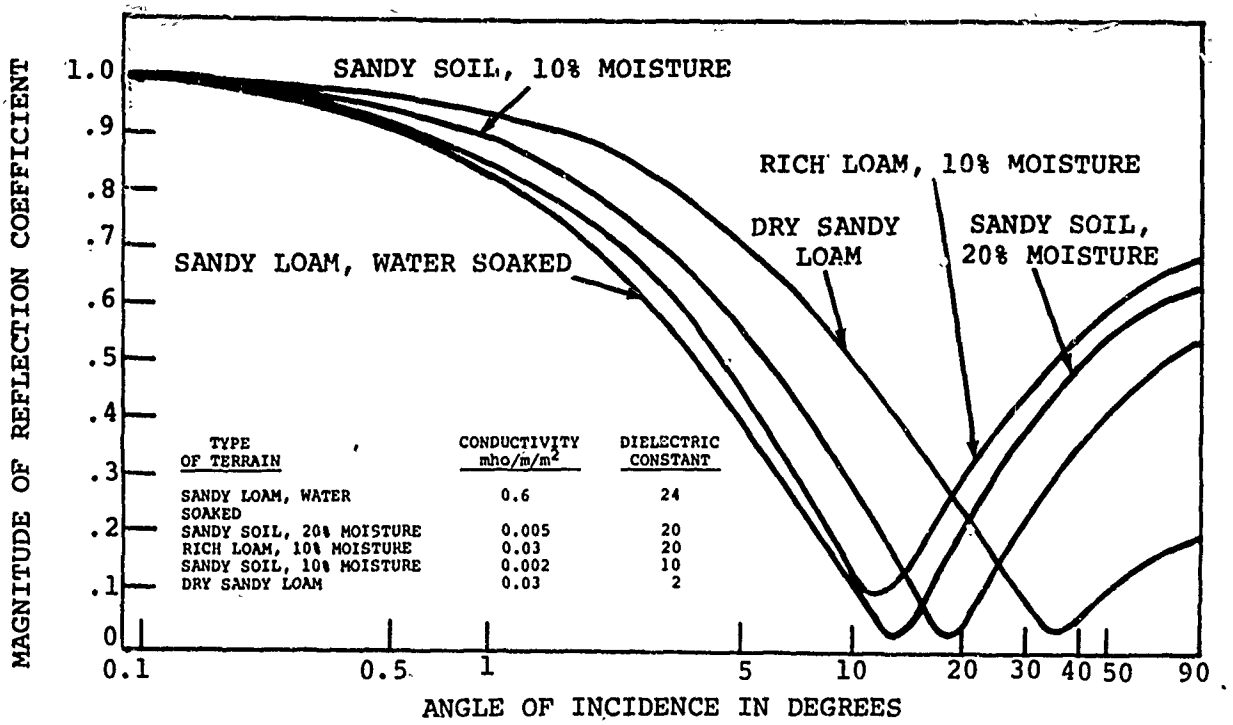

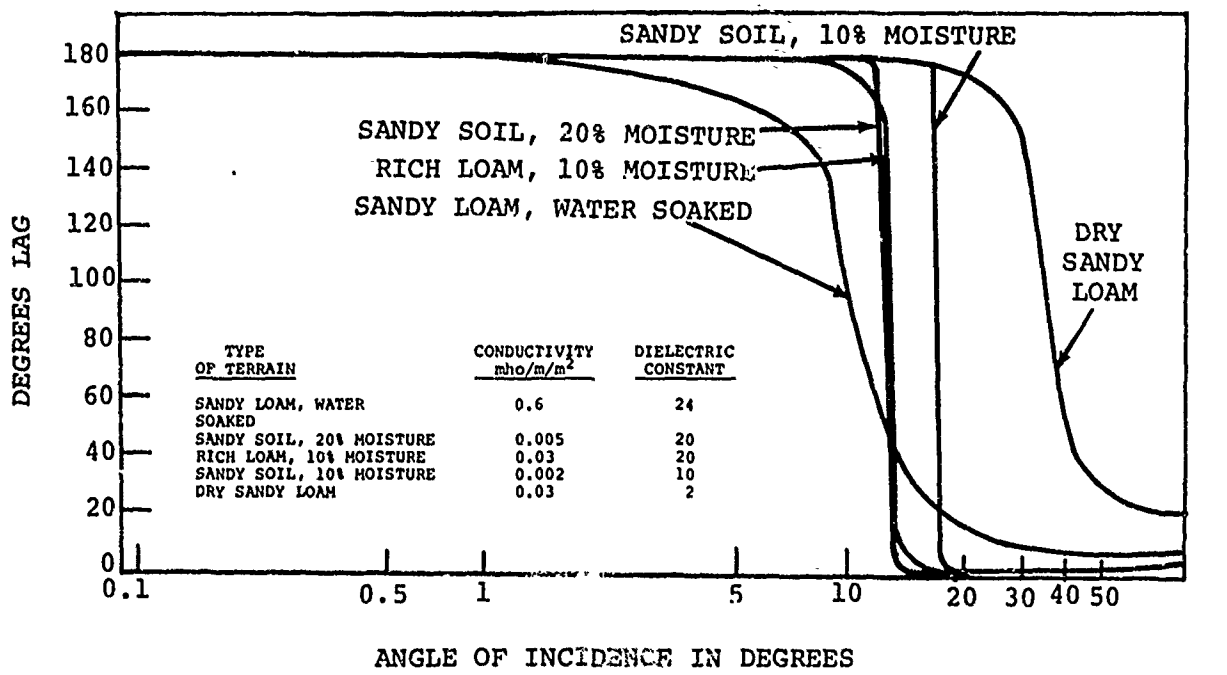

Figure F2. Magnitude and Phase of the Surface Reflection Coefficient Plotted Vs Angle of Incidence for Different Types of Terrain (Ref. F-5)

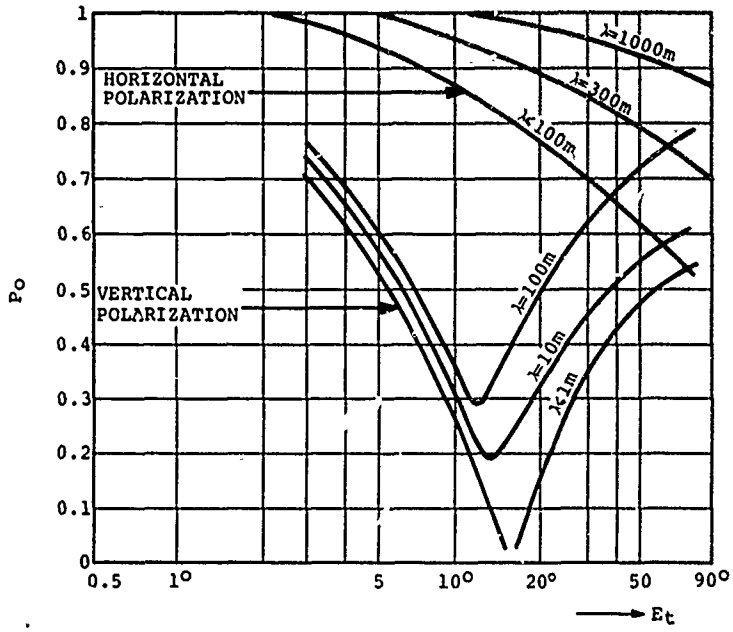

Figure F3a. Reflection Coefficient of a Perfectly Plane Earth vs Angle of Incidence, with $\varepsilon/\varepsilon_o=10$, $\sigma=10^{-3}$ mho m (The parameter is the free-space wavelength.)

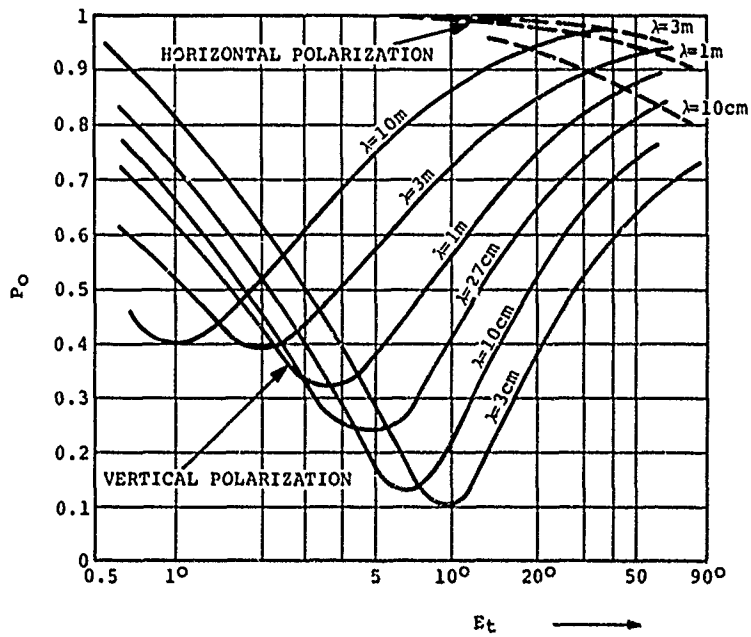

Figure F3b. Reflection Coefficient of a Very Smooth Sea vs Angle of Incidence, $\varepsilon/\varepsilon_o=80$, $\sigma=4$ mho m (The parameter is the free-space wavelength.)

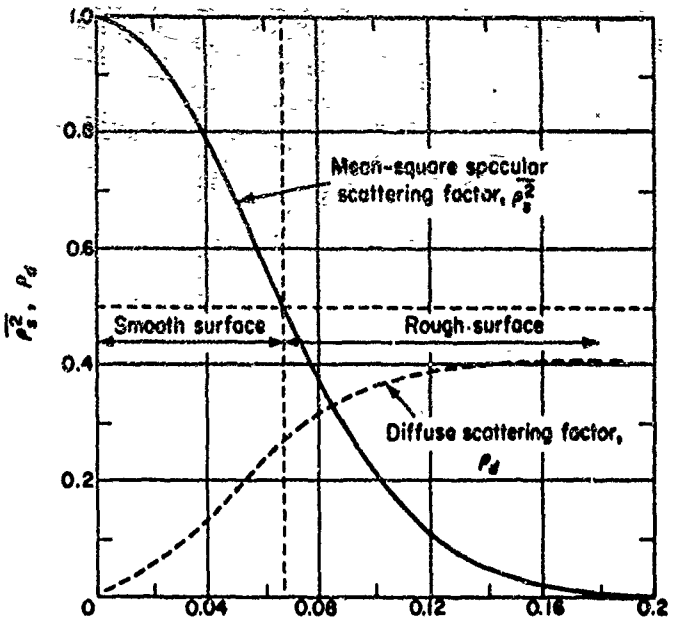

Figure F4. Scattering Factor vs Surface Roughness (Ref. F-1)

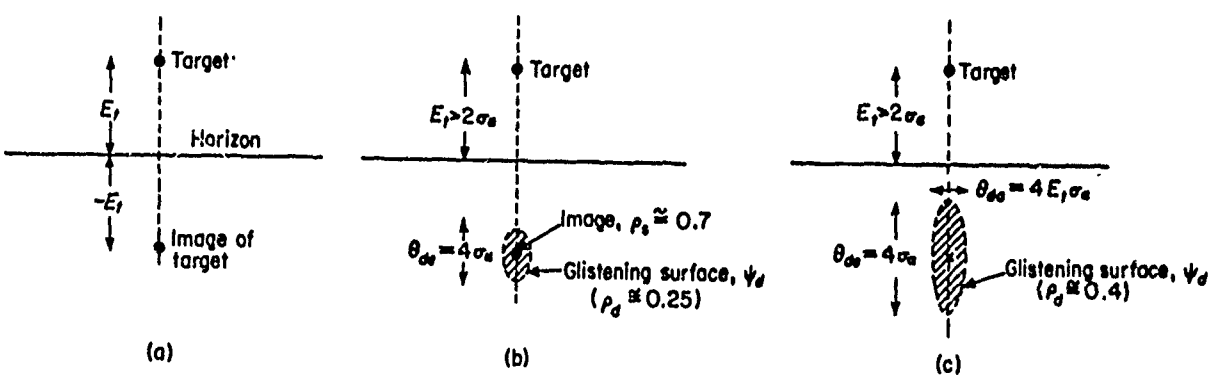

Figure F5. Glistening Surface Associated with Various Degrees of Surface Roughness (Ref. F-1)
a) Specular reflection, b) slight roughness, c) rough surface

ground reflections will be carried out below.

Since it would be impractical to consider all varieties of terrain, the calculations will be made on the basis of the reflection coefficient curves of Figure F3, as these were derived for representative values of conductivity and dielectric constant. Reflections from both land and sea surfaces will be considered.

REFLECTIONS FROM THE SEA

The azimuth multipath error introduced by reflections from the sea will now be computed. Table F2 lists the wave height for various states of sea agitation; no azimuth error can result from specular reflection from a calm sea.

The multipath error will be derived for the following conditions:

The sea state is assumed to be moderate; the wave height is 1.4 meters. σ_h, the rms height = 0.30 meters

V_w, the wind velocity = 15m/sec (30 knots)
σ_α, the rms slope of the surface = 0.25 radians

TABLE F2. WAVE HEIGHT ENCOUNTERED FOR VARIOUS SEA STATES

No.	Sea State	Wave Height Vh
0	Calm	0
1	Smooth	0-30cm
2	Slight	30cm-1m
3	Moderate	1m-1.50m
4	Rough	1.50m-2.50m
5	Very rough	2.50m-4m
6	High	4m-6m
7	Very high	>6m

The critical angle γ_c (where $\overline{\rho_s}^2 = 0.5$) then is

$$\gamma_c = \sin^{-1}\left[\frac{0.065\lambda}{\sigma_h}\right] = 3.49^o$$

First, we assume that the target elevation falls in the vicinity of the critical angle, say two degrees. The glistening surface then covers an area bounded by (see Figure F4)

$$\theta_{da} = 2E_t\sigma_\alpha = 2^o$$

$$\theta_{de} = 4\sigma_\alpha = 1^o$$

The azimuth error is given by (Ref. F-1, pq. 151)

$$\sigma_A = \frac{\theta_{da}\rho K_e}{2\sqrt{2\overline{G_{sr}}n_e}} \qquad (\theta_{da}<\theta_a) \qquad (F.7)$$

where $\overline{G_{sr}}$ is the average sidelobe ratio, evaluated at the horizon. This average is taken over the glistening surface ψ_d.

$$\overline{G_{sr}} = \frac{G_1\psi_d}{\int_\psi G_r d\psi}$$

K_e is the elevation-pattern gain reduction factor. This coefficient accounts for the fact that the reflections are being received at an elevation angle of $-E_t$, whereas the gain $\overline{G_{sr}}$ was evaluated at the horizon. K_e is defined by

$$K_e \triangleq \sqrt{\frac{G(0, -E_t)}{G(0,0)}}$$

n_e is the number of independent error samples.

We can now proceed to calculate σ_A. From measurements on a calm sea (Figure 3b), at 4 degrees, ρ^o equals 0.26. The roughness factor ($\sigma_h \sin\gamma/\lambda$), equals 0.075 which corresponds to a diffuse scattering coefficient of ρ_d=0.29. Therefore, the reflection parameter for diffuse scattering is $\rho=\rho_o\rho_d$=0.075.

The number of error samples n_e is a function of the correlation time of the reflections. For reflections from the sea, the correlation time can be related to the wind speed by (Ref. F-1, pg. 152, Eq. 5.32)

$$t_c = \frac{1.6\lambda}{V_\omega} = 0.03 \text{ sec}$$

Therefore, the received signal is correlated over the duration of the pulse, and consequently $n_e = 1$.

The average sidelobe ratio is given by

$$\overline{G_{sr}} = \frac{G_1 \psi_d}{\int_{\theta_{de}} \int_{\theta_{da}} G_r d\eta d\varepsilon} \qquad (F.8)$$

Since the dispersion in elevation is small, $G_r(\eta,\theta)$ can be considered invariant with elevation, so the above expression becomes

$$\overline{G_{sr}}\Big|_{-E_t} = \frac{G_1 \theta_{da}}{\int G_r(\eta,-E_t)d\eta} \qquad (F.9)$$

This expression can be rewritten as

$$\overline{G_{sr}}\Big|_{-E_t} = \frac{\theta_{da}}{2K_e^2 \int_o^{\theta_{da}/2} \frac{G_r(\eta)}{G_1} d\eta} \qquad (F.10)$$

The normalized antenna gain ratio, $G_r(\eta)/G_r(0)$ is plotted in Figure F6. From this curve, when $\theta_{da} = 2$ degrees, the integral equals 0.83 and the sidelobe ratio assumes the value $\overline{G_{sr}} = 1.20$.

The variation of antenna gain with elevation, K_e, is given in Figure F7 (Ref. F-6). The voltage gain reduction at $-E_t$ for the elevation under consideration is given by

$$K_e = 0.91$$

This is based on a decrease in gain of 0.8 dB as read from Figure F7.

Substituting the calculated values of ρ, n_e, $\overline{G_{sr}}$, and K_e into Equation (F.7) yields

$$\sigma_A = 0.045^o \qquad (E_t = 4^o)$$

For the case where the elevation angle, E_t, is 10 degrees, the reflections differ from the previous case in that the glistening area extends over a larger azimuth sector, $\theta_{da} = 4\ E_t \sigma_\alpha$ (see Figure F-5). In addition, the azimuth

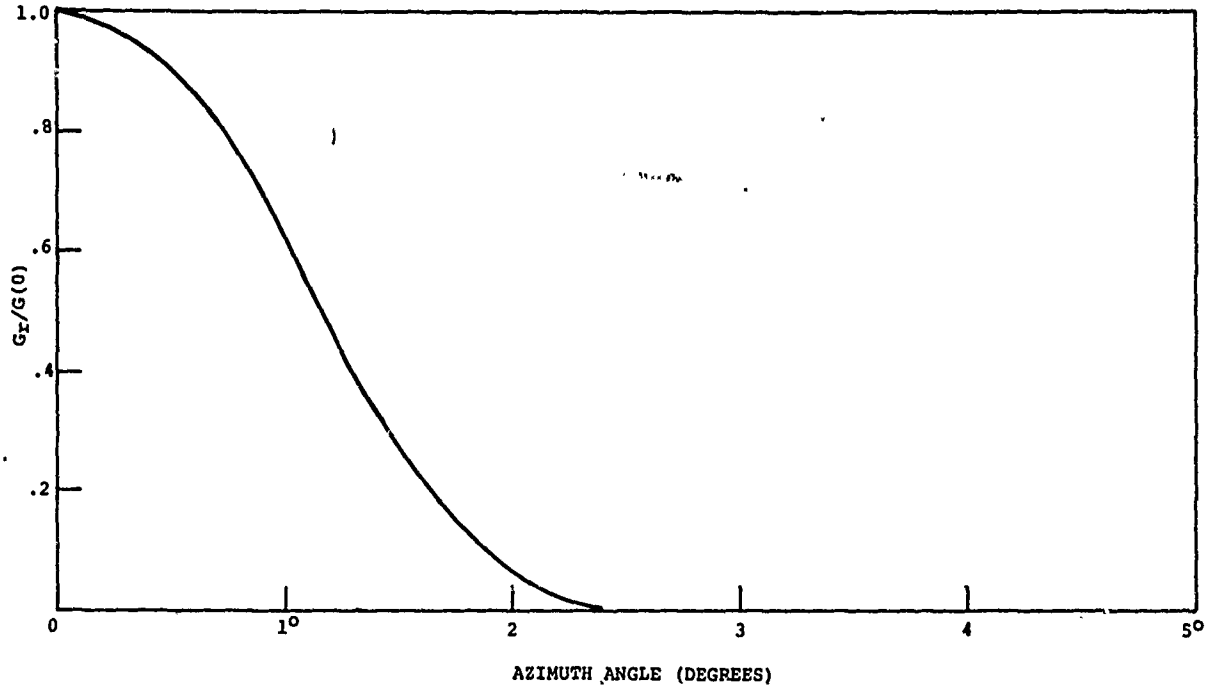

Figure F6. Normalized Antenna Gain Ratio $G_r/G(0)$ vs Azimuth Angle, FA 7202 Antenna Sum Pattern

error is now given by (Ref. F-1, pg. 152)

$$\sigma_A = \frac{\rho\theta_a K_e}{K_m\sqrt{2\hat{G}_{sr}n_e}} \qquad (\theta_{da}>\theta_a) \qquad \text{(F.11)}$$

The following numerical values are applicable:

$\theta_{da} = 10^o$

$\rho_o = 0.4$

$\rho_d = 0.4$

$K_e = 0.75$

$\sigma_h \sin E_t/\lambda = 0.186$

This yields a pointing error (boresight shift) of

$\sigma_A = 0.104^o \qquad (E_t = 10^o)$

The azimuth error was also evaluated for other elevation angles, and this information is listed in Table F3

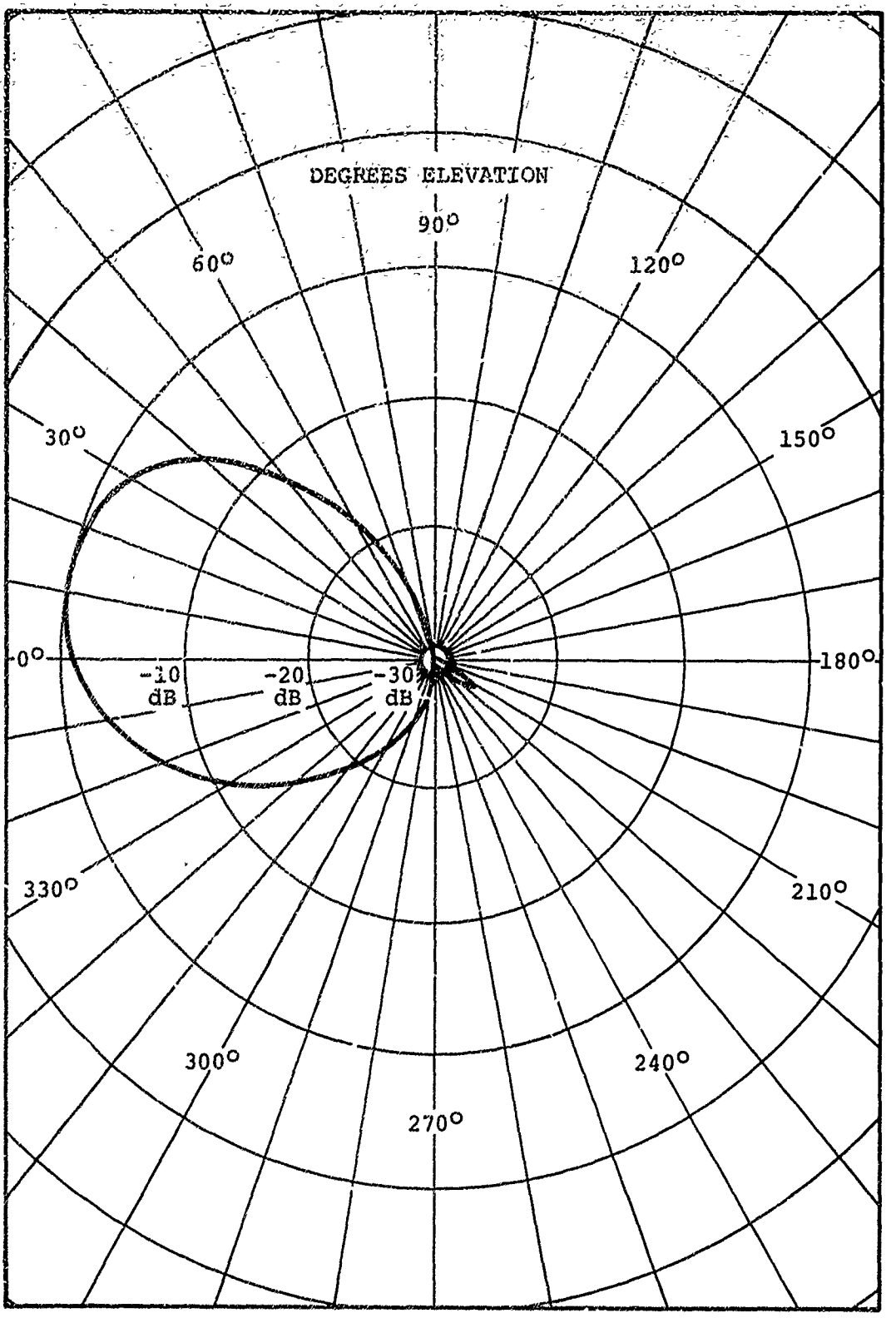

Figure F7. Variation of
Antenna Gain with Elevation, FA 7202 Antenna

TABLE F3. AZIMUTH MULTIPATH ERROR INTRODUCED BY SCATTERING FROM THE SEA

Elevation	ρ_o	ρ_d	ρ	K_e	σ_A
2°	0.46	0.13	0.059	0.98	0.020
4°	0.26	0.29	0.075	0.91	0.045
10°	0.4	0.4	0.16	0.75	0.104
15°	0.55	0.4	0.22	0.631	0.116
20°	0.65	0.4	0.26	0.531	0.118
30°	0.74	0.4	0.296	0.31	0.079
40°	0.78	0.4	0.31	0.20	0.053
50°	0.82	0.4	0.32	0.12	0.033

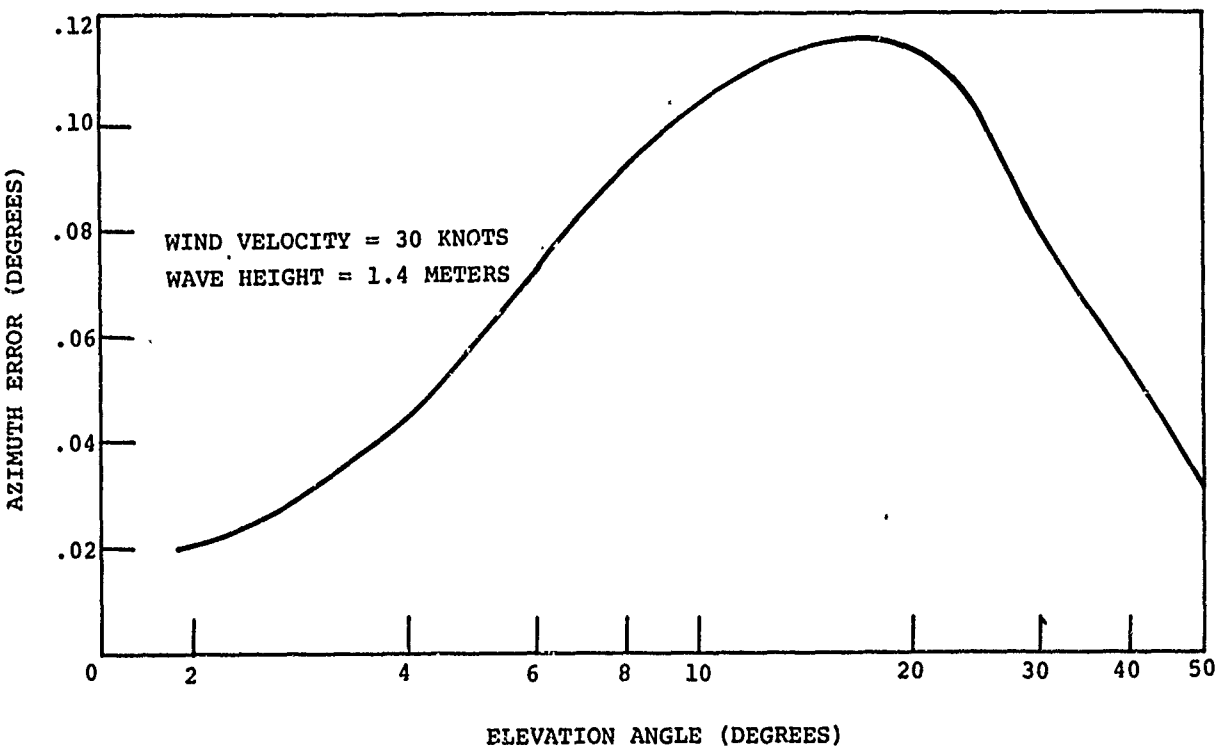

Figure F8. Azimuth Multipath Error Introduced by Diffuse Reflections from the Sea vs Elevation Angle for the FA 7202 Antenna

and plotted vs elevation angle in Figure F8. This error reaches a peak of 0.118 degrees in the vicinity of E_t = 18 degrees. Beyond this point, the antenna gain factor, K_e, goes down faster than the reflection coefficient ρ_o increases. As a result, there is a monotonic reduction in the azimuth error. It must be emphasized that this analysis takes into account only the diffuse component of reflection; the specular component is ignored since it does not influence azimuth accuracy.

REFLECTIONS FROM THE GROUND

The impact of ground reflections on azimuth accuracy will now be considered. The reflection properties have been given previously for the mean values of ground conductivity and dielectric constant (Fig. F3). In addition, the following parameters characterizing surface irregularity are assumed.

σ_h = 0.15 meters

σ_α = 0.2 radians (this is a typical value for land, Ref. F-1, pg. 150)

The critical angle for these conditions then is

$\gamma_c = 7.46^o$

Evaluation of the azimuth error is carried out in a manner similar to that employed previously when dealing with reflections from the sea. A sample calculation for one elevation angle will be presented.

Consider an elevation of 8 degrees, which places the target in the region of the critical angle. The pertinent system parameters are

$\rho_o = 0.32$ (From Fig. F3a)

$\sigma_h \sin E_t / \lambda = 0.0746$

$\rho_d = 0.27$

$\theta_{da} = 3.2^o$

$K_e = 0.79$

The correlation time is related to the velocity spread of the scatterers, σ_v, in the following manner:

$$t_c = \frac{\lambda}{2\sqrt{2}\pi\sigma_v}$$

If the terrain is covered with wooded hills and the wind speed is 25 knots, then from Table F4, $\sigma_v = 0.38$ ft/sec, and the correlation time is

$$t_c = 0.09 \text{ sec}$$

Therefore, the reflected signal will be correlated over the entire return and n_e equals one. The resulting azimuth error is calculated from Equation (F.11) as

$$\sigma_A = 0.062^o$$

Similar results were obtained for other target elevation angles and these data are listed in Table F5 and plotted in Figure F9.

An examination of Figure F9 reveals a series of peaks and nulls. These arise in the following manner.

Region I: $\{E_t \leq 10^o\}$

For small elevation angles, the azimuth multipath error increases with E_t. The dominant factor in this region is the growth of the glistening surface as the target elevation increases. This is accompanied by a rapid increase in the diffuse scattering coefficient, ρ_d, which more than compensates for the decline in ρ_o.

Region II: $\{10^o < E_t < 30^o\}$

In this region, the increase in ρ_d has leveled off, and the error variation is determined by ρ_o. This reflection coefficient, ρ_o, decreases dramatically, reaching a null in the vicinity of 16 degrees. The decrease is reflected in a corresponding reduction in the azimuth error. Beyond 16 degrees, ρ_o increases, and σ_A grows, reaching a peak of 0.034 near 30 degrees.

Region III: $\{30^o \leq E_t\}$

The azimuth error in this region is shaped by the decrease in the antenna gain with elevation. As a result, there is a gradual decline in σ_A.

TABLE F4. CHARACTERISTICS OF CLUTTER SPECTRA (REF. F-1)

Source of clutter	Wind speed (knots)	Ratio m^2	Barlow's a	$\sigma_c\lambda$ (cm/sec)	σ_v (ft/sec)	Reference
Sparse woods	(calm)		3.9×10^{19}	3.5	0.057	Barlow
Rocky terrain	10	30				Goldstein, p.583
Wooded hills	10	5.2	7.2×10^{18}	8	0.13	Goldstein, pp. 583-85
Wooded hills	20		2.3×10^{17}	45	0.74	Barlow
Wooded hills	25	0.8	9×10^{17}	23	0.38	Goldstein, pp. 583-85
Wooded hills	40	0	1.1×10^{17}	65	1.06	Goldstein, pp. 583-85
Sea echo			2.4×10^{16}	140	2.3	Wiltse, et al., p. 226
Sea echo		0	$(1-2)\times10^{16}$	165-205	2.5-3.3	Goldstein, pp. 580-81
Sea echo	8-20		$(0.6-2.6)\times10^{16}$	100-220	1.5-3.5	Hicks, et al., p. 831
Sea echo	(windy)		1.4×10^{16}	183	3.0	Barlow
Chaff	0-10	0	$(1.4-8)\times10^{16}$	75-180	1.2-3.0	Goldstein, p. 472
Chaff	25	0	7×10^{15}	250	4.1	Goldstein, p. 472
Chaff			10^{16}	215	3.5	Barlow
Rain clouds		0	$(0.7-3)\times10^{15}$	370-800	6-13	Goldstein, p. 576
Rain clouds			2.8×10^{15}	410	6.7	Barlow

Basic relationships: $\sigma_v = \frac{\sigma_c\lambda}{2}(\text{cm/sec}) = \frac{\sigma_c\lambda}{61}(\text{ft/sec})$ $\quad \sigma_c = 0.85f^{0.5}$

$\sigma_v = \frac{c}{\sqrt{8a}} = \frac{10^9}{\sqrt{8a}}(\text{ft/sec})$ $\quad a = \frac{c^2}{8\sigma_v^2}$

TABLE F5. AZIMUTH MULTIPATH ERROR INTRODUCED BY GROUND REFLECTIONS

Elevation	ρ_o	ρ_d	ρ	K_e	σ_A (degrees)
2^o	0.78	0.06	0.046	0.98	0.012
4^o	0.63	0.12	0.075	0.91	0.037
6^o	0.50	0.18	0.09	0.83	0.053
8^o	0.32	0.27	0.086	0.79	0.062
10^o	0.30	0.34	0.102	0.75	0.066
12^o	0.10	0.40	0.04	0.70	0.024
15^o	0.03	0.40	0.012	0.631	0.006
20^o	0.15	0.40	0.06	0.531	0.027
30^o	0.34	0.40	0.13	0.31	0.034
40^o	0.41	0.40	0.16	0.20	0.027
50^o	0.46	0.40	0.186	0.12	0.019

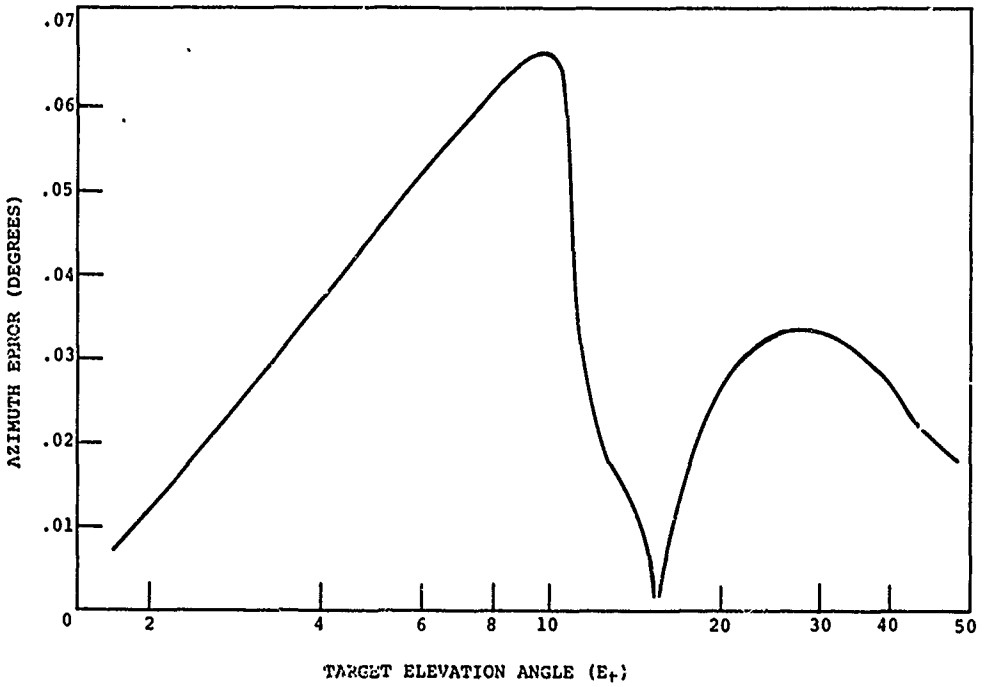

Figure F9. Azimuth Multipath Error Introduced by Ground Reflections

References

F-1. D. F. Barton and H. R. Ward, Handbook of Radar Measurement, Prentice-Hall, Inc., Englewood Cliffs, N. J., 1969.

F-2. D. E. Kerr, editor, Propagation of Short Radio Waves, McGraw-Hill Book Co., New York, 1951.

F-3. P. Beckman and Andre Spizzichino, The Scattering of Electromagnetic Waves from Rough Surfaces, Pergamon Press, New York, 1963.

F-4. ITT Handbook, "Reference Data for Radio Engineers," Fifth Edition, 1970.

F-5. G. F. Spingler, "Experimentation and Analysis of Siting Criteria," Report No. NA-69-36 (RD-69-43), FAA National Aviation Facilities Experimental Center, Atlantic City, N. J. 08407, Sept. 1969.

F-6. ATC Radar Beacon Interrogator, ATCBI-3, Theory of Operation, FAA Manual FR-527-1, FAA Aeronautical Center, Oklahoma City, Oklahoma, June 1970.

APPENDIX G

MULTIPATH ERROR INTRODUCED BY BUILDING REFLECTIONS

A serious problem encountered at many airports is the extraneous replies due to reflection from the surrounding buildings. With the increasing tendency to construct high rise structures close by airport sites, this problem is becoming more significant.

A detailed analysis of surface reflections involves describing each building in terms of *elementary reflecting surfaces* and characterizing these by an associated scattering matrix (Refs. G-1, G-2). The contribution of the individual scatterers is then summed to obtain the reflection properties of the object. Following this procedure, the radar cross-section can be expressed in terms of the discrete scattering centers by the following relation (Ref. G-3):

$$\sigma = \left| \sum_{k=1}^{N} \sqrt{\sigma_k}\, e^{j\phi_k} \right|^2 \qquad \text{(G.1)}$$

where

σ = the effective radar cross-section

N = number of discrete scattering surfaces

σ_k = radar cross-section of kth scattering surface

ϕ_k = phase of field scattered by kth reflector relative to that of the first scattering surface.

The use of the above approach is impractical, since most structures are composed of numerous scattering surfaces whose reflection properties are only roughly known. As a result, even an approximate solution of Equation (G.1) requires a great deal of computation. Therefore, another technique will be employed, and this second approach is based on the premise that a reflecting structure will behave in a manner analogous to an antenna.

THE REFLECTING STRUCTURE VIEWED AS AN ANTENNA

The problem of building reflections is an example of so-called bistatic scattering, where the building is illuminated by the source (the aircraft transponder) and emits a secondary signal that is observed by the receiver (the IFF antenna). As viewed by the receiving antenna, the reflecting structure acts as an additional RF source and can be replaced by an equivalent antenna transmitting a signal similar to the reflected signal.

A typical reflection situation is portrayed in Figure G1; here, a tall structure close to the airport has energy impinging upon it from a responding aircraft. When the replying craft is more than five miles away (a condition met for most en route surveillance), the received wavefront will be essentially planar. Under these conditions, the reflecting structure is considered to be uniformly illuminated, with a linear phase taper determined by the angle of incidence α_i (Fig. G2). Neglecting the effect of windows and other small irregularities, the building can be represented as a uniformly illuminated antenna tramsmitting a pattern following a sinx/x distribution (Ref. G-4, pg. 2-25). The main lobe will lie along d_{BA}, and the angle α_R is equal to the angle of incidence α_i. The incident signal is reradiated with the gain $G_R = 4\pi A/\lambda^2$ where A is the reflecting surface area.

If W is the width of the reflecting surface, then the bistatic radar cross-section seen by the receiving antenna is given by the worst-case cross-section modified by a phased array pattern function and an area reduction factor,

$$\Omega(\alpha_A,\alpha_i) = \frac{4\pi A^2 C_R}{\lambda^2}\left[\frac{\sin\{kW\sin(\alpha_A-\alpha_R)\}}{kW\sin(\alpha_A-\alpha_R)}\right]^2\cos^2\alpha_i \qquad (G.2)$$

where

A = the area of the reflecting surface

α_i = the angle of arrival of the incident wavefront defined with respect to the building normal $\vec{N}_R$ (see Fig. G2)

α_R = the angular position of the main lobe of the reradiated signal

α_A = the aspect angle of the antenna, seen as a point source from the reflecting building

C_R = a parameter characterizing the (generally imperfect) reflection properties of the material comprising the structure (this coefficient defines the percentage of incident energy which is reradiated)

$k = 2\pi/\lambda$, the free-space propagation constant.

When $\alpha_A = \alpha_i$, the above expression defines the monostatic radar cross-section. For this case, Equation (G.2) reduces to the relation derived by Kerr for the radar cross-section

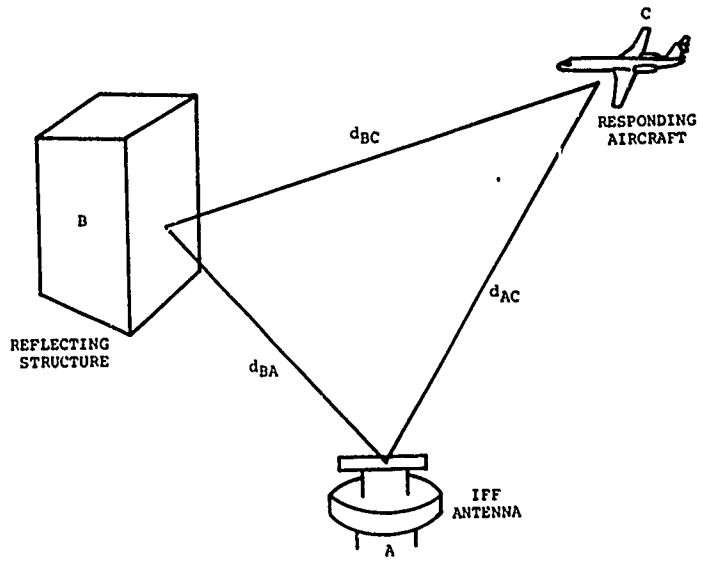

d_{BC}: DISTANCE FROM TRANSPONDER TO REFLECTOR

d_{AC}: DISTANCE FROM TRANSPONDER TO IFF ANTENNA

d_{BA}: DISTANCE FROM THE REFLECTING SURFACE TO ANTENNA

Figure G1. Target Reflector Geometry

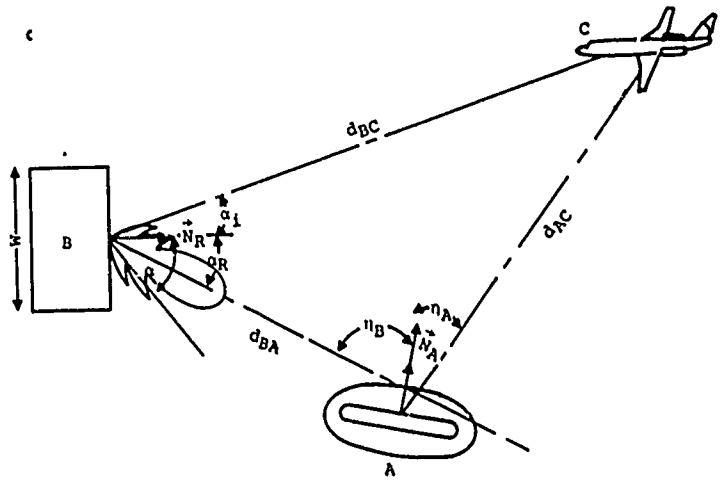

$\vec{N}_R$ IS THE NORMAL TO THE REFLECTING SURFACE

$\vec{N}_A$ IS THE NORMAL TO THE SURFACE OF THE IFF ANTENNA

Figure G2. Target Reflector Geometry Projected Upon the Ground Plane

of a flat plate (Ref. G-1, pg. 457).

The pattern followed by the reflected signal strength is plotted vs aspect angle in Figure G3 for two buildings of widths W and W/2, respectively. These curves exhibit the peaks and nulls commonly observed with multipath phenomena. In practice, the nulls would not be as deep as indicated here, since buildings are not perfectly smooth. As a result of surface irregularities, the phase relations required to establish a null are not maintained, and these troughs are partially filled in.

From Figure G3, it is apparent that reflections from wider buildings will cause the most serious problems due to their greater intensity. However, the reradiated energy from these structures is confined to a narrow azimuth sector spanning λ/W radians. This information can be used to define *critical zones*, areas where an interrogation reply gives rise to serious reflection problems. Once these zones are identified, it would be useful to study the impact on total system performance resulting from a reduced interrogation rate, for aircraft passing through them.

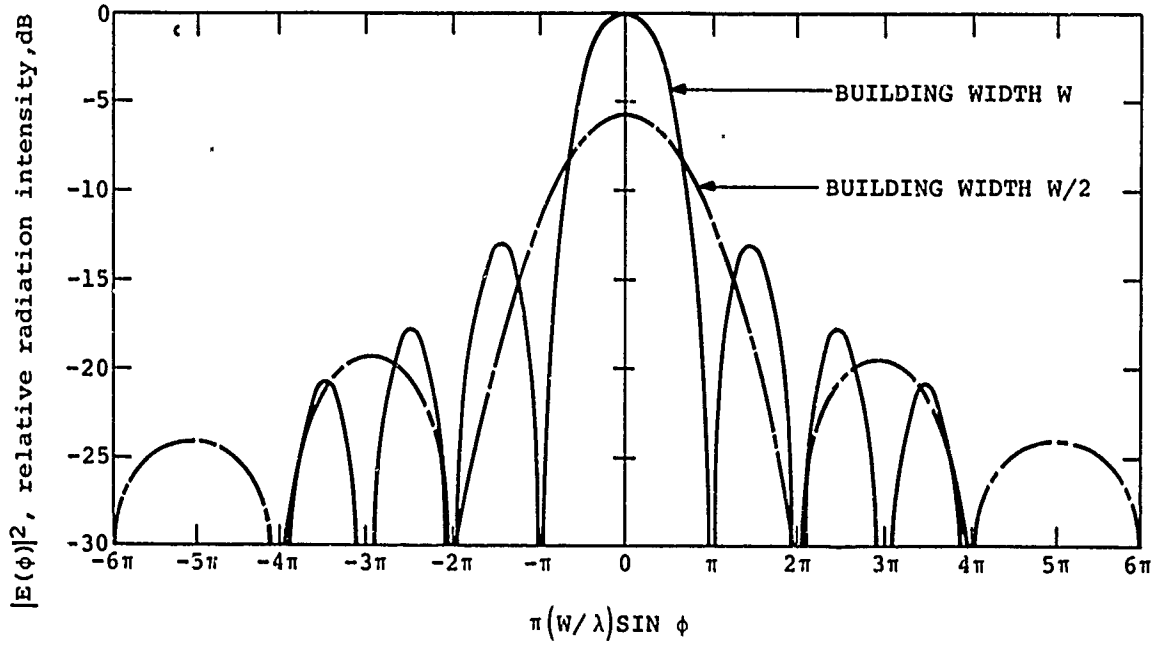

Figure G3. Relative Reflection Strength From Two Buildings of Widths W and W/2

WORST-CASE POINTING ERROR INTRODUCED BY BUILDING REFLECTIONS

In this section, the azimuth accuracy degradation caused by building reflections will be evaluated. A computation will be made for the worst-case conditions. These are

1. The direct path reply and the interfering signal arrive simultaneously at the receiver.

2. The receiving antenna is situated along the main lobe of the reradiated signal and therefore receives the peak interference signal.

With these assumptions, Equation (G.2) reduces to

$$\Omega(\alpha_i) = \frac{4\pi A^2 C_R \cos^2 \alpha_i}{\lambda^2} \tag{G.3}$$

The power incident upon the reflecting surface is

$$(P_I)^B = \frac{P_T G_T}{4\pi (d_{BC})^2} \tag{G.4}$$

where P_T is the transponder power, G_T is the aircraft antenna gain, and d_{BC} is the distance between the aircraft and reflecting surface (see Fig. G1).

The reflected signal is related to the incident energy by

$$P(\alpha_i) = (P_I)^B \Omega(\alpha_i) \tag{G.5}$$

Combining Equations (G.4) and (G.5), the reradiated power received at the antenna can be expressed as

$$(P_A)^R(\alpha_i) = \frac{P_T G_T \Omega(\alpha_i)}{(4\pi)^2 (d_{BA})^2 (d_{BC})^2} \tag{G.6}$$

The pointing error introduced by this extraneous reply can be determined by applying the results of the multiple target analysis. In using these relations, the reflected signal is assumed originating from an aircraft located at angle η_B along the line-of-sight from the antenna to the reflecting building. The voltage ratio of the two returns, g_v, is then specified by

$$g_v = \frac{d_{AC}}{d_{BC}d_{BA}}\sqrt{\frac{\Omega(\alpha_i)}{4\pi}} \qquad (G.7)$$

The distances d_{AC} and d_{BC} are approximately the same, so that the energy ratio reduces to

$$g_v = \frac{1}{d_{BA}}\sqrt{\frac{\Omega(\alpha_i)}{4\pi}} \qquad (G.8)$$

The amplitude ratio at the receiver depends not only on relative target strength, but also on relative antenna gain in the direction of both targets, g_A, so that

$$g = g_v g_A$$

The pointing error was evaluated for a building 12 stories (120 feet) high and 50 feet wide. Additional system parameters are as follows:

d_{BA} = 1 mile

C_R = 0.30

η_B = 10 degrees

α_i = 30 degrees

These conditions produced a signal voltage ratio of g_v = 0.562, resulting in the pointing error

$\sigma = 0.062^o$

Similar calculations were made for other building heights. These results are presented in Figure G4. From these curves, a building 80 feet high, which is located one-half mile from the antenna, could introduce an azimuth error of

$\sigma = 0.083^o$

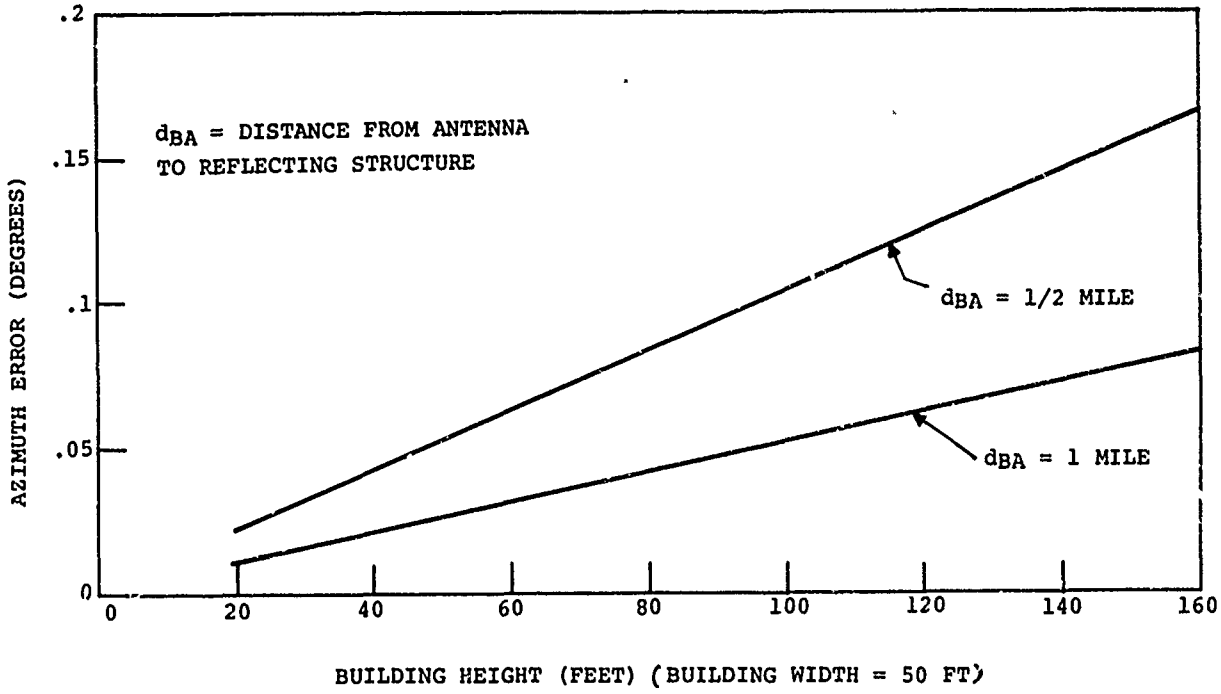

Figure G4. Azimuth Error Caused by Reflections from Buildings

References

G-1. Donald E. Kerr, Propagation of Short Radio Waves, M.I.T. Radiation Laboratory Series, vol. 13, McGraw-Hill, New York, 1951.

G-2. R. M. Kalafus et. al., "Derivation of Aerospace Antenna Coupling-Factor Interference Prediction Techniques," University of Michigan, Radiation Laboratory, Technical Report AFAL-TR-66-57, April 1966.

G-3. J. W. Crespin and A. L. Maffett, "Radar Cross Section Estimation for Simple Shapes," Proc. of the IEEE, vol. 53, Number 8, Aug. 1965.

G-4. Henry Jasik, editor, Antenna Engineering Handbook, McGraw-Hill, New York, 1961.

REFERENCES

1. Report of the DOT Air Traffic Control Advisory Committee (ATCAC), December 1969.

2. J.C. Doty, "ATCBI-2 Linear System and ATCBI-3 Logarithmic System," FAA/SRDS Report No. RD-65-28, March 1965.

3. W. Goldberg, H. Safran, H. Yamins, "The Use of Monopulse Techniques in the Radar Beacon System," Report M71-84, The MITRE Corporation, 5 April 1971.

4. Litton IFF Antennas, TM-20001C, Amecom Division, Litton Systems, Inc., College Park, MD, October 1969.

5. "Antenna Radome Groups AN/GPA-123 and AN/GPA-128," Specification sheet issued by Hazeltine Corporation, Little Neck, N. Y. 11362.

6. "AN/FYQ 47, 48, 49 Common Digitizer," Report No. D-774A, Burroughs Corporation, pp. 1-2 to 1-26, July 1968.

7. A. D. Bradley, "Technical Evaluation of Interrogator Set AN/TPX42 Type III and Type IV Systems," Final Report, NAFEC, Atlantic City, N. J. 08405, May 1970.

8. "Monopulse Antenna, Brief Description," Report No. N1/0/V-1, AEG-Telefunken (N1), 79 Ulm, W. Germany, July 1969.

9. D. K. Barton and H. R. Ward, Handbook of Radar Measurement, McGraw-Hill, New York, 1969.

10. D. R. Rhodes, Introduction to Monopulse, McGraw-Hill, New York, 1959.

11. M. I. Skolnik, Radar Handbook, McGraw-Hill, New York, 1970.

12. D. K. Barton, Radar System Analysis, Prentice-Hall, Englewood Cliffs, New Jersey, 1964.

13. R. S. Berkowitz, ed., Modern Radar, J. Wiley, New York, 1965.

14. Detailed Technical Discussion of Progress during September 1971 on Task A of PPA FA 209, Letter to FAA, RD-235, October 7, 1971.

REFERENCES (CONT.)

15. R. M. Kalafus and G. J. Bishop, "The Effective Phase Perturbation on Beam Pointing Errors in Phased Arrays," to be published in Trans. IEEE, Ant. and Propag.

16. ATC Radar Beacon Interrogator, ATCBI-3, Theory of Operation, Manual FR 527-1, FAA Aeronautical Center, FAA Academy, Oklahoma City, Oklahoma, June 1970.

17. Richards, C. J., editor, Mechanical Engineering in Radar and Communications, Van Nostrand Reinhold Co., New York, 1969.

18. "Wind Forces on Standard Antennas with Radomes," Microwave Engineers' Handbook, Horizon House, Dedham, MA , February 1970, p. 59.

19. Norman L. Fox and Bain Dayman, Jr., "Preliminary Report on Parabolsidal Reflector Antenna Wind Tunnel Tests," Int. Mem. CP-3, Jet Propulsion Laboratory, Pasedena, CA., 28 February 1962.

20. S. Sharenson, "Angle Estimation Accuracy with a Monopulse Radar in the Search Mode," Trans. IRE Aerospace & Nav. Electr., vol. ANE-9, pp. 175-179, September 1962.

21. E. T. Bayliss, "Design of Monopulse Antenna Difference Patterns with Low Sidelobes," Bell System Technical Journal, v. 47, no. 5, pp. 623-650, 1968.

22. Samuel Sherman, "Complex Indicated Angles Applied to Unresolved Radar Targets and Multipath," Trans. IEEE Aerospace & Electronic Systems, vol. AES-7, no. 1, January 1971.

23. C40 Final Test Report, MTR 4414, The MITRE Corp., Washington, D.C., March 23, 1970.